

7-2-2011

Interpreting Early Triassic (Smithian) sea-level change and climate using sequence stratigraphy and oxygen isotopes of conodont apatite

Stephanie Yurchyk

Follow this and additional works at: https://digitalrepository.unm.edu/eps_etds

Recommended Citation

Yurchyk, Stephanie. "Interpreting Early Triassic (Smithian) sea-level change and climate using sequence stratigraphy and oxygen isotopes of conodont apatite." (2011). https://digitalrepository.unm.edu/eps_etds/101

This Thesis is brought to you for free and open access by the Electronic Theses and Dissertations at UNM Digital Repository. It has been accepted for inclusion in Earth and Planetary Sciences ETDs by an authorized administrator of UNM Digital Repository. For more information, please contact disc@unm.edu.

Stephanie Yurchyk

Candidate

Earth and Planetary Sciences

Department

This thesis is approved, and it is acceptable in quality and form for publication:

Approved by the Thesis Committee:

 _____, Chairperson

 _____

 _____

**INTERPRETING EARLY TRIASSIC (SMITHIAN)
SEA-LEVEL CHANGE AND CLIMATE
USING SEQUENCE STRATIGRAPHY AND
OXYGEN ISOTOPES OF CONODONT APATITE**

BY

STEPHANIE LYNN YURCHYK

B.S. Geology, University of Rochester, 2007

THESIS

Submitted in Partial Fulfillment of the
Requirements for the Degree of

**Master of Science
Earth and Planetary Sciences**

The University of New Mexico
Albuquerque, New Mexico

May, 2011

Acknowledgements

There are many mentors and colleagues over the last few years that provided invaluable insight, support and guidance. Most importantly, this thesis would not have been possible without my advisor, Dr. Maya Elrick, committee member and field advisor, Dr. Viorel Atudorei, and dedicated third committee member, Dr. Gary Weissmann. Thank you for imparting your wisdom, exercising patience, and offering countless hours of your time over the past 3 years.

As many who have undergone the masters thesis process would agree, it takes a village to raise a grad student. I would like to thank the Earth and Planetary Sciences department from the front office staffers, to my professors, to my fellow grad students for helping me complete this process. A special thank you to Dr. Laura Crossey for your mentorship and support while I was a teaching fellow in the G K-12 program.

Many thanks to the US field crew: Dr. Viorel Atudorei, Vivek Shah, and Andy Darling who endured the summer heat while literally collecting 2 tons of rock samples, fording a river, and narrowly escaping the fangs of a rattle snake. I wouldn't have done it any other way. Thanks for sticking by me!! Another big thank you goes out to Jim and Ruby Jenks for their hospitality every time we visited northeast Utah and to Jim for his help locating outcrops and knowledge of Triassic ammonoids.

Thank you to the Indo-US research consortium lead by Dr. Asish Basu from the University of Rochester in Rochester, NY and Dr. Arundee Ahluwalia from Panjab University in Chandigarh, India for affording me the opportunity to travel to

the Indian Himalayas and to Dr. Leopold Krystyn for helping me identify the Smithian section.

Many words of gratitude go out to my friend, Nina Lanza for always being there. Your support meant the world to me; to Bethany Theiling, as you walked every step of the past 3 years right along with me; to Zach Wallace and Phil Ragonese who will continue to carry on the Elrick lab legacy; to the rest of my fellow grad students, thanks for the memories!

And last, but certainly not least, thank you Robin Tanner for your love and support from the northeast to the southwest and back east again. And a final thanks goes out to my mom, dad, and sister, Taylor. You are my inspiration.

This project was funded in part by the following: Department of Earth and Planetary Sciences at the University of New Mexico, the National Science Foundation, the Geological Society of America, the New Mexico Space Grant, UNM graduate student grants (RPT and SRAC), and Sigma Xi.

**UNDERSTANDING EARLY TRIASSIC (SMITHIAN)
SEA-LEVEL CHANGE AND CLIMATE
USING SEQUENCE STRATIGRAPHY AND
OXYGEN ISOTOPES OF CONODONT APATITE**

BY

STEPHANIE LYNN YURCHYK

ABSTRACT OF THESIS

Submitted in Partial Fulfillment of the
Requirements for the Degree of

**Master of Science
Earth and Planetary Sciences**

The University of New Mexico
Albuquerque, New Mexico

May, 2011

INTERPRETING EARLY TRIASSIC (SMITHIAN) SEA-LEVEL CHANGE AND CLIMATE USING SEQUENCE STRATIGRAPHY AND OXYGEN ISOTOPES OF CONODONT APATITE

Stephanie Lynn Yurchyk

B.S., Geology, University of Rochester, 2007

M.S., Earth and Planetary Sciences, University of New Mexico, 2011

ABSTRACT

The Early Triassic is conventionally interpreted to have a warm and ice-free climate. During this time, three globally recognized depositional sequences developed in response to ~My-scale sea-level changes. The Lower Triassic Lower Thaynes Formation records the Smithian (2nd sea-level cycle in the Early Triassic) in the western United States (Confusion Range and Weber Canyon, Utah). The Smithian portion of the Mikin Formation records an approximately time-equivalent sea-level cycle in northern India (Guling, Himachal Pradesh). The maximum flooding zone combined with existing age-diagnostic biostratigraphy allows for correlation between two sections in the western United States and one section in northern India suggesting the Smithian My-scale sea-level change was likely eustatic.

Samples were collected for oxygen isotopic analyses of conodont apatite from the two field locations (in Utah) in a sequence stratigraphic framework to better understand the Smithian paleoclimate. Due to an up to ~1.5 ‰ disparity of values between the two locations, additional conodont elements were analyzed from the Guling, Himachal Pradesh, northern India, Bear Lake, southern Idaho, Wapiti Lake area in eastern British Columbia, Canada, and Sverdrup Basin in the Canadian Arctic. Conodont Alteration

Index or CAI (a measure of post-burial thermal alteration based on color) was estimated for each of the locations listed above and range from 1.5 for Wapiti Lake and the Confusion Range to 5 for Guling. In addition, SEM images were taken to identify potential physical alteration of the conodonts for the Confusion Range (smooth surface with no signs of alteration), Weber Canyon (pitted surface with signs of potential alteration), and Guling (visibly the most pitted surface with signs of potential dissolution).

The $\delta^{18}\text{O}$ values for Weber Canyon range from ~ 14.4 to 15.8 ‰, the Confusion Range from ~ 16 to 16.9 ‰, northern India from ~ 15.8 to 16.5 ‰, Wapiti Lake from ~ 17.2 and 17.6 ‰, Sverdrup Basin range from ~ 14.5 and 14.8 ‰, and the Bear Lake value was ~ 16.5 ‰. Conodonts with a CAI of ≤ 3 or lower produced $\delta^{18}\text{O}$ values that most likely reflect the primary Smithian ocean isotopic values. Assuming an ice-free ocean value of -1 ‰, sea-surface temperatures were calculated as ~ 35 to 38 °C for the paleotropical and ~ 32 to 34 °C for the paleosubtropical regions, which make sense given their latitudinal position. Warm ocean currents in the neo-Tethys Sea can potentially explain this discrepancy. All six locations indicate that the Smithian ocean was significantly warmer than the present ocean, and instead, most resemble the extreme greenhouse sea-surface temperatures calculated for mid- to late Cretaceous.

TABLE OF CONTENTS

LIST OF FIGURESx

LIST OF TABLES xii

PREFACE xiii

CHAPTER 11

 1.1 Introduction.....3

 1.2 Geologic Background: Paleogeography and Lower Triassic Stratigraphy.....6

 1.2.1 Western North America7

 1.2.2 The Thaynes Formation (Smithian-Spathian)9

 1.3 Facies Descriptions and Depositional Environment Interpretations16

 1.3.1 Weber Canyon, northern Utah16

 1.3.2 Confusion Range, western Utah27

 1.3.3 Guling, Himachal Pradesh, northern India35

 1.3.4 The Lilang Supergroup: Mikin Formation (Lower Triassic).....37

 1.4 Sequence Stratigraphy42

 1.4.1 Sequence stratigraphy terminology42

 1.4.2 Weber Canyon, northern Utah44

 1.4.3 Confusion Range, western Utah49

 1.4.4 Guling, Himachal Pradesh, northern India51

 1.5 Global Correlation52

 1.6 Conclusions.....55

CHAPTER 2.....57

 2.1 Introduction.....58

2.2 Geologic Background	59
2.3 Early Triassic Climate	59
2.4 $\delta^{18}\text{O}$ paleoclimate studies.....	62
2.5 Methods	63
2.6 Results.....	65
2.6.1 CAI and SEM images of Conodonts	65
2.6.2 $\delta^{18}\text{O}$ values	67
2.7 Discussion.....	67
2.7.1 $\delta^{18}\text{O}$ values	67
2.7.2 Paleoclimate interpretations.....	73
2.7.3 What is driving My-scale sea-level change?	77
2.8 Conclusions.....	78
APPENDICES	79
APPENDIX A STRATIGRAPHIC COLUMNS	
WEBER CANYON.....	80
CONFUSION RANGE	94
GULING	98
APPENDIX B OXYGEN ISOTOPE DATA	
OXYGEN ISOTOPE DATA.....	101
REFERENCES	103

LIST OF FIGURES

Figure 1.1: Phanerozoic sea-level curve with the Early Triassic highlighted.	5
Figure 1.2: Early Triassic paleogeography	8
Figure 1.3: Chronostratigraphy and biostratigraphy of the western United States and northern India.....	10
Figure 1.4: Outcrop photograph of the Weber Canyon, northern Utah section.	12
Figure 1.5: Outcrop photograph of the Confusion Range, western Utah section.....	14
Figure 1.6: Field photograph of thin and medium bedded silty lime-mudstone subfacies.	19
Figure 1.7: Field photograph of the abraded bivalve wackestone-packstone outcrop	20
Figure 1.8: field and hand sample photograph of the bivalve wackestone subfacies.....	22
Figure 1.9: Field photograph of the dark calcareous mudshale interbedded with lime mudstone subfacies (rhythmites).	25
Figure 1.10: Field photograph of the dark calcareous mudshale subfacies.....	26
Figure 1.11: Field photograph of the vuggy lime mudstone subfacies.....	30
Figure 1.12: Field photograph of the ammonoid-micro-gastropod wackestone and the lime mudstone interbedded with light calcareous mudshale subfacies.	33
Figure 1.13: Field photograph of the Lower Triassic (Smithian) portion of the Mikin Formation in Guling, northern India.....	36
Figure 1.14: Field photographs four subfacies defined for the Smithian portion of the Mikin Formation in Guling, northern India	41
Figure 1.15: Sequence stratigraphy interpretation.....	45
Figure 1.16: Platform depositional model for the Weber Canyon section	48

Figure 2.1: Paleogeography of the Early Triassic	60
Figure 2.2: SEM images of conodonts	66
Figure 2.3: Oxygen isotope data for the six locations and association temperatures plotted by latitude	68
Figure 2.4: Oxygen isotope data plotted next to the Confusion Range and Weber Canyon stratigraphy and sea-level curve	69
Figure 2.6: Oxygen isotope data from the six sections plotted vs. CAI	72
Figure 2.7: All oxygen isotope data from conodont apatite published from the Early Ordovician through the Late Triassic	74

LIST OF TABLES

Table 1.1 Weber Canyon Facies Table	17
Table 1.2 Confusion Range Facies Table	28
Table 1.3 Guling Facies Table	39
Table 2.1 Conodont CAI Estimates	65

Preface

The aim of this research project is to better understand the interaction between Early Triassic (Smithian) climate and sea-level changes through a detailed sedimentological and sequence stratigraphic perspective (Chapter 1), as well as through the use of $\delta^{18}\text{O}$ of conodont apatite as a proxy for sea surface temperature and temperature gradients between the equator and mid paleolatitudes (Chapter 2). This project is important because it adds to the growing amount of detailed stratigraphic work during the recovery period after the Permo-Triassic extinction and evaluates the relatively new tool of using $\delta^{18}\text{O}$ of conodont apatite to better understand the Smithian climate.

The purpose of Chapter 1 is to create a sequence stratigraphic framework for the Early Triassic (Smithian), specifically looking at developing a more detailed global correlation. This chapter takes the previous research one step further by combining modern advances in biostratigraphy with detailed sedimentary facies analyses and depositional environment interpretations of the Smithian in the western United States and northern India. This will allow for both a more complete global sequence stratigraphic picture, as well as help to create a framework for understanding the Smithian climate.

In addition to the detailed stratigraphic analysis, samples were collected in a sequence stratigraphic framework for conodont apatite. Chapter 2 will focus on the reliability of $\delta^{18}\text{O}$ values from conodont apatite, and the potential for using this tool as a proxy for seawater temperature, ice volume, evaporation, and freshwater influx. Those samples interpreted to retain primary or near primary ocean $\delta^{18}\text{O}$ values were used to address the Smithian climate.

To date, it is difficult to identify diagenetic alteration that would allow for the exchange of oxygen between pore waters and conodont elements. This chapter will investigate a number of Smithian conodont elements with Conodont Alteration Indexes (CAIs) ranging from 1.5 (little thermal alteration) to 5 (moderate to extreme thermal alteration), as well as SEM images of the conodonts to look for physical evidence of alteration to better understand why there is an up to ~1.5 ‰ difference between relatively closely spaced samples collected for this study.

Chapter 1: Sequence Stratigraphy of the Lower Triassic (Smithian) Lower Thaynes Formation (Weber Canyon and Confusion Range, Utah) and the Smithian portion of the Mikin Formation (Guling, Himachal Pradesh, India)

Abstract

The mixed siliciclastic and carbonate Lower Triassic (Smithian) Lower Thaynes Formation at Weber Canyon, northern Utah and the Confusion Range, western Utah are interpreted as ~My-scale transgressive-regressive cycles. They were deposited in an inland sea on the western edge of Pangaea separated from the Panthalassa Ocean by a volcanic arc. The Lower Thaynes Formation conformably overlies the siliciclastic-rich, restricted shallow subtidal to continental Woodside Shale to the north and east and carbonate-rich, shallow marine Dinwoody Formation to the west and south. It is overlain by the Decker Tongue to the north and east and its shallow subtidal to marginal marine red siltstone and shale facies equivalents to the south and west. Facies relationships between the Woodside Shale, Lower Thaynes Formation, and the Decker Tongue and marginal marine equivalents indicate a deepening into open marine facies dominated by bivalves, gastropods, echinoderms, and ammonoids in the transgressive systems tract to deep subtidal, dark shale in the maximum flooding zone, and a shallowing into shallow and restricted shallow subtidal facies in the highstand systems tract. The two sections are correlated both by sequence stratigraphy and existing ammonoid and conodont biostratigraphy.

The carbonate-rich Lower Triassic Smithian portion of the Mikin Formation in Guling, Himachal Pradesh, northwestern India represents the time-equivalent My-scale sea-level change from the southern neo-Tethys Sea on the eastern Margin of Pangaea. The Smithian portion of the Mikin Formation conformably overlies the Griesbachian Lower Limestone Member and the Dienerian portion of the Limestone and Shale Member. The Spathian portion of the Niti (Nodular) Limestone Member of the Mikin Formation overlies the Smithian portion of the Mikin Formation. The Indian section is correlated with the western United States sections using the maximum flooding zone, defined as the deposition that occurs during the maximum transgression. Further support for the correlation comes from ammonoid and conodont biostratigraphy.

The transgressive-regressive sequence for all three sections falls within the bounds of the Smithian time period based on the known biostratigraphy. Thus, it is possible that the sea-level changes are eustatic in origin. However, due to the complexities involving regional changes in accommodation and lack of absolute age dates and the scarcity of age-diagnostic fossils in the Early Triassic, determining the timing of the sea-level change between the two regions is challenging.

1.1 Introduction

The Permian-Triassic extinction (~252 Ma) is recognized as one of the “big five” extinctions in Earth’s history marked by the loss of 84-93% of marine genera (Raup, 1979; Sepkoski, 1989; Stanley, 1990; Erwin, 2006; 2008). The ~5 My recovery period (Early Triassic) is characterized by low biotic diversity (Schubert and Bottjer, 1995; Rodland and Bottjer, 2001; Payne et al., 2006), the absence of corals and sponges (Hallam and Wignall, 1997), the persistence of cosmopolitan marine fauna (Hallam, 1981, Boyer et al., 2004; Fraiser and Bottjer, 2004), continued low deep-water oxygen levels (Wignall and Hallam, 1996), and a hiatus of coal deposition (Retallack et al., 1996). The prolonged recovery is thought to be the result of persistent, unfavorable paleoenvironmental conditions throughout the Early Triassic, though the nature of these paleoenvironmental conditions are not well understood (Erwin, 2006; 2008; Hallam and Wignall, 1997; Payne et al., 2004).

The climate during the Early Triassic is thought to have been warm and stable; however, the assumed stability may be the result of a lack of detailed paleoclimate studies. Evidence to support a globally-warm Early Triassic is based on increased weathering rates in high paleolatitude soils (Retallack, 1999; Michaelsen and Henderson, 2000; Michaelsen, 2002), migration of characteristically warm-water taxa to higher latitudes (i.e., calcareous algae into the Svalbard Basin); (Wignall et al., 1998) and warm weather flora (i.e. the appearance of cycads in the Greenland record); (Looy et al., 2001). The lack of glacial deposits suggests that the poles were not cold enough to sustain permanent ice caps (Frakes et al., 1992). Ammonoid fauna are found at a wide paleo-latitudinal range through the Smithian suggesting that there is a gentle low to high

latitude temperature gradient (Brayard et al., 2006). General circulation models across the Permo-Triassic boundary (Kidder and Worsley, 2004; Kiehl and Shields, 2005) and geochemical models (Berner et al., 2002; Royer et al., 2004) suggest that there was a 6 to 8 °C increase in the temperature.

Although the Early Triassic is an important and unique period in Earth history, relatively few detailed stratigraphic studies exist, which are necessary to build a framework for global marine sequence correlation. The groundbreaking work identifying genetically related sedimentary packages (or depositional sequences) involved seismic stratigraphy, which lacked relative and absolute time controls (Vail et al., 1977; Haq et al., 1987; 1988) (Figure 1.1a). Embry (1988) combined Triassic outcrop and well-log stratigraphic study from the Sverdrup Basin in the Canadian Arctic to test the Triassic portion of the Phanerozoic eustatic sea-level curve developed by Vail et al. (1977), Haq et al. (1987; 1988). From this study, three sea-level changes were described for the Early Triassic (Figure 1.1b). Additional Early Triassic stratigraphic studies (Embry, 1997; Paull and Paull, 1994; Baud et al., 1996) have broadly identified a similar three Lower Triassic transgressive-regressive sequences: the first in the Griesbachian-Dienerian, the second in the Smithian, and the third in the Spathian. Embry (1997) attempted to correlate the Triassic across seven globally distributed regions; however, this project lacked both adequate biostratigraphic control for these regions and detailed stratigraphy to prove that the sequences were, in fact, correlative.

The purpose of this project is to 1) identify depositional environments within the Lower Triassic Lower Thaynes Formation (western United States) and the Smithian

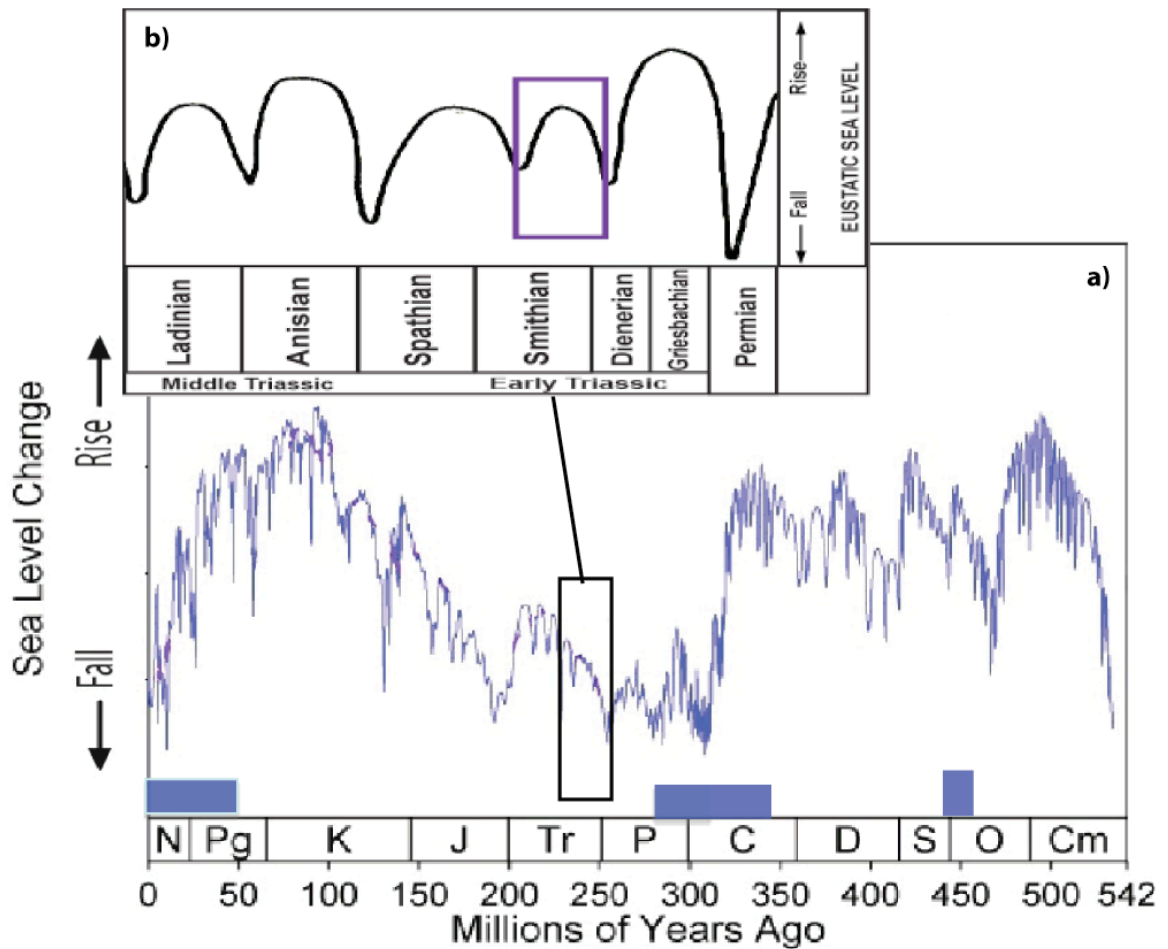


Figure 1.1: **a)** The Phanerozoic sea-level curve interpreted from both seismic stratigraphy, well logs and outcrops studies, highlighting known ice ages with blue bars (modified from a compilation of seismic stratigraphy completed by Haq et al., 1988, Ross & Ross 1987, Ross & Ross 1988). **b)** The above sea level curve highlights the Early and Middle Triassic sea-level curve developed from both seismic and outcrop studies in the Sverdrup Basin in the Canadian Arctic with the Smithian sea-level rise and fall highlighted in the purple box (modified from Embry, 1988).

portion of the Mikin Formation (Guling, Himachal Pradesh, northern India), 2) characterize vertical stacking patterns in each section in order to develop a sequence stratigraphic framework for the Smithian and 3) use published ammonoid and conodont biostratigraphy (Smith, 1969; Garzanti et al., 1994; Krystyn et al., 2004; 2007; Galfetti et al., 2007; Brayard et al., 2009; Guex et al., 2010; Stephen et al., 2010; Beatty, personal communication; Jenks, personal communication) to constrain the age and help correlate the Smithian sequences, which will provide the framework for understanding the origin of the Smithian sea-level change. The Lower Thaynes Formation in Weber Canyon and the Confusion Range and the Smithian portion of the Mikin Formation in Guling, India are chosen for this study because they have well-exposed marine strata with established biostratigraphic age control in geographically diverse locations.

1.2 Geologic Background: Paleogeography and Lower Triassic Stratigraphy

The Pangaeon supercontinent and the Panthalassa Ocean (Figure 1.2) dominated the Early Triassic paleogeography. Pangaea remained a single landmass transected by the paleoequator until the Early to Middle Jurassic (Blakey, 2010; Scotese, 2010). Global sea level was relatively low during the late Paleozoic through the early Mesozoic due to low mid-ocean ridge activity (Forney, 1975; Holser and Magaritz, 1987; Ross and Ross, 1987) (Figure 1.1b).

1.2.1 Western North America

During the Early Triassic, western North America lay between ~5 and 35 °N paleolatitude (Figure 1.2) (Blakey, 1974; 2010; Scotese, 2010). This region underwent a complex tectonic history that resulted from the initiation and evolution of two temporally distinct subducted lithospheric slabs: a pre-Farallon plate and the Farallon plate beneath the western edge of North America (Lawton, 1994). Subduction of the pre-Farallon plate was initiated in the Early Triassic following the latest Permian to early Triassic Sonoma Orogeny, which marked the closure of a marginal basin west of North America (Lawton, 1994). Following the brief formation of the earliest Triassic flexural basin (including the Havalleh Basin) adjacent to the Golconda allochthon, initiation of subduction created a north-westward-thickening wedge of marine sedimentary rocks in the marine foreland basin (Smith, 1969; Silberling, 1975). During the Smithian maximum transgression, this inland sea extended from southeastern Utah to British Columbia with an ~160 to 500 km-wide ramp and was separated from the Panthalassa Ocean by a volcanic arc to the west (Blakey, 1974).

Subsidence within the foreland basin is attributed to the viscous flow of the mantle above the slab of the subducted oceanic crust, tectonic loading by the thrust sheets and crustal loading by sediments following the closure of a backarc basin during the Sonoma Orogeny (Lawton, 1994). Significant orogenic features that influenced siliciclastic sedimentation in the Havalleh basin included the Uncompahgre Highland, the Kaibab Uplift, the Ancestral Rocky Mountains, and the Mogollon Highland to the east and south (Blakey, 1974; Paull and Paull, 1994). Fluvial sediment transport into the basin occurred from the east and southeast (Marzolf, 1994).

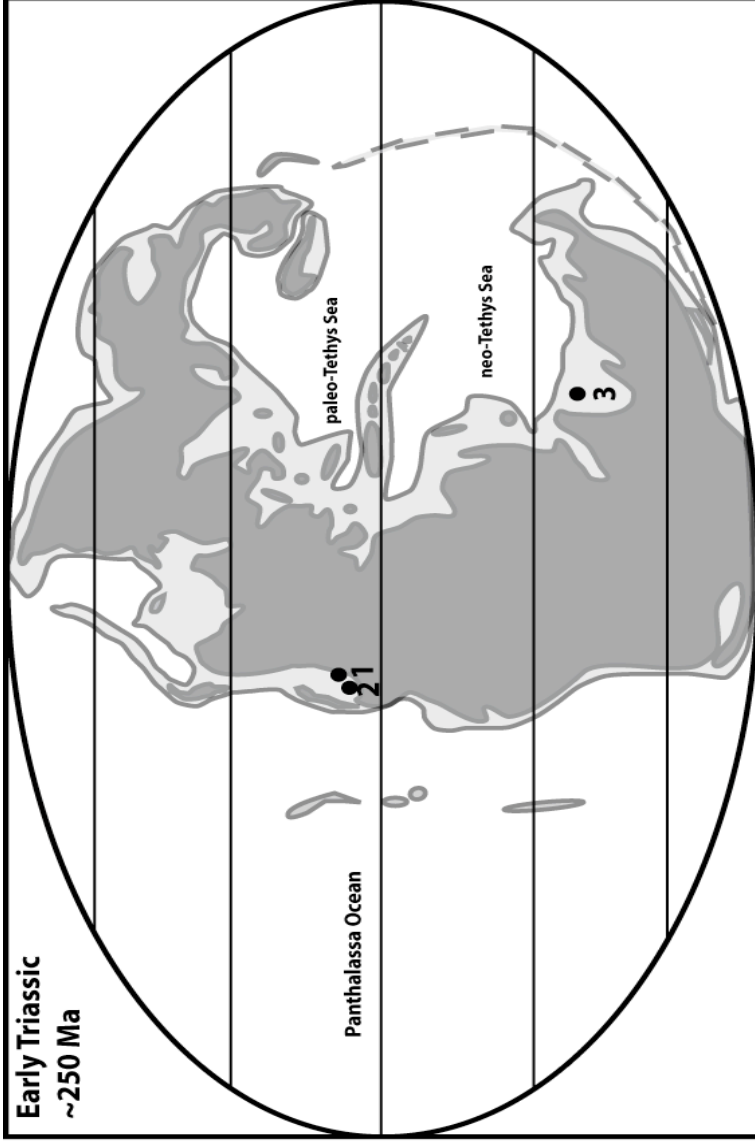


Figure 1.2: Early Triassic paleogeographic map. The supercontinent of Pangaea is fully assembled with the Panthalassa Ocean surrounding the eastern margin and the paleo- and neo-Tethys Seas bordering the eastern margin, dotted with micro-continents and volcanic arcs. Exposed land masses are dark gray and submerged continental platforms are light gray. Sites 1 and 2 are Weber Canyon, northern Utah and Confusion Range, western Utah, respectively, and were deposited in an intracratonal basin separated from the open Panthalassa Ocean by a volcanic arc. Site 3 is Guling, northern India deposited on a passive margin that dipped to the north towards the neo-Tethys Sea (modified from Blakey, 2010 and Scotese, 2010).

1.2.2 The Thaynes Formation (Smithian and Spathian)

The Thaynes Formation (~300 to 1100 m thick) was originally described by Boutwell (1907) in Park City, Utah and ranges from deep subtidal to marginal marine deposits that commonly consist of skeletal limestone, calcareous siltstone and shale facies. The Thaynes Formation overlies the Griesbachian-Dienerian shallow marine to continental Woodside Shale in northern and eastern Utah and the shallow-water carbonates of the Dinwoody Formation to the north and west in Idaho, western Utah, Nevada, and Montana (Kummel, 1943; 1954) (Figure 1.3). The Woodside Shale and Dinwoody Formation unconformably overlie the Upper Permian Phosphoria Formation in most of the basin; however, in western Utah and Nevada, the Thaynes Formation unconformably overlies the Upper Permian Gerster Formation (Kummel, 1954; Collinson, 1976).

The Thaynes Formation is separated into the Lower Thaynes (Smithian) and the Upper Thaynes (Spathian) Formations divided by the Decker Tongue to the east and very shallow marine deposits to the west (Kummel, 1954; Smith, 1969) (Figure 1.3). The Ankareh Formation of the Moenkopi Group is characterized by continental sandstone and shale and overlies the Thaynes Formation (Kummel, 1954). Regional correlation between the Thaynes Formation in Utah, Idaho, and Nevada were originally defined using ammonoid biostratigraphy (early Smithian *Meekoceras* ammonoid zone (Boutwell, 1912). Lucas et al. (2007) argued that some of the ammonoids that were originally defined as *Meekoceras* were, in fact, misidentified due to poor preservation. Instead, the ammonoid zone used for regional correlation of the maximum transgression is the mid- to late Smithian *Anasibirites* ammonoid zone (Lucas et al., 2007).

More recently, advancements in ammonoid and conodont biostratigraphy have made it possible to build a framework for global correlation. Using the absolute U/Pb ages from the time-equivalent Jinya section in China combined with ammonoid and conodont biostratigraphy, the Griesbachian through Smithian is ~2 My in duration and the Spathian as ~3 My (Ovtcharova et al., 2006). This suggests that the entire Smithian represents ≤ 2 My.

The mixed carbonates and siliciclastics of the Lower Thaynes Formation at Weber Canyon (~240 m thick) was measured and described on the north and south sides of the Weber River, adjacent to the Union Pacific Railroad tracks and west of Devils Slide in Morgan County, Utah (Exit 108 off of I-84E; GPS location: 12 T 0452004 UTM 4545695) (Figure 1.4; Appendix A). Weber Canyon is the best-known exposure of the Lower Thaynes Formation in western North America (Figure 1.4). Most outcrops of the Thaynes Formation only expose the base and the top of the formation because the middle portion is composed of fine-grained silty lime mudstone and mudshale facies, which are often covered. At this locality, the marine Lower Thaynes Formation conformably overlies red-brown sandstone, siltstone, and shale of the Woodside Shale (Griesbachian-Dienerian) and is conformably overlain by a similar red-brown marginal marine to continental siliciclastic unit (Decker Tongue) at Weber Canyon (Kummel, 1954; Smith, 1969). The lower contact is defined by the first and the upper contact by the last beds containing marine macrofossils (Smith, 1969).

At Weber Canyon, the Lower Thaynes Formation consists of three depositional units: 1) the carbonate-rich lower unit composed primarily of gray, silty lime mudstone containing sparse to rare fossils and wackestones to grainstones containing bivalves,

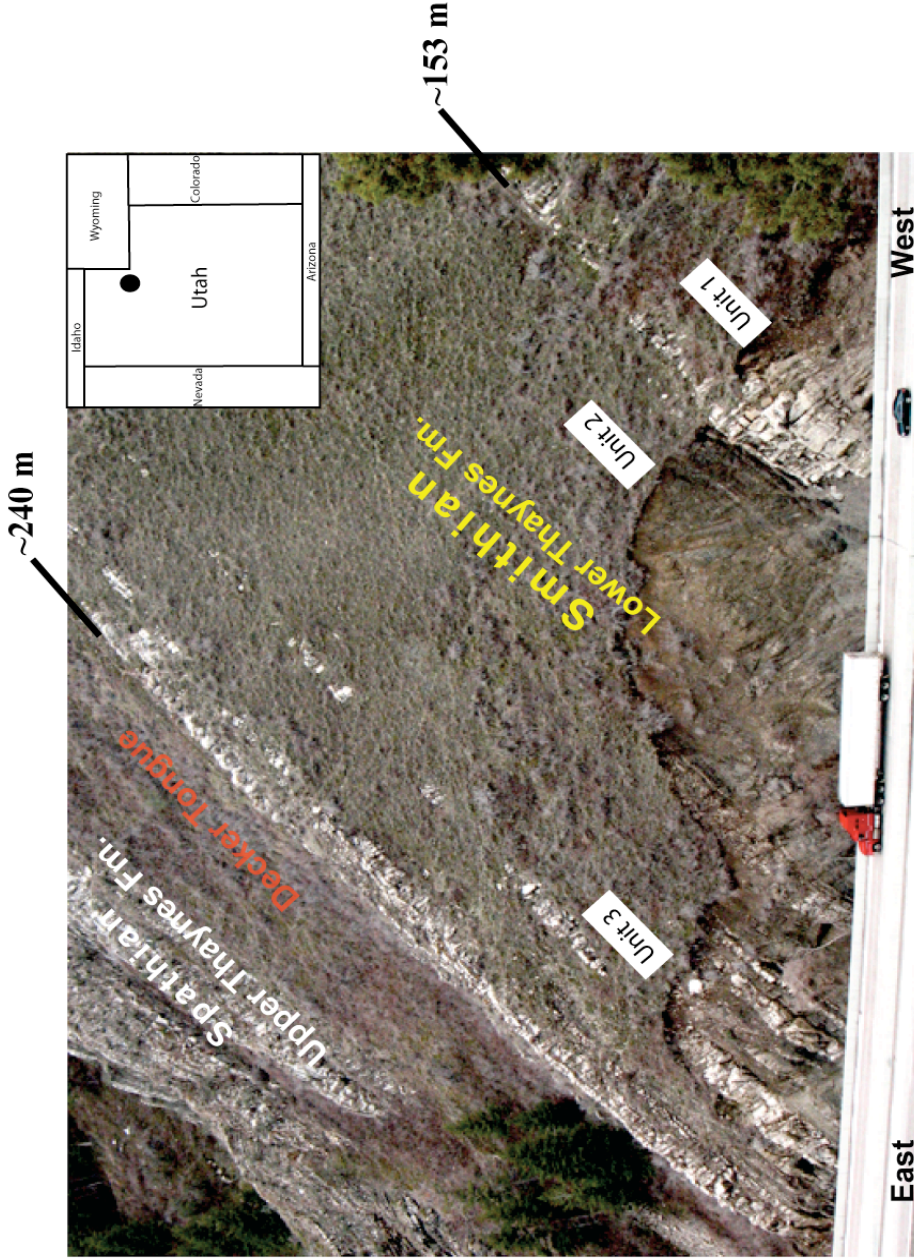


Figure 1.4: The Lower Triassic Lower and Upper Thaynes Formations exposed at Weber Canyon along I-84 east of Ogden, Utah. The contact between the silty lime mudstone (top of unit 1) and the dark calcareous shale (unit 2) is labeled (~153 m). Also, the top of the Lower Thaynes Formation (~240 m; top of unit 3) is labeled. The Decker Tongue conformably overlies the Lower Thaynes Formation and the Spathian Upper Thaynes Formation, which conformably overlies the Decker Tongue, are also labeled.

echinoderms, and gastropods (~150 m), 2) a dark shale devoid of fossils that shallows into a calcareous mudstone interbedded with thin carbonates (~40 m), and 3) an upper mixed siliciclastic and carbonate unit of silty lime mudstone and calcareous siltstone, interbedded with whole bivalve wackestones (~70 m). Age-diagnostic fossils in the Lower Thaynes Formation, though scarce, consists primarily of upper Smith ammonoids (*Anasibirites*) and mid- to upper Smithian conodonts (*N. waageni*) (Beatty, T., written communication; Jenks, J., personal communication; Smith, 1969). The first beds containing early Spathian conodonts are stratigraphically above the Decker Tongue and help constrain the marine Lower Thaynes Formation as likely Smithian in age.

The Lower Thaynes Formation in the Confusion Range (~250 m) was measured and described at two locations: Disappointment Hills (GPS location: 12S 0268549 UTM 4365751) and Cowboy Pass, separated by ~11 kilometers (Figure 1.5). In the Confusion Range, four depositional units comprise the Lower Thaynes Formation: 1) a resistant, light olive-gray and pinkish wackestone to grainstone (~10 m), 2) primarily light olive-gray to yellowish calcareous mudshale occasionally capped by ammonoid and micro-gastropod rich limestone beds (.25 to 2 m thick) (~70 m), 3) a light yellow mudshale (~100 m) (Hose and Repenning, 1959), and 4) a red mudshale to fine sandstone interbedded with bivalve-rich limestone beds (~70 m) (Collinson, 1979). Due to the post-depositional complex tectonic history at Cowboy Pass, only the first and fourth

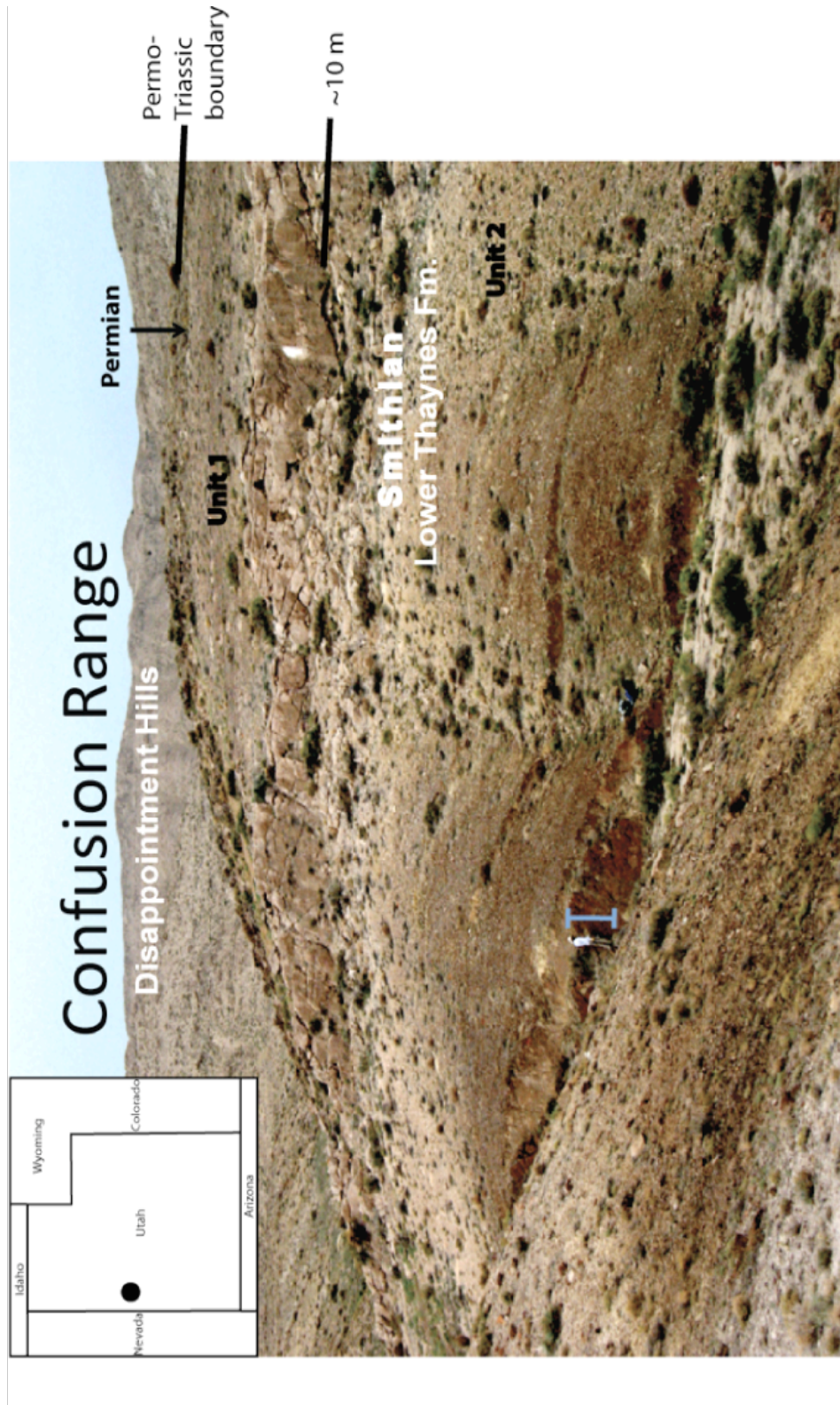


Figure 1.5: The Lower Triassic Lower Thaynes Formation exposure in western Utah (Confusion Range, Disappointment Hills). Units 1 (~70 m) and 2 (~10 m) are labeled. Here the Lower Thaynes Formation overlies the Permian Gerster Formation.

depositional units are well exposed, whereas at Disappointment Hills only the first and second units can be examined in a continuous section. Unit 3, a yellow mudshale, does not outcrop well at either location, but is estimated to have a thickness of ~100 m (Hose and Repenning, 1959). Despite having to piece together the Confusion Range, these sections were chosen for this study due to the abundance of age-diagnostic fossils.

The Lower Thaynes Formation in the Confusion Range unconformably overlies the Permian Gerster Formation, which is overlain by a conglomerate varying in thickness from 0 to 1.5 m. This unconformity extends from western Utah to eastern Nevada and has been recorded by several authors (Newell, 1948; Wheeler et al., 1949; Clark, 1956; 1959; Bissell, 1962a, 1962b; Collinson, 1968). Collinson et al. (1976) investigated the origin of this unconformity and concluded that it resulted in significant time loss likely caused by uplift and erosion related to the Sonoma Orogeny. Newell (1973) suggested that a eustatic drop in sea level caused the hiatus. Shallow marine red-brown sandstones and siltstones conformably overlie the Lower Thaynes Formation (~50 m; Atudorei, V., personal communication).

Ammonoid fossils representing the *Meekoceras*, *Inyoites* and *Anasibirites* zones are abundant near the base of the Lower Thaynes Formation at the Confusion Range (Brayard et al., 2009; Stephen et al., 2010). At the top of the Lower Thaynes Formation, however, no age diagnostic marine fossils have been recovered (Hose and Repenning, 1959; Newell, 1959). Thus, the only marker to distinguish the Lower from the Upper Thaynes is the first Spathian ammonoid-bearing bed in the field area (*Tirolites*) (Guex et al., 2010). The *Tirolites* lies above the red sandstone and shale facies (Guex et al., 2010).

1.3 Facies Descriptions and Depositional Environment Interpretations

Two Lower Thaynes Formation from sections from Weber Canyon and the Confusion Range were measured and described on a bed-by-bed basis for facies descriptions and paleoenvironmental analysis (Table 1; Appendix A). Facies and internal subfacies were originally defined in the field based on grain size, bedding characteristics, sedimentary structures, biota, and facies associations; 27 thin sections were utilized to refine the facies descriptions and interpretations (Tables 1.1, 1.2, 1.3). Facies stacking patterns were used to define ~My-scale depositional sequences. Interpretations of paleoenvironmental change and sea-level change were then derived from facies stacking patterns. The inner- to outer-ramp terminology, defined by Burchette and Wright (1992), is used for depositional environment interpretations. Vertical facies relationships of the cycles will be used to describe changes in ramp morphology through time.

1.3.1 *Weber Canyon, northern Utah*

At Weber Canyon, four depositional facies and seven subfacies are recognized, including: restricted shallow subtidal (silty lime mudstone, abraded bivalve wackestone-packstone), shallow subtidal (echinoderm grainstone), intermediate subtidal (bivalve wackestone), and deep subtidal (silty skeletal lime mudstone, lime mudstone interbedded with silty dark mudshale interbeds (rhythmites), and dark calcareous mudshale) (Table 1.1).

Weber Canyon		Lower Thaynes Formation		Table 1
Subfacies	Bedding	Skeletal components	Sedimentary-biologic features	Environment of deposition
Silty lime mudstone	Thin-medium	none observed	suspension laminations, sparse symmetric ripples	Restricted shallow subtidal, low to moderate energy, inner ramp
Abraded bivalve wackestone-packstone	Medium-thick	bivalves, sparse echinoderms, micro-gastropods, (conodonts)	bioturbation, occasional cross bedding	Restricted subtidal, moderate energy, inner ramp
Echinoderm grainstone	Medium	echinoderms, abraded bivalves, (conodonts), sparse abraded micro-gastropods	cross bedding	Shallow subtidal, high energy, inner to mid ramp
Bivalve wackestone	Medium	bivalves, sparse to rare micro-gastropods, and echinoderms, (conodonts)	bioturbation	Intermediate subtidal, low energy, inner to mid ramp
Silty skeletal lime mudstone	Thin-medium	sparse-rare abraded bivalves, micro-gastropods, echinoderms (conodonts)	locally disrupted laminae (bioturbation), strongly laminated toward the top, sparse symmetric ripples and thin ripples with clay drapes	Deep subtidal, low energy, periodically poorly oxygenated (at times), outer ramp
Lime mudstone interbedded with silty dark mudshale (rhythmites)	Thin bedding	rare abraded bivalves (conodonts) only in the lime mudstone	lime mudstone is bioturbated	Deeper Subtidal, low energy, poorly oxygenated, outer ramp
Dark calcareous mudshale	Thin	none observed	none observed	Deepest subtidal, low energy, outer ramp

Restricted shallow subtidal facies

Silty lime mudstone subfacies:

The silty lime mudstone subfacies ranges in thickness from <1 to 30 cm and is deposited near the base and top of the Lower Thaynes Formation (Figure 1.6). This subfacies was deposited in moderate energy, poorly oxygenated shallow subtidal, inner-ramp environments. This interpretation is supported by a lack of subaerial exposure features, fine-grain size, suspension laminations, sparse symmetric ripples, and lack of both fossils and bioturbation. In addition, this subfacies is in a conformable stratigraphic position above the interpreted continental beds of the Woodside Shale and below open-marine subfacies. The abundant, well-sorted quartz silt grains indicate a consistent current energy and/or eolian source and the fine-grain size indicates that this subfacies was deposited distal from its source.

Abraded bivalve wackestone-packstone subfacies:

The abraded bivalve wackestone-packstone subfacies ranges in thickness from 0.1 to 1 m and was deposited in moderate energy, shallow subtidal open marine, inner-ramp environments (Figure 1.7). The bioclasts are abraded, disarticulated, and moderately to well sorted, which suggests that they were extensively reworked in and transported from higher energy environments. The abundance of lime mud suggests moderate energy environments. The bivalves and gastropods likely filled an open marine, shallow subtidal niche that was vacated by organisms, such as brachiopods, during the time of ecosystem recovery following the end-Permian extinction (Boyer et al., 2004). Sparse echinoderm grains further suggest occasional open-marine circulation or onshore transport of offshore



Figure 1.6: Field photograph of thin and medium bedded silty lime-mudstone subfacies. Field book for scale.



Figure 1.7: Field photograph of the abraded bivalve wackestone-packstone outcrop. Rock hammer for scale.

crinoid bioclasts (Lehrmann et al., 2001). Based on its stratigraphic association with inner-ramp silty lime mudstone, the wackestone-packstones are interpreted to have been deposited during times of increased energy when either waves were able to surpass the shoal barrier (echinoderm grainstone subfacies) and/or when the shoal barrier was absent.

Shallow subtidal facies

Echinoderm grainstone subfacies:

The echinoderm grainstone subfacies ranges in thickness from 0.5 to 1 m and was deposited in open marine, high energy, mid-ramp environments. This interpretation is based on the relatively high faunal abundance and diversity, cross bedding, and lack of mud. In addition, its stratigraphic association with both fine-grained, low-energy inner- and outer-ramp suggests that it may have served as a barrier and sediment source for the lower energy deposition (i.e. abraded bivalve wackestone-packstone and the silty skeletal lime mudstone). The well-sorted and abraded nature of the bioclasts indicates significant transport and, thus, the organisms were likely not living in this environment.

Intermediate subtidal facies

Bivalve wackestone subfacies:

The bivalve wackestone subfacies ranges in thickness from 0.1 to 0.5 m and was deposited in low energy, inner- to mid-ramp environments indicated by the presence of bioturbation and stratigraphic association with both deep subtidal (rhythmites subfacies) and restricted shallow subtidal (silty lime mudstone) deposits (Figure 1.8). The whole, unabraded shells indicate that the bivalves were not extensively transported or reworked



Figure 1.8: Field and hand sample photograph of the bivalve wackestone subfacies. The facies is lighter in color and the calcareous mudshale is interbedded and dark in color. Gallon-size plastic bag for scale.

and represent local communities living in or very close to this environment. Boyer et al. (2004) reports similar bivalve-dominated facies in Lower Triassic rocks as monospecific shell beds and interpreted that they were deposited in a low to moderate energy, mixed carbonate-siliciclastic mid-ramp environments.

Deep subtidal facies

Silty skeletal lime mudstone subfacies:

The ~90 m-thick silty skeletal lime mudstone subfacies, located in the middle of the Lower Thaynes Formation (~50% of unit 1), represents the most abundant subfacies and was deposited in low energy, poorly to moderately oxygenated outer-ramp environments. Evidence to support this interpretation include the fine-grain size, sparse to rare fossils, clay draped symmetric ripples at the base and horizontal laminations near the top. Terrigenous silt was likely sourced from the exposed craton to the east and south via rivers associated with the Moenkopi Formation and/or eolian sources. This interpretation is further supported by its association with shallower, high-energy deposits at the base and the deepest water subfacies at the top indicating a deepening upward trend. The intensity of bioturbation varies throughout indicating variable dissolved oxygen contents during deposition. Smith (1977) interpreted a similar dark lime mudstone facies as being deposited in deep subtidal environments in the Mississippian Lodgepole Formation.

Lime mudstone interbedded with dark silty mudshale subfacies (rhythmites):

This subfacies ranges in thickness from 0.5 to 30 m with individual beds from <1 cm to ~5 cm. It was deposited in low energy, poorly oxygenated, outer-ramp environments (Figure 1.9). This interpretation is based upon the fine grain size, lack of current-generated sedimentary structures and bioturbation, sparse to rare fossil content, and its association with the deepest water subfacies at the base. The rhythmic interbedding of 1-10 cm thick lime mudstone and mudshale was likely the result of periodic fluctuations in detrital carbonate influx and/or changes in siliciclastic fluvial influx into the marine basin (Elrick et al., 1991; Elrick and Hinnov, 1996; Elrick and Hinnov, 2007). There is an increase in number and thickness of lime mudstone interbeds up section, concurrent with an increase in fossil content and bioturbation corresponding with a decrease in number and thickness of calcareous mudshale, suggesting an overall upward-shallowing trend.

Dark calcareous mudshale subfacies:

This ~30 m thick, platy subfacies was deposited in low energy, poorly oxygenated outer ramp environments (Figure 1.10). This interpretation is based upon its fine-grain size, lack of current-generated sedimentary structures, and lack of bioturbation and fossils. This subfacies is deposited in an upward-deepening portion of the sequence and the two storm beds at the base (skeletal packstones) indicate that initial deposition took place near storm wave base. The absence of storm beds above the contact between this facies and the shallower water facies below indicates that deposition continued below storm wave base for the majority of time. Toward the top of the subfacies, the shale



Figure 1.9: Field photograph of the lime mudstone interbedded with silty dark mudshale subfacies (rhythmites). Field pack and gallon-sized plastic bag to the right for scale

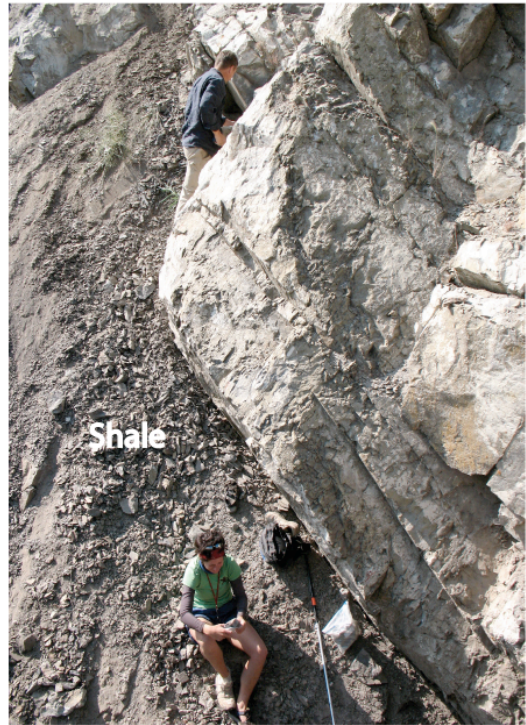
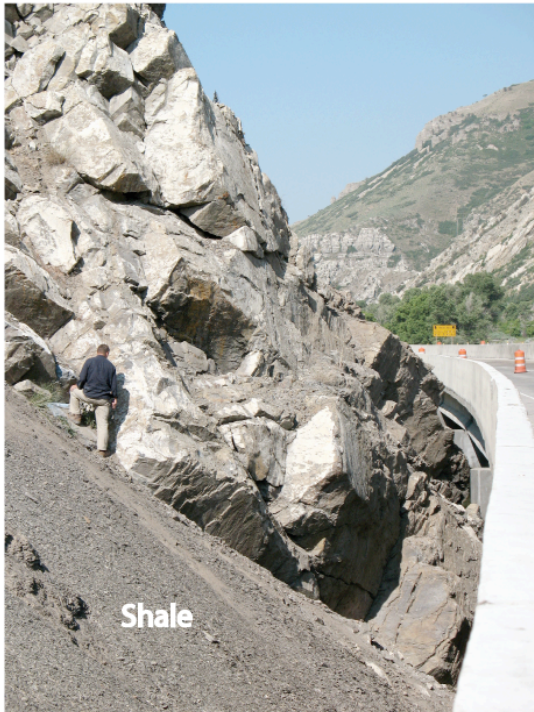


Figure 1.10: Field photographs of the dark calcareous mudshale subfacies. There is a sharp contact between the light-colored, silty skeletal lime mudstone subfacies and the dark mudshale.

becomes less fissile, indicating an increase in bioturbation. Dark shale facies can form in a variety of depositional regimes; however, based on the stratigraphic position of the subfacies, it is best interpreted as an anoxic to dysoxic, low energy, outer-ramp environments (Arthur and Sageman, 1994).

1.3.2 Confusion Range, western Utah

In the Confusion Range, four depositional facies and eight subfacies were also identified, with two subfacies similar to those found in Weber Canyon (Table 1.2). In descending water depths they include: restricted shallow subtidal (red silty lime mudstone, vuggy (subtidal microbialite) lime mudstone, and bivalve wackestone), shallow subtidal (clast-supported chert-quartz pebble conglomerate, and micro-gastropod-skeletal packstone-grainstone), intermediate subtidal (ammonoid-micro-gastropod wackestone), and deep subtidal (lime mudstone interbedded with calcareous mudshale (“rhythmites”), and light yellow calcareous clayshale) (Table 2; Appendix A).

Confusion Range		Lower Thaynes Formation		Table 2
Subfacies	Bedding	Skeletal Components	Sedimentary and biologic features	Environment of deposition
Red silty-lime mudstone	Thin-medium	none observed	Laminations, symmetric ripples, rare cross bedding	Restricted shallow subtidal, low energy, inner ramp
Vuggy (subtidal microbialite) lime mudstone	Thin-medium	none observed	vugs	restricted shallow subtidal, low energy, inner ramp
Bivalve wackestone	Thin-medium	whole bivalves, micro-gastropods	bioturbation	Restricted shallow subtidal, low energy, inner ramp
Clast-supported chert-quartz pebble conglomerate	Medium-thick	Sparse bivalves and micro-gastropod fragments, chert	poorly sorted, angular clasts	shallow subtidal, high energy, inner ramp
Micro-gastropod skeletal packstone-grainstone	Medium-thick	Abraded bivalves and crinoids, micro-gastropods, ammonoid fragments	massive, cross bedding, graded beds	shallow subtidal, high energy, shoal barrier, mid to inner ramp
Ammonoid/micro-gastropod wackestone	Thin-medium	Ammonoids, micro-gastropods, bivalves	Bioturbation	intermediate subtidal, medium energy, mid to outer ramp
Lime mudstone-calcareous mud- shale rhythmites	Thin bedding	none observed	Bioturbation in mudstone	deeper subtidal, low energy, outer ramp
Light (yellow) calcareous clayshale	thin	none observed	none observed	deepest subtidal, low energy, outer ramp

Restricted shallow subtidal facies

Red silty lime mudstone:

The red silty lime mudstone subfacies ranges in thickness from <1 cm to 10 cm and is only found at the top of the formation. This subfacies was deposited in low energy, low oxygen, inner-ramp environments. This interpretation is based on lack of both fossil and bioturbation, and the occurrence of suspension laminations, sparse symmetric ripples. The depositional environment of this facies is up for debate (McKee, 1949; Picard, 1967; McCormic and Picard, 1969; Blakey, 1974), but has been interpreted as peritidal to tidal flat environments based on evidence of periodic submersion and its relationship with shallow water carbonate deposits (bivalve wackestone subfacies).

Vuggy (subtidal microbialite) lime mudstone:

The vuggy (subtidal microbialite) lime mudstone subfacies (~0.25 m thick) was deposited in low energy, inner-ramp, shallow subtidal-intertidal environments (Figure 1.11). This interpretation is based on fine-grain size, primary vugs, and stratigraphic relationship with other restricted shallow subtidal subfacies.

Bivalve wackestone:

The bivalve wackestone subfacies ranges in thickness from 0.2 to 1 m and was deposited in low energy, inner- to mid-ramp restricted subtidal environments. This interpretation is based on the presence of bioturbation and its stratigraphic

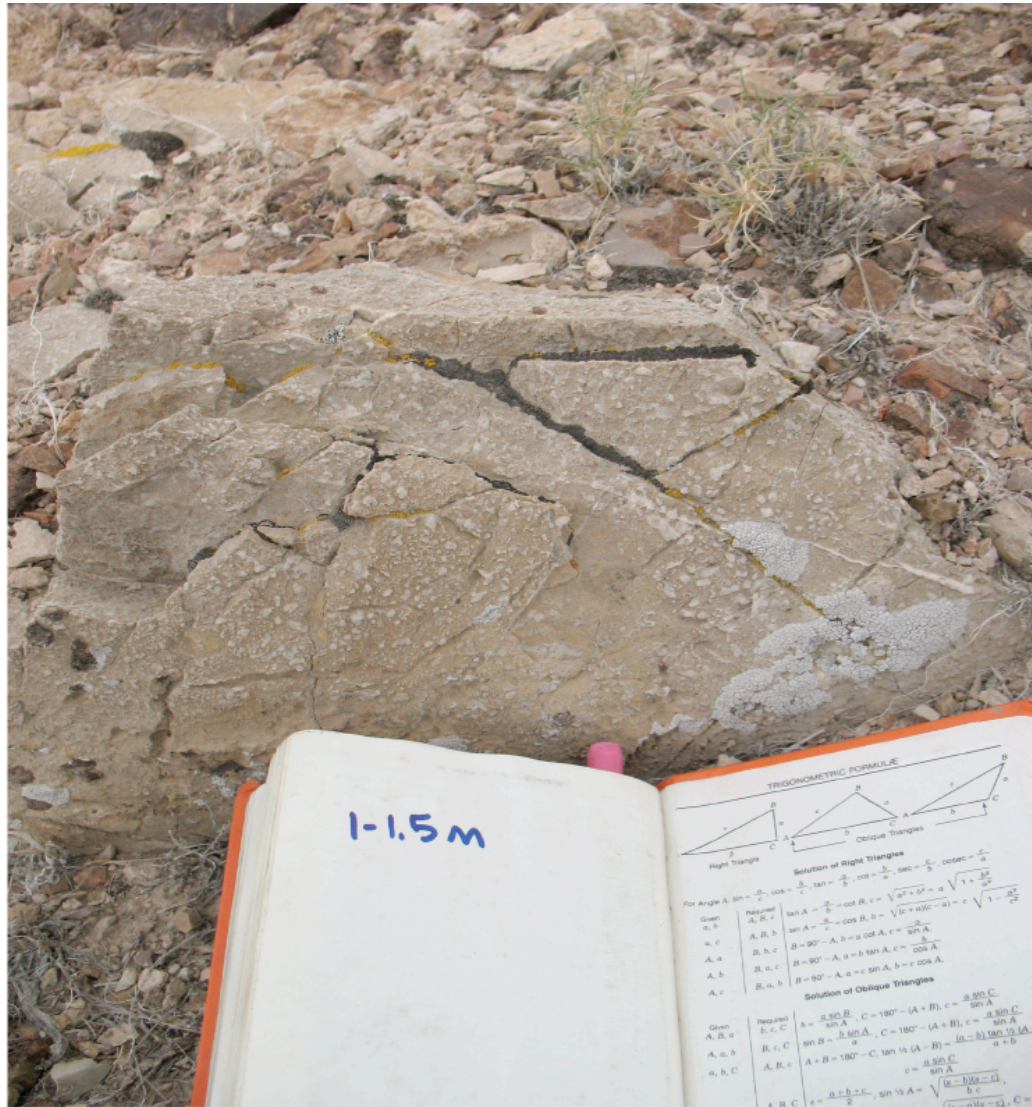


Figure 1.11: Field photograph of the vuggy (subtidal microbialite) lime mudstone subfacies. This subfacies is only present near the base of the Confusion Range Lower Thaynes Formation. Field book for scale.

relationship with other restricted shallow subtidal subfacies. Boyer et al. (2004) suggests that similar facies with monospecific taxa from other Lower Triassic deposits in western North America indicate a period of recovery. The whole, unabraded nature of the bivalves demonstrates that they were not extensively transported or reworked.

Shallow subtidal facies

Clast-supported chert-quartz pebble conglomerate:

The clast-supported chert conglomerate subfacies vary laterally in thickness from ~0-0.3 m at Cowboy Pass to ~0-1.5 m at Disappointment Hills (Collinson, 1976) and are interpreted to represent conglomerates shed off a local fault scarp related to the Sonoma Orogeny (Collinson, 1976) or transgressive lag conglomerates deposited during sea-level rise (Newell, 1973). These high energy events took place in the inner-ramp, shallow subtidal environments evidenced by poor sorting of the clasts indicating changes in depositional energies, marine fossil content in the matrix, lack of mud, and stratigraphic position within other shallow subtidal subfacies.

Micro-gastropod-skeletal packstone-grainstone:

The micro-gastropod-skeletal packstone-grainstone subfacies is ~6 m thick and was deposited in high energy, well-oxygenated, inner- to mid-ramp environments. This interpretation is based on poor sorting, cross bedding, abundant, abraded fossil content, and its stratigraphic relationship with both restricted shallow subtidal and deep subtidal facies. Like the echinoderm grainstone subfacies from the Weber Canyon section, this subfacies was deposited in a high energy environment that resulted in a sand bar or shoal.

Fraiser and Bottjer (2004) report that these gastropod species (ecological opportunists) could have occupied any of the ramp environments in other Lower Triassic stratigraphic units and, thus could have been transported here from inner to mid-ramp environments. The micro-gastropod-skeletal packstone subfacies is also documented in the time-equivalent, inner-ramp Sinbad Formation in eastern and southeastern Utah (Davidson, 1967; Fraiser and Bottjer, 2004; and Lucas et al., 2007) further suggesting that the fossils were likely transported from a shallower environment where they were living during times of maximum transgression.

Intermediate subtidal facies

Ammonoid-micro-gastropod wackestone:

The ammonoid-micro-gastropod wackestone subfacies (Figure 1.12) ranges in thickness from 0.1 to 0.5 m and was deposited in low-energy, mid- to outer-ramp environments. This interpretation is based on abundance of mud and sharp stratigraphic contacts with deep subtidal subfacies. The abraded nature of the ammonoids and gastropods suggests that they were not likely living in this environment and were instead transported here from the inner- to mid-ramp environments where they were likely living. In addition, Stephen et al. (2010) documented that the ammonoid shell sizes range from <1 cm to >30 cm; however, ammonitellas (embryonic and early juvenile phases) were not found suggesting that the ammonoids may have reproduced elsewhere. The ammonoid species documented here are *Meekoceras*, *Inyoites*, and *Anasibirites*, which span the entire Smithian (Brayard et al., 2009; Stephen et al., 2010)



Ammonoid-micro-gastropod wackestone

lime mudstone interbedded with light calcareous mushale

Figure 1.12: Field photograph of the maroon-colored, more resistant ammonoid-micro-gastropod wackestone subfacies, which occasionally caps the buff- to yellow-colored lime mudstone interbedded with light calcareous mushale subfacies. Spray paint container for scale.

Deep subtidal facies

Lime mudstone interbedded with light calcareous mudshale (rhythmites):

The lime mudstone interbedded with light calcareous mudshale subfacies (Figure 1.12) ranges in total thickness of ~0.5 to 15 m and represents the majority of the transgressive facies at the Confusion Range. It was deposited in low energy, poorly oxygenated, outer-ramp environments based on the fine-grain size, lack of current-generated sedimentary structures and bioturbation, rare to absent fossils, and its association with the deepest water subfacies. The meter-thick rhythmite intervals are occasionally capped by the Ammonoid-micro-gastropod wackestone-packstone subfacies (0.1 to 0.5 m thick). Similar to the Weber Canyon rhythmites subfacies, the rhythmic interbedding of 1-10 cm thick lime mudstone and mudshale was likely the result of periodic fluctuations in detrital carbonate influx and/or changes in siliciclastic fluvial influx into the marine basin (Elrick et al., 1991; Elrick and Hinnov, 1996; Elrick and Hinnov, 2007).

Light (yellow) calcareous clayshale:

The poorly exposed, light yellow calcareous clayshale subfacies is ~100 m thick, (Collinson, 1976; Hose and Repenning, 1959) and was deposited in low-energy, poorly oxygenated, outer-ramp environments. This interpretation is based on its fine-grain size, and lack of both bioturbation and fossils.

1.3.3 Guling, Himachal Pradesh, northern India

The main focus of the study was to understand the depositional facies relationships in the western United States; however, I also had the opportunity to participate in a research expedition to the Spiti Valley, Himachal Pradesh, northern India (Himalayas) and observe several well-exposed and biostratigraphically well-constrained Lower Triassic sections (Figure 1.13). In the Early Triassic, Northern India sat at ~40 °S paleolatitude in the southern neo-Tethys Sea (Ogg and von Rad 1994). The neo-Tethys Sea, which began to open in the Permian, contained many micro-continents and volcanic arcs and was surrounded on three sides by continents (Baud et al., 1984) (Figure 1.2).

The Mikin Formation was deposited on a passive margin in the southern neo-Tethys Sea during the Early Triassic (Baud et al., 1984). Subsidence of the passive margin in the mid- to late Triassic is likely related to the extensional tectonics that were involved in opening the neo-Tethys Sea (Baud et al., 1984). Uniformity within the Lilang Supergroup in the northern Indian Himalayas (Spiti Valley) suggests that the sediments were deposited on a homogenous epicontinental ramp with little variations in subsidence (Krystyn et al., 2004).

The marine Triassic in the Indian subcontinent is confined to the Himalayas and the Triassic sequence in the Spiti Valley, Himachal Pradesh is considered to have well developed biostratigraphy and stratigraphic continuity (Bhargava et al., 2004; Krystyn et al., 2004; 2007). Originally described by Hayden (1904), with recent updates in the



Figure 1.13: The Lower Triassic Smithian portion of the Mikin Formation in the town of Guling in Himachal Pradesh, northern India. It is bounded by a fault at the base and the Spathian Mikin Formation at the top. Packs for scale.

stratigraphy by Krystyn et al. (2004; 2007) puts the entire Lower Triassic within the Lilang Supergroup (up to 1250 m thick), Tamba Kurkur Group, Mikin Formation (~35 m) (Bhargava et al., 2004). The Mikin Formation is divided into four members: the Lower Limestone Member, the Limestone and Shale Member, the Niti (Nodular) Limestone, and the Himalayan Muschelkalk and is generally composed of concretionary, nodular limestone, cherty argillaceous, sporadic fine shale partings (Bhargava et al., 2004).

1.3.4 The Lilang Supergroup: Mikin Formation (Lower Triassic)

The Lilang Supergroup disconformably overlies on the Upper Permian Gungri Formation and conformably underlies the Lower Jurassic Kioto Group Tagling Formation (Bhargava, 2008). The Lilang Supergroup is subdivided into four groups and ten formations based on detailed ammonoid and, when available, conodont biostratigraphy (see Bhargava et al., 2004 and Krystyn et al., 2004; 2005 for full description). Of the ~1250 m of stratigraphy, the Lower Triassic and half of the Middle Triassic (Tamba Kurkur Group Mikin Formation) occupy ~35 m (Bhargava et al., 2004). The Lower Triassic Mikin Formation is subdivided into the Griesbachian Lower Limestone Member, the Dienerian and Smithian Limestone and Shale Member, and the Spathian Nodular (Niti) Limestone Member.

This study focuses on the Smithian portion of the Mikin Formation (~14 m thick) measured and described in the town of Guling (Appendix A). Five ammonoid zones, *Rohilites*, *Flemingites flemingianus*, *Meekoceras gracilitatis*, and *Wasatchites-Anasibirites*, and *Xenocelites*, and one conodont zone, *N. waageni*, define the Smithian

and are used for global sequence correlation (Carr and Paull, 1983; Carr, 1983; and Krystyn et al., 2007). Combining sequence stratigraphic methods with recent advances in ammonoid and conodont biostratigraphy (Krystyn et al., 2004; 2007; Galfetti et al., 2007, Brayard et al., 2009; Stephen et al., 2010) allows for the correlation of the western United States with the northern India Smithian sequence (Figure 1.15).

Smithian portion of the Mikin Formation at Guling, Himachal Pradesh

In Guling, Himachal Pradesh, northern India two facies (intermediate and deep subtidal) and six subfacies (*nodular skeletal wackestone, skeletal wackestone, skeletal mudstone, skeletal mudstone-wackestone with mudshale interbeds, dark mudshale interbedded with skeletal packstones, and dark mudshale*) are identified (Table 1.3; Figure 1.14).

The two intermediate subtidal subfacies are the *nodular skeletal wackestone* and the *skeletal wackestone subfacies*. The *nodular skeletal wackestone subfacies* ranges in thickness from ~0.5 to 1 m and was deposited under low energy, open marine, mid-ramp environments evidenced by its fine-grain size, nodular bedding, sparse fossil content, and association with other mid- and outer-ramp deposits (Figure 14.d). The *skeletal wackestone subfacies* ranges in thickness from 0.03 to 0.25 m and was deposited under low energy, moderately oxygenated, mid-ramp environments below fair weather wave base (Figure 14.c). This interpretation is based on its relationship with other deeper water facies (mudshale), occurrence of whole-fossil clasts, the shale interbeds, and the presence of bioturbation.

Guling, northern India		Mikin Formation		Table 3
Subfacies	Bedding	Skeletal Components	Sedimentary and biologic features	Environment of deposition
Nodular skeletal wackestone	Medium to thick (massive)	Abraded bivalves, gastropods, echinoderms, (conodonts)	Bioturbation	Intermediate subtidal, low energy, intermediate ramp between storm wave base and fair weather wave base
Skeletal wackestone	Thin to medium	unabraded ammonoids, sparse bivalves, gastropods, conodonts	Bioturbation	Intermediate subtidal, low energy, mid ramp between storm wave base and fair weather wave base
Skeletal mudstone	Medium	Sparse abraded bivalves, gastropods, echinoderms, (conodonts)	Bioturbation	Deep subtidal, low energy, outer ramp
Skeletal mudstone-wackestone with mudshale interbeds	Medium	Sparse to rare fragments of bivalves, echinoderms, (conodonts)	Bioturbation, shale partings	Deep subtidal, low energy, outer ramp
Dark mudshale interbedded with skeletal packstones	Thin	Shale: none Packstone: ammonoids, bivalves, gastropods, echinoderms (conodonts)	Graded layers, packstone lenses	Deep subtidal, outer ramp, above storm wave base
Dark mudshale	Thin	None observed	None observed	deepest subtidal, low energy, outer-ramp, below storm wave base

The four deep subtidal subfacies are *skeletal mudstone*, *skeletal mudstone-wackestone with mudshale interbeds*, *dark shale interbedded with skeletal packstones*, and *dark mudshale*. The *skeletal mudstone subfacies* (~1 m) subfacies was deposited in low energy, moderately oxygenated, outer-ramp environments evidenced by the occurrence of bioturbation, abundant mud, and sparse skeletal clasts (Figure 1.14a). The *skeletal wackestone with mudshale interbeds subfacies* ranges in thickness from 0.1 to 0.9 m and was deposited under low energy, poorly to moderately oxygenated, outer-ramp environments below fair weather wave base evidenced by the abundant shale partings, lack of bioturbation and sparse, abraded skeletal clasts, and its stratigraphic relationship with the deeper mudshale subfacies. The *dark mudshale interbedded with skeletal packstones subfacies* ranges in thickness from 0.05 to 2 m and was deposited above storm wave base in poorly oxygenated, outer-ramp environments (Figure 1.14b, c). This interpretation is based on the lack of fossils and sedimentary structures in the mudshale and the abraded, densely packed nature of the packstone lenses, and its facies relationship with the deepest water dark mudshale subfacies. The deepest subtidal *dark mudshale subfacies* (~1.5 m) was deposited under low energy, low oxygen outer-ramp environments below storm wave base evidenced by its fine-grain size, lack of fossils, bioturbation, and current-generated sedimentary structures, and its association with other interpreted deep subtidal subfacies.

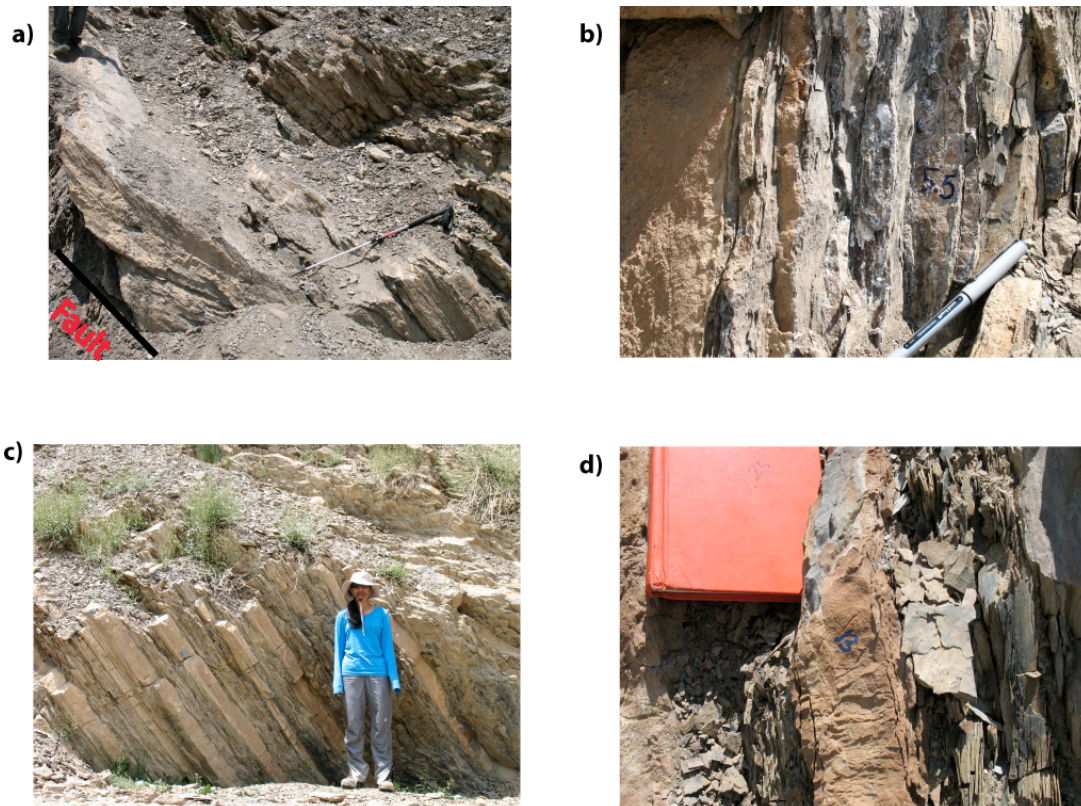


Figure 1.14: Field photographs from the Guling, northern India section. a) In Guling, the base of the Smithian Mikin (skeletal wackestone subfacies (buff colored)) sits on a fault. Hiking pole (~1 m) for scale. b) The dark skeletal mudstone-wackestone with mudshale interbeds subfacies (pen for scale). c) Skeletal wackestone subfacies (buff) and the dark mudshale interbedded with skeletal packstones subfacies (person (~1.5 m) for scale). d) The nodular skeletal wackestone at the top of the section and with the dark mudshale interbedded with skeletal packstones (field book for scale).

1.4 Sequence Stratigraphy

1.4.1 *Sequence Stratigraphy Terminology*

Sequence stratigraphy is the study of genetically related sedimentary facies within the framework of chronostratigraphically significant surfaces. The fundamental unit of sequence stratigraphy is the sequence, which is defined as a relatively conformable, genetically related succession of strata bounded by unconformities or their correlative conformities (Mitchum, 1977). Parasequences and parasequence sets are the building blocks of sequences. Parasequences (or cycles) are defined as a relatively conformable, genetically related succession of beds or bedsets bounded by marine-flooding surfaces or their correlative surfaces and parasequence sets are parasequences that form a distinctive stacking pattern often bounded by major marine flooding surfaces and their correlative surfaces (Van Wagoner, 1988). Parasequences usually mimic the overall trend of the sequence, but on a shorter time scale.

Concepts associated with sequence stratigraphy were originally outlined using seismic stratigraphy and were based upon the vertical and lateral relationships of observed stratal geometries (Vail et al., 1977) and later evolved to include well log and outcrop studies (e.g. Van Wagoner et al., 1988; 1990). Since lateral facies trends and stratal geometries cannot be directly observed in the three outcrop field sites due to lack of seismic data and extensive lateral exposure, the traditional definitions and sequence stratigraphic concepts will be de-emphasized. Instead, the vertical stacking patterns and relationships will be used to infer lateral facies (i.e. Walther's Law). The facies trends were used to infer depositional environments. The facies and associated subfacies were

ordered from shallowest to deepest (Tables 1-3). Based on the relative facies changes in the sections, a relative sea-level curve for each section was interpreted (Figure 1.15).

Systems tracts are defined as the linkage of contemporaneous depositional systems in a three-dimensional assemblage of lithofacies genetically linked by active (modern) or inferred (ancient) processes and environments (Fisher and McGowen, 1967; Brown and Fisher, 1977). The following will go through the original definitions of systems tracts, which will be used to describe and aid in the correlation of the three Smithian sections in the following sections. Once again, it is important to note that the descriptions used in this thesis will only loosely follow these definitions, as systems tracts terminology was intended to be used in cases extensive seismic data, lateral exposure, core and well logs.

The sequences are enveloped by sequence boundaries (SB), which are defined as significant erosional unconformities and their correlative conformities (Mitchum, 1977). These boundaries are the product of sea level falling faster than subsidence and sedimentation rate producing an unconformity or minimum accommodation (shallowest water sedimentation). The lowstand systems tract (LST) is the stratigraphically oldest systems tract and is represented by the sedimentary accumulation that straddles the lowest position of the relative sea level curve, often forming a prograding wedge at the base of a shelf margin (Van Wagoner, 1988). The transgressive systems tract (TST) follows the lowstand systems tract and is comprised of the deposits accumulated from the onset of the transgression until the time of maximum sea level rise rates (Van Wagoner, 1988). The TST represents a period of increasing accommodation space, which leads to a landward migration of facies and upward-deepening vertical facies patterns. The zone

that marks the time of maximum flooding or sea-level rise and separates the TST from the highstand systems tract (HST) is called the maximum flooding zone (MFZ) (Van Wagoner, 1988). The deposits that accumulate when sedimentation rates exceed accommodation rate increases constitute the HST (Van Wagoner et al., 1988; Jervey, 1988). The HST is characterized by shallowing-upward vertical stacking patterns.

1.4.2 Weber Canyon, northern Utah

The mixed carbonate-siliciclastic depositional sequence at Weber Canyon (~250 m) was measured and described on the north and south sides of the Weber River, adjacent to I-84 just west of Devil's Slide. The underlying sequence boundary (SB) is characterized by the shallowest portion of fine-grained continental to marginal marine siliciclastics of the Woodside Shale (Smith, 1969), which contains mudcracks and lacks marine fossils. These observations suggest subaerial exposure and although, no evidence of an erosional surface was documented at Weber Canyon, the Woodside shale is interpreted to be the units deposited during a time of minimum accommodation. The Permian (Phosphoria Formation) and Triassic (Thaynes Formation) marine deposits bracket the Woodside Shale (Smith, 1969).

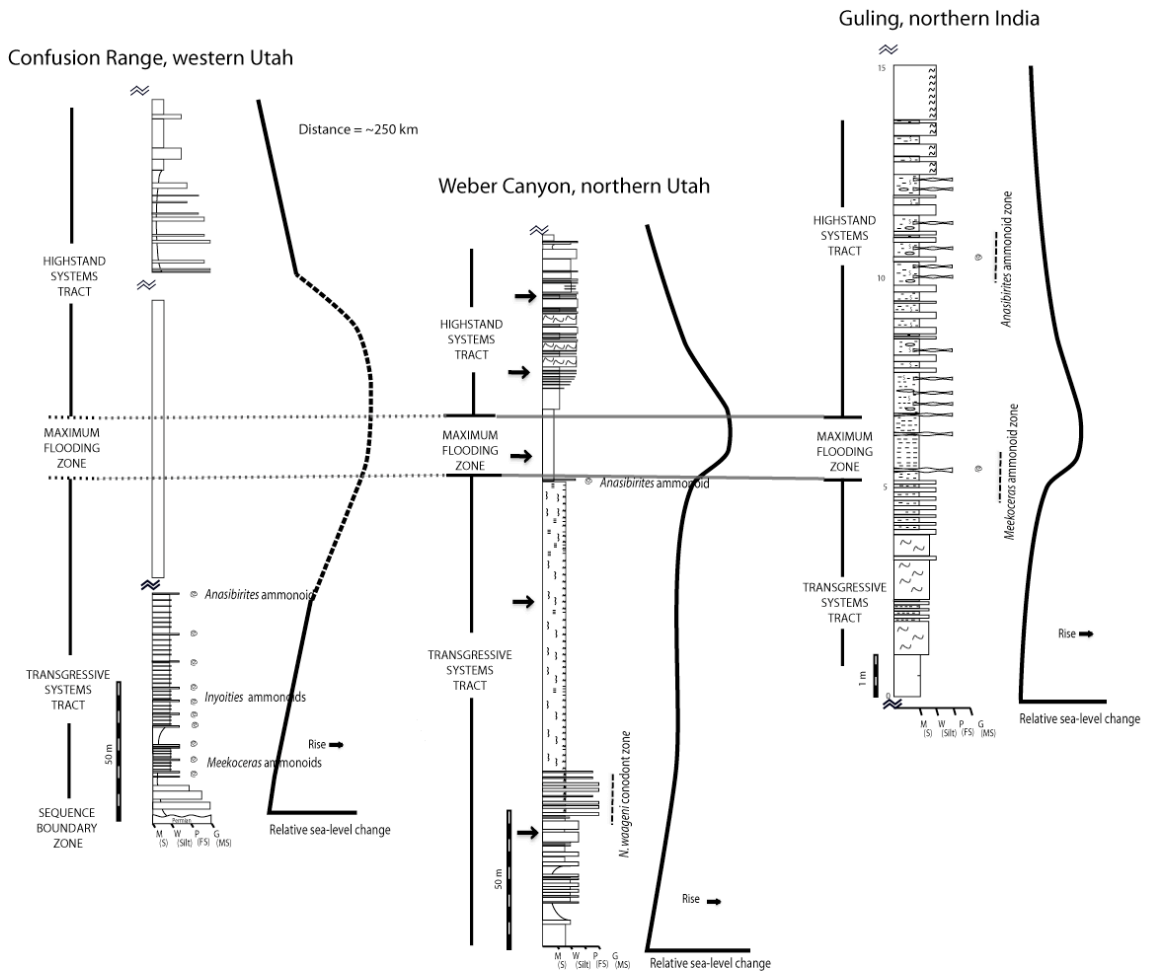


Figure 1.15: Smithian sequences from western North America (left and center; ~250 km apart) and northern India are correlated using sequence stratigraphy and biostratigraphy. The *Anasibirites* ammonoid zone has been identified by Stephen et al. (2010) for the Confusion Range section, Smith (1969) for the Weber Canyon section, and Krystyn (2004) for the Guling section. In addition, the *Meekoceras* ammonoid zone (Krystyn, 2004) is labeled for the Guling section and the *Neospathodus waageni* conodont zone (Beatty, personal communication) for the Weber Canyon section to further constrain these sections to roughly Smithian time. The arrows on the Weber Canyon section indicate where each of the sketches in figure 1.16 are interpreted from.

The overlying transgressive systems tract (TST; ~150 m) is characterized by upward-deepening subfacies trends, including the silty lime mudstone, the abraded bivalve wackestone-packstone, the echinoderm grainstone, the silty skeletal lime mudstone. Superimposed upon these upward-deepening facies trends are ~1 to 3 meter-thick upward shallowing cycles. Biostratigraphy, although limited, provides insight into the relative time of deposition of the Lower Thaynes Formation. Beatty (personal communication) reports mid- to late Smithian *N. waageni* conodonts in the TST (~45 m). At the top of the TST (~153 m) there is an occurrence of the late Smithian *Anasibirites* ammonoid zone is documented (Smith, 1969).

The MFZ is composed of deep subtidal, dark calcareous mudshale (~15 m). The Sinbad Formation of central and eastern Utah represents the maximum landward extent of the marine limestones into the Thaynes seaway and it also contains the *Anasibirites* ammonoid zone (Lucas et al., 2007), suggesting that this interval represents the maximum flooding (Figure 1.3).

Upward-shallowing trends of the HST (~75 m) are represented by the following subfacies: lime mudstones interbedded with silty dark mudshale, the bivalve wackestone, and the silty lime mudstone. Superimposed in this upward-shallowing succession, are ~1 to 4 meter-scale upward-shallowing cycles.

The overlying SB is represented by the Decker Tongue (~20 m), which is composed of red siltstones and shales, which are interpreted as continental to restricted peritidal environments evidenced by occasional mudcracks and a lack of marine fossils (Smith, 1969). The Decker Tongue is the diagnostic unit used to separate the marine Lower Thaynes Formation from the Upper Thaynes Formation (Spathian).

Depositional Model for the Weber Canyon Platform

The Weber Canyon section is used as an example of how the stacking pattern for a single outcrop allows for lateral paleoenvironmental interpretations to be made across a basin. According to Walther's Law, it is assumed that conformable vertically facies were deposited adjacent to one another in a basin. Using the four facies and seven subfacies defined above and their interpreted depositional environments to interpret relative (Figure 1.16).

Two of the three most prevalent and conformable subfacies at the base of the section, the silty lime mudstone and abraded bivalve wackestone-packstone are interpreted to have been deposited in a restricted shallow subtidal environment due to their relatively low energy, grain size, and abundance of mud. The third most abundant subfacies near the base is an echinoderm grainstone, which is interpreted to have been deposited in a high energy, open marine environment and is likely to have created a protective shoal barrier, so that the shallower facies listed above did not experience as much winnowing away of mud as would be expected for a typical shallow subtidal, open marine environment (Figure 1.16). Moving up section, the echinoderm grainstone is interbedded with a silty skeletal lime mudstone, which is interpreted as being deep subtidal based on the abundance of mud, parallel laminations, more abundant bioturbation at the base and increase in parallel laminations up section, indicating an overall decrease of oxygen and its relationship with the deepest subtidal facies, the dark calcareous mudshale up section. From these relationships, sea level is interpreted to be

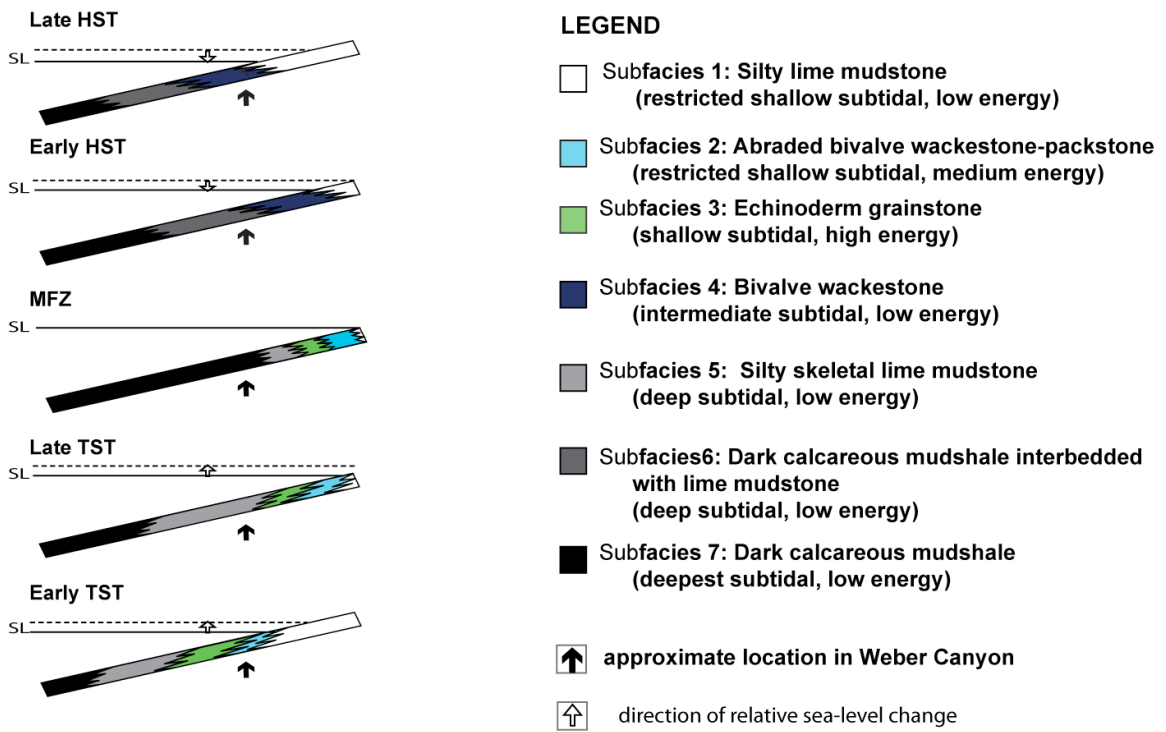


Figure 1.16: Platform depositional model for the Weber Canyon section from Early TST to Late HST. There are seven subfacies that make up the Weber Canyon described on the right. The solid arrow corresponds to the location of Weber Canyon during deposition. These arrows are also marked on the stratigraphic column in figure 1.15.

rising, characterized by deeper water facies are depositing on top of shallower water facies.

Above the silty skeletal lime mudstone subfacies is the deepest subtidal subfacies, the dark calcareous mudshale, which represents the deepest water facies. The dark calcareous mudshale grades into the dark calcareous mudshale with interbedded lime mudstone facies, which is interpreted to have been deposited in the second deepest subtidal environment. This interpretation is based on the increased number of lime mudstone beds up section that contain sparse fossils, which indicated an environment of increasing oxygen and subsequent life, yet remains in a relatively low energy environment. This subfacies is also interbedded further up section with an intermediate subtidal, bivalve wackestone. This indicates that sea level is likely falling and the oxygen-poor deep subtidal facies are moving basin ward.

Further up section, the bivalve wackestone is interbedded with the same restricted shallow subtidal, low energy, devoid of fossils facies found at the base, which was interpreted to be the shallowest facies of the sequence. From these vertical relationships and some knowledge of other sections in the basin, it is evident that the Smithian at Weber Canyon represents a full sea-level transgression and regression (Figure 1.16).

1.4.3 Confusion Range, western Utah

The composite depositional sequence in the Confusion Range was measure and described at Cowboy Pass and Disappointment Hills, which are separated by ~16 km. Its total thickness (~240 m) is estimated from outcrop descriptions in this study combined with previous studies (Hose and Repenning, 1959; Collinson, 1976). The underlying SB

is represented by the unconformity between the Upper Permian Gerster Formation and the quartz-chert pebble conglomerate lying at the base of the Lower Thaynes Formation. Development of this unconformity has been attributed to uplift and subsequent erosion related to the Sonoma Orogeny (Collinson, 1976) or a drop in relative sea level (Newell, 1973). In either interpretation, at ~1 My of time is lost based on the fact that there have been no Griesbachian or Dienerian index fossils identified above the Permian Gerster Formation. The first diagnostic fossil occur ~10 m above the unconformity and include lower Smithian *Meekoceras* ammonoid fossils (Stephen et al., 2010). Chemostratigraphy ($\delta^{13}\text{C}$), which is a tool used to correlate stratigraphic sections throughout the Phanerozoic, further supports that the Griesbachian and Dienerian stages are likely missing (Atudorei et al., 2007).

Deepening-upward characteristics of the overlying TST (~60 m) are characterized by the following subfacies: the clast-supported chert-quartz conglomerate, the vuggy (subtidal microbialite) lime mudstone-wackestone, the micro-gastropod-skeletal packstone-grainstone, the lime mudstone interbedded with calcareous mudshale rhythmites, and the ammonoid-micro-gastropod wackestone. Smithian ages for the TST are provided by the *Meekoceras*, *Inyoites*, and *Anasibirites* ammonoid zones located in the ammonoid wackestone subfacies (Brayard et al., 2009; Stephen et al., 2010; Jenks, personal communication).

The MFZ is recognized by poorly exposed deep subtidal light (yellow) calcareous clayshale (~100 m thick) (Hose and Repenning; 1959). There have been no diagnostic fossils recorded in this stratigraphic unit; however, the first *Anasibirites* ammonoids are

recognized in the last recorded ammonoid-mirco-gastropod wackestone layer before the shale (Guex et al., 2010).

Upward-shallowing trends of the HST (~60 m) are represented by the bivalve wackestone subfacies overlain by the red silty limestone subfacies. Although there have been no age-diagnostic fossils identified, the first Spathian ammonoid bed is well above the marginal marine to continental red beds, which I interpret as the SBZ.

Marginal marine to continental red sandstones and shales of the Moenkopi Group (~75 m thick) define the upper SBZ (Guex et al., 2010). This unit is defined as the SBZ because it contains the shallowest marine deposits. This unit separates the marine Lower Thaynes Formation from the marine Upper Thaynes Formation (Spathian).

1.4.4 Guling, Himachal Pradesh, northern India

In northern India (Guling, Himachal Pradesh), the Smithian My-scale sequence (~14 m) is composed of mixed carbonate and siliciclastic TST (~5.5 m), siliciclastic dominant MFZ (~2 m), and a mixed carbonate and siliciclastic HST (~6.5 m) and was measured and described in the village of Guling, Himachal Pradesh (Appendix A). The underlying sequence boundary was not observed due to faulting, but at the Mud section ~10 km away it was characterized by nodular limestone subfacies (Krystyn et al., 2004), which represents the shallowest water facies for the Smithian and contains the *Flemingites* ammonoid zone (Krystyn et al., 2004; Galfetti et al., 2007). The upward deepening facies of the TST are characterized by nodular limestone and skeletal wackestone subfacies, overlain by dark shale. The *Meekoceras* ammonoid zone is found at the top of the TST. The maximum flooding zone is defined by the deepest water facies

and is composed of the deep subtidal (dark calcareous mudshales) (~1 m). The maximum flooding zone is above the *Meekoceras* ammonoid zone and below the *Anasibirites* ammonoid zone (Krystyn, 2004).

The upward shallowing facies trends of the highstand systems tract (HST) are characterized dark shale with abundant storm beds interbedded with skeletal wackestones and overlain by nodular limestone (~10 m). Twelve upward shallowing subtidal cycles occur in the HST characterized by dark shale with abundant storm beds (0.15 to 0.5 m thick) overlain by skeletal wackestone (0.08 to 0.3 m thick). Unlike Weber Canyon, the *Anasibirites* ammonoid zone is identified above the MFZ in the HST (Krystyn et al., 2004). Evidence of minimum accommodation (SB) is characterized by the nodular skeletal wackestone (Krystyn et al., 2004).

1.5 Global Correlation

Three Lower Triassic My-scale transgressive-regressive sequences are documented in the western United States (Embry et al., 1987; Paull and Paull, 1984), northern India (Embry, 1997; Krystyn et al., 2004), the Canadian Arctic (Haq, et al., 1987; Embry, 1997), northern Germany (Aigner and Bachmann, 1992; Embry, 1997), the northern Italian Alps (De Zanche et al., 1993; Ruffer and Zuhlke, 1995; Embry, 1997), Svalbard-Barents Shelf (northern Norway) (Van Veen et al., 1992; Embry, 1997), and eastern Siberia (Mørk et al., 1994; Embry, 1997). If these sequences can be correlated using biostratigraphy, then the sea-level changes generating the sequences could be eustatic in origin.

The Weber Canyon and Confusion Range are ~250 km away from each other and were deposited in the same basin. The TST for each section is confirmed to be Lower Thaynes based on existing ammonoid and conodont biostratigraphy (Stephen et al., 2010, etc.). For both locations, an occurrence of the Anasiberites ammonoid zone is directly below the MFZ. Further on shore, Anasirites is also documented in the Sinbad Formation, which is interpreted as the maximum extent of the Smithian transgression (Lucas et al., 2007). The sequence stratigraphic interpretation is based on the MFZ in Figure 1.15.

The TST at Weber Canyon has no known documentation of early Triassic biostratigraphy, which suggests that the conodonts and ammonoids were not living in this region during the early Triassic or that there is potentially time missing from the base of the WC section. The first identified age-diagnostic fossils are Middle to Upper Smithian in age and are located in the middle of the TST (*N. waageni* conodonts) and the top of the TST (*Anasiberites*). Since there is no known evidence of erosion, it is unlikely that there is missing time in the WC section. Instead, the water conditions (water depth, temperature, salinity, dissolved oxygen, etc.) were probably not favorable for the conodonts and ammonoids during the early Smithian.

The CR section, on the other hand, does have documentation of early, middle, and late Smithian ammonoids in the TST, suggesting that there is little Smithian time missing; however, it is likely that the G/D deposits were eroded away, since the Lower Thaynes Formation sits on top of the Permian Gerster Formation. Although, there are no age-diagnostic fossils in the HST, the first occurrence of an early Spathian Ammonoid (*Tirolites*) is stratigraphically above the interpreted SB. With

this in mind, it is likely that the HST is wholly or partially within the Upper Smithian, however, more data would be necessary to confirm this.

In the summer of 2009, I had the opportunity to measure and describe the Smithian section in Guling, India while on a research expedition with the intention of attempting a global correlation of the Smithian using the biostratigraphy outlined in Kristen et al. (2004; 2007). The Smithian portion of the Mikin Formation (~14 m) is much thinner than the Smithian of the western United States (~240 m) due to lower subsidence and sedimentation rates. The ammonoid and conodont biostratigraphy for the Guling, India section suggests that the entire transgressive-regressive sequence is within the Smithian.

The major difference between northern India and the western United States is that the Anasiberites ammonoid zone is located in the HST, rather than the TST and MFZ. Several scenarios could explain this. One situation is that the sea-level change, if in fact eustatic, did not happen all at once in the Smithian and, perhaps happened sooner in the Tethys Sea, which would mean that the sea-level change may not have been eustatic. Another solution is that the Anasiberites does continue through the interpreted HST for the western United States; however, there could be a preservation problem or the ocean conditions in the Panthalassa at that location were not conducive for the ammonoids to live there at that time. In either case, a more detailed study of the entire Lower Triassic is necessary to fully understand the global extent of the three transgressive-regressive sequences, which is beyond the scope of this thesis.

1.6 Conclusions

1. The Lower Triassic (Smithian) Lower Thaynes Formation in northern (Weber Canyon; ~250 m) and western (Confusion Range; ~240 m), Utah is composed of seven and eight subfacies, respectively. These subfacies can be grouped into four depositional facies representing restricted shallow subtidal, shallow subtidal, intermediate subtidal, and deep subtidal environments.

2. The Woodside Shale (marginal marine to continental) and the Decker Tongue (marginal marine) brackets the sequence at Weber Canyon. Mid- to late Smithian *N. waageni* conodont horizons occur within the TST and the Late Smithian *Anasibirites* ammonoid horizon at the top of the TST, which help to constrain the age of the sequence. The first Spathian (*Tirolites*) ammonoid horizon is found above the Decker Tongue.

3. An unconformity and conglomerate at the base of the Confusion Range section indicates that the section was subaerially exposed with at least 1 My of time missing between the Permian and Early Triassic. A very shallow marine red silty lime mudstone unit overlies the Lower Thaynes Formation at the Confusion Range. Early (*Meekoceras* and *Inyoites*) and Late (*Anasibirites*) ammonoid horizons have been identified in the TST. The first Spathian-diagnostic ammonoid horizon (*Tirolites*) is found above the restricted shallow marine red silty lime mudstone subfacies.

4. The Lower Triassic Smithian portion of the Mikin Formation (~14 m thick) in Guling, Himachal Pradesh, northern India is composed of two depositional facies and six subfacies that are grouped into representing intermediate and deep subtidal environments. Ammonoid biostratigraphy suggests that the entire transgressive-regressive sequence is within the Smithian. Unlike the western United States, the *Anasibirites* ammonoid zone is not found below the MFZ.

5. Using the maximum flooding zones defined for both the Confusion Range and Weber Canyon sections, as well as ammonoid and conodont biostratigraphy, it appears as though the two sections are roughly time equivalent.

6. The correlation between the two sections in the western United States was based on the maximum flooding zone and further constrained using the *Anasibirites* ammonoids and extended to the other side of the globe to a roughly time-equivalent India section based on the maximum flooding zone and ammonoid and conodont biostratigraphy. This correlation suggests that there could be a roughly time equivalent sea-level change between the three locations.

Chapter 2: Understanding the Early Triassic Climate using $\delta^{18}\text{O}$ of conodont apatite

Abstract

Samples were collected for oxygen isotopic analyses of conodont apatite from the two field locations (western North America) in a sequence stratigraphic framework to better understand the Smithian paleoclimate. Due to the an up to ~ 1.5 ‰ disparity of values between to two locations, additional samples were collected from Guling, northern India, the Sverdrup Basin in the Canadian Arctic, Wapiti Lake area in eastern British Columbia, Canada, and Bear Lake, southern Idaho. Conodont Alteration Index or CAI (a measure of thermal alteration based on color) was estimated for each of the locations listed above and range from 1.5 for Wapiti Lake, British Columbia and the Confusion Range to 5 for Guling, India. In addition, SEM images were taken to identify potential physical alteration of the conodonts for the Confusion Range (smooth surface with no signs of alteration), Weber Canyon (pitted surface with signs of potential alteration), and Guling (visibly the most pitted surface with signs of potential dissolution of the apatite).

The $\delta^{18}\text{O}$ values for the Weber Canyon range from ~ 14.4 to 15.8 ‰, Confusion Range range from ~ 16 to 16.9 ‰, Guling range from ~ 15.8 to 16.5 ‰, Wapiti Lake range from ~ 17.2 and 17.6 ‰, Sverdrup Basin range from ~ 14.5 and 14.8 ‰, and the Bear Lake value was ~ 16.5 ‰. Conodonts with a CAI of 3 or lower produced $\delta^{18}\text{O}$ values that most likely reflect the primary Smithian ocean isotopic values. From these values, the isotopic difference between tropical and subtropical latitudes is ~ 1 ‰. Assuming an ice-free ocean value of -1 ‰, sea-surface temperatures were calculated as 35 to 38 °C for the tropical and 32 to 34 °C for the subtropical regions. Both of these temperatures

indicate that the Smithian sea-surface temperatures were significantly warmer than the present ocean, and instead, most resemble the intense greenhouse sea-surface temperatures calculated for mid- to Late Cretaceous.

2.1 Introduction

Despite the range of multi-disciplinary research conducted to understand the potential causes and the recovery patterns of the Permo-Triassic extinction, little work has focused on establishing a detailed climate record during the ~5 My recovery interval after the extinction. Previous Early Triassic studies focus on the biotic recovery (Erwin 1996; Erwin 1996; Erwin and Hua-Zhang 1996; Hallam and Wignall 1997; Payne, Lehrmann et al. 2004; Payne, Lehrmann et al. 2004; Guex et al., 2010) and many of these studies cite climatic changes as a potential cause of the extinction and delayed biotic recovery; however, to date few studies have utilized $\delta^{18}\text{O}$ as a proxy for paleoenvironmental changes in this time interval.

$\delta^{18}\text{O}$ studies of marine minerals provide detailed insight into paleoclimate and paleoenvironmental studies including changes in ice volume, temperature, and seawater $\delta^{18}\text{O}$ composition (Urey et al., 1951; Longinelli, 1966; Kolodny et al., 1983; Luz et al., 1984; Kolodny and Luz 1991). $\delta^{18}\text{O}$ studies using biogenic phosphates are preferred over calcite because they are less prone to diagenetic alteration and non-equilibrium oxygen isotope fractionation has not been observed during biogenic apatite precipitation. Even though it is generally accepted that apatite is a good proxy for paleoclimate, there few published reports of how diagenesis affects primary isotopic values. The purpose of this

study is to 1) report the results from $\delta^{18}\text{O}$ apatite studies of Early Triassic (Smithian) marine successions in western North American and northern India, and 2) evaluate the reliability of conodont apatite $\delta^{18}\text{O}$ values in deep time (pre-Cenozoic) paleoclimate studies.

2.2 Geologic Background

Early Triassic paleogeography is dominated by the Pangaeian supercontinent, which extended from $\sim 85^\circ\text{N}$ to 90°S and the globally extensive Panthalassa Ocean with its subtropical paleo-Tethys seaway extending into eastern Pangaea (Figure 2.1) (Ziegler et al., 1983; Blakey, 2010; Scotese, 2010). This study focuses on stratigraphic sections from the inland seaway in tropical, subtropical, and mid-latitudes along the western margin of Pangaea (western North America) and a southern subtropical passive margin within the southern Tethys Ocean on the eastern side of Pangaea (India) (Dubiel, 1994; Blakey, 2010; Scotese, 2010) (Figure 2.1). The locations for this study include Weber Canyon (northern Utah), Confusion Range (western Utah), Guling, Himachal Pradesh (northern Indian Himalayas), Wapiti Lake area (northeastern British Columbia, Canada), and the Sverdrup Basin (Canadian Arctic).

2.3 Early Triassic Climate

Previous studies of the Late Permian to Early Triassic suggest that the climate was uniformly warm with ice-free poles (e.g., Dickins, 1993, Frakes and Francis, 1988;

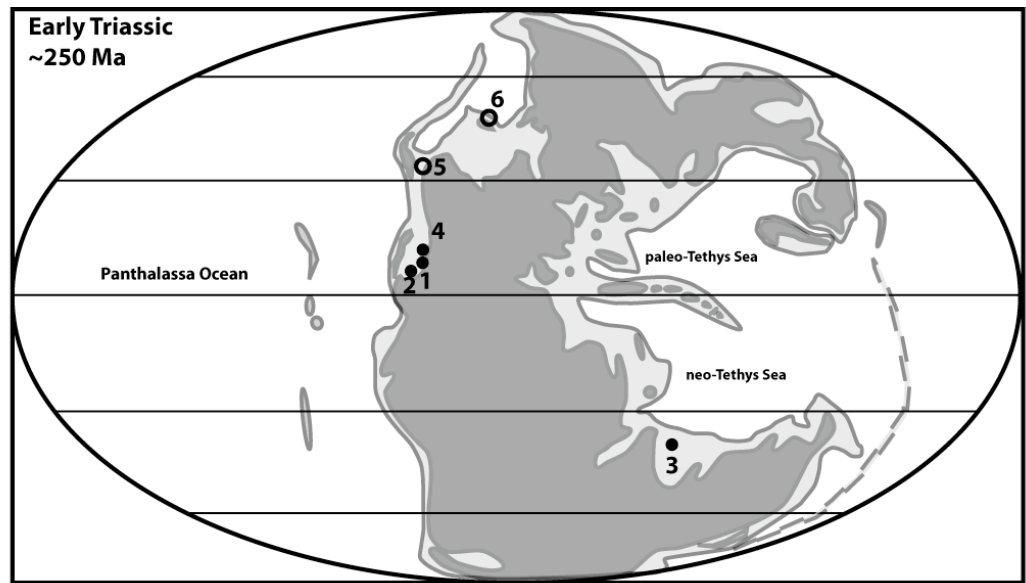


Figure 2.1: The supercontinent of Pangaea is fully assembled with the Panthalassa Ocean surrounding the eastern margin and the paleo- and neo-Tethys Seas bordering the eastern margin. Exposed land masses are dark gray and submerged continental platforms are light gray. Sites 1 and 2 are Weber Canyon, northern Utah and Confusion Range, western Utah, respectively, and were deposited in an intercratonic basin separated from the open Panthalassa Ocean by a volcanic arc. Site 3 is Guling, northern India deposited on a passive margin dips to the north towards the neo-Tethys Sea. Site 4 is Bear Lake, southern Idaho, site 5 is Wapiti Lake, northeastern British Columbia, and site 6 is the Sverdrup Basin, Canadian Arctic. Closed circles represent locations where I collected the samples and open circles are samples that were collected by Dr. Mike Orchard from the Canadian Geological Survey (modified from Blakey, 2010 and Scotese, 2010).

Frakes, 1992; Spalletti et al., 2003). Evidence for this climate include: increased weathering rates determined from high latitude paleosols (Retallack, 1999; Michaelsen and Henderson, 2000), the migration of typically warm-water and warm-temperature flora and fauna to higher latitudes, such as calcareous algae in the Svalbard Basin (Wignall et al., 1998) and the appearance of cycads in Greenland (Looy et al., 2001). Particular ammonoid species have been found from tropical through mid-latitudes indicating only minor seawater temperature gradients (Brayard et al., 2006). No Early Triassic glacial deposits have been discovered suggesting polar to high-latitude regions did not have permanent ice or that the glacial deposits were not preserved (Frakes et al., 1992).

Several major negative shifts in $\delta^{13}\text{C}$ of up to 6 ‰ at the Permian-Triassic boundary and in the Early Triassic indicate major changes in the global carbon budget (Holser and Magaritz, 1987; Payne et al., 2004). The negative shifts are attributed to the release of methane gas hydrates and subsequent rapid oxidation of methane to CO_2 (Hallam and Wignall 1997). The increase in CH_4 and CO_2 , increases the greenhouse affect and warms the climate (Berner, 1999; 2002).

In addition to geologic evidence of a globally warm climate, discussed above, general climate models across the Permo-Triassic boundary (Kidder and Worsley 2004) Kiehl and Shields, 2005), and geochemical modeling (Berner et al., 2002) suggests increase in the temperature at the boundary of 6-8 °C (Royer et al., 2004). This increase comes from an intensified greenhouse effect related to greenhouse gases in the atmosphere. Berner's (2002) pCO_2 models were conducted at 10 My time steps, which cannot detect shorter-scale climatic events and variability. In fact, the data available for

determining the Early Triassic paleoclimate is not abundant nor is it available for time scales of < 1 My. Even though there is abundant evidence to suggest that the Early Triassic was warm, Jefferson and Taylor (1983), Payne et al. (2004), Brayard et al. (2006), Preto et al., (2010) suggest that the climate was quite variable and much more complex than originally thought.

2.4 $\delta^{18}\text{O}$ paleoclimate studies

Oxygen exists as three isotopes: ^{16}O , ^{17}O , and ^{18}O with relative abundances of 99.759 %, 0.037%, and 0.204%, respectively. Urey et al. (1951) pioneered the research efforts to fully understand the potential for oxygen isotopes to be applied as a paleothermometer. This is possible because $^{18}\text{O}/^{16}\text{O}$ of calcite is dependent on a limited number of parameters: temperature and the composition of the ocean. $\delta^{18}\text{O}$, defined as:

$$\delta^{18}\text{O} = \left(\frac{\left(\frac{^{18}\text{O}}{^{16}\text{O}} \right)_{\text{sample}}}{\left(\frac{^{18}\text{O}}{^{16}\text{O}} \right)_{\text{standard}}} - 1 \right) * 1000 \text{ ‰}$$

and can be measured in minerals containing oxygen, such as CaPO_4 , H_2O , CaCO_3 (Craig, 1965). Emiliani (1955) was the first to apply this method of measurement and interpretation of the isotopic composition of oxygen to modern and ancient foraminifera, which set the stage for high-resolution paleoclimate studies.

One potential problem with using calcite is its susceptibility to diagenetic alteration in rocks older than the Late Mesozoic. Oxygen isotopic values in carbonates

can be altered during diagenesis by the addition of carbonate cement and the dissolution and re-precipitation processes. Early studies indicate that PO_4^{3-} does not exchange oxygen with water during inorganic reactions (Tudge, 1960) and from there, later researchers began to test this method on fish bone apatite (Kolodny et al., 1983), phosphorite rocks (Shemesh et al., 1988), and conodonts (Luz et al. 1984) Conodonts are composed of carbonate fluorapatite and its composition is approximated by $\text{Ca}_5\text{Na}_{0.14}(\text{PO}_4)_{3.01}(\text{CO}_3)_{0.016}\text{F}_{0.73}(\text{H}_2\text{O})_{0.85}$ (Pietzner et al, 1968). Oxygen occurs in the apatite lattices in at least three sites; however, the method that we use isolates the PO_4^{3-} group. Because apatite is less susceptible to diagenetic alteration than calcite, it is more likely to reflect the original temperature and composition of the ocean (Luz et al., 1984; Sharp et al., 2000). In addition, conodont apatite has been shown to produce reasonable paleotemperature estimates for the Silurian (Wenzel et al., 2000), Pennsylvanian (Joachimski, 2006) and Devonian (Joachimski et al., 2002; 2004; 2009; Elrick et al., 2009); therefore, we utilize conodonts as a proxy for deep-time paleoclimate reconstructions, much like foraminifera in the Cenozoic.

2.5 Methods

Three Early Triassic (Smithian) marine stratigraphic sections were measured and described (Chapter 1). Samples for $\delta^{18}\text{O}$ analysis of conodont apatite were collected every 0.5 to 10 m from Weber Canyon and Confusion Range. Additional Smithian conodonts were obtained from Bear Lake, southern Idaho and from Wapiti Lake, northeastern British Columbia, the Sverdrup Basin in the Canadian Arctic (Canadian

samples were obtained from Dr. Mike Orchard at the Canadian Geological Survey), and Guling, northern India.

Bulk rock samples weighing between 10-25 kg were collected for each conodont sample. Samples were processed using standard preparation methods (Harris and Sweet, 1989); a density separation was performed using lithium metatungstate (LMT), and conodonts were handpicked under a binocular microscope. Conodont alteration index (CAI) values were estimated in order to determine the degree of thermal alteration based on the study by Epstein (1977). Representative examples were also mounted and imaged with a scanning electron microscope (SEM).

Conodont elements (0.3-1.2 mg) were converted to Ag_3PO_4 using a modified version of the methods described by O'Neil et al. (1994) and Bassett et al. (2007). The $\delta^{18}\text{O}$ values were measured by reducing the Ag_3PO_4 to CO in a high-temperature conversion-elemental analyzer (TC/EA) connected to a Finnigan Mat 253 at the University of New Mexico, Albuquerque, New Mexico and New Mexico Tech, Socorro, New Mexico. Samples were run in duplicate, triplicate and occasionally quadruplicate to ensure reproducibility. All $\delta^{18}\text{O}$ values were reported in ‰ relative to SMOW. The overall reproducibility was detected by replicate analyses of internal standards with an uncertainty of < 0.35 ‰ (1σ). The samples were normalized to the Tu-1 standard with a value of 21.11 ‰.

2.6 Results

2.6.1 CAI and SEM images of conodonts

Epstein (1977) developed the conodont alteration index (CAI), which measures the thermal alteration of the conodonts on a scale of increasing alteration from 1 to 8 based on the color of the conodont. Corresponding temperatures range from $< 50\text{ }^{\circ}\text{C}$ for a CAI of 1 to $> 300\text{ }^{\circ}\text{C}$ for a CAI of 5. The CAI estimates for each of the sections are shown in Table 2.1 and range from 1.5 to 4. SEM images of conodonts show varying

Location	CAI	Estimated temperature of alteration $^{\circ}\text{C}$
Confusion Range, western Utah	1.5	50-90 $^{\circ}\text{C}$
Wapiti Lake, eastern British Columbia (Canada)	1.5	50-90 $^{\circ}\text{C}$
Bear Lake, southern Idaho	3	60-140 $^{\circ}\text{C}$
Weber Canyon, northern Utah	4	190-300 $^{\circ}\text{C}$
Sverdrup Basin, Canadian Arctic	4	190-300 $^{\circ}\text{C}$
Guling, Himachel Pradesh, northern India (Himalayas)	5	$>300\text{ }^{\circ}\text{C}$

Table 2.1

degrees of physical alterations (Figure 2.2). Conodonts with a CAI of ≤ 2 have a smooth and vitreous surface, whereas conodonts with a CAI of ≥ 3 become increasingly more pitted and rough on the outer surfaces and on fractured surfaces.

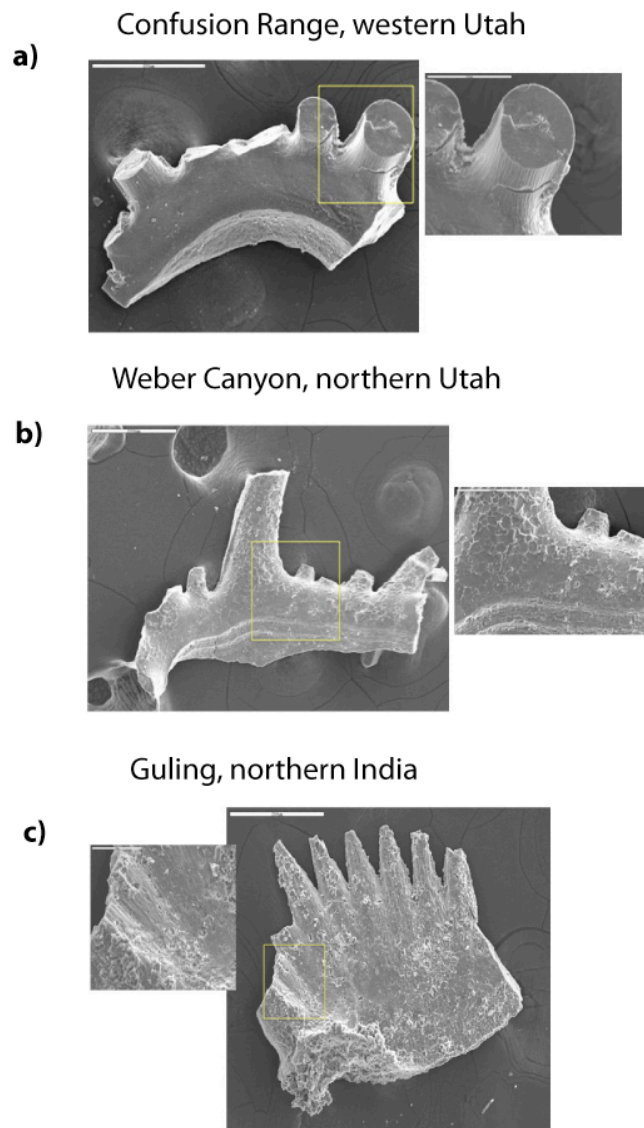


Figure 2.2: SEM images of typical conodont elements from a) the Confusion Range, western Utah, b) Weber Canyon, northern Utah, and c) Guling sections, northern India. Note the change in physical appearance of the elements, in particular, the Confusion range element is smooth, whereas the Weber Canyon and Guling elements are rough with possible evidence of dissolution.

2.6.2 $\delta^{18}\text{O}$ values

The measured $\delta^{18}\text{O}$ values range from 14.4 to 15.8 ‰ for Weber Canyon, from 16 to 16.9 ‰ for the Confusion Range, and 15.8 to 16.5 ‰ for Guling (Appendix B). The single Bear Lake sample has a value of 16.5 ‰ and two samples from Wapiti Lake have values of 17.2 and 17.6 ‰ and two samples from the Sverdrup Basin have values of 14.5 and 14.8 ‰ (Figure 2.3; Appendix B). When isotopic values are compared to the sequence stratigraphy at Weber Canyon or the Confusion Range, there are no systematic correlation, which would indicate a relationship between relative sea-level change and isotopic changes (Figure 2.4). Figure 2.6 illustrates the relationship between CAI and $\delta^{18}\text{O}$ values. With the exception of the two India samples, the observed trends show higher $\delta^{18}\text{O}$ values correspond to lower CAI values. This will be discussed further in the next section.

2.7 Discussion

2.7.1 $\delta^{18}\text{O}$ values

The measured Smithian $\delta^{18}\text{O}$ values range from ~14.4 to 17.6 ‰ across the western United States, the Canadian Arctic, and India. Of particular interest is that average $\delta^{18}\text{O}$ values between the two coeval Utah successions (Weber Canyon and the Confusion Range) record differences of up to 1.5 ‰ (Figure 2.3 and 2.4; Appendix B). This suggests that the seawater $\delta^{18}\text{O}$ values or seawater temperatures between the two localities, which

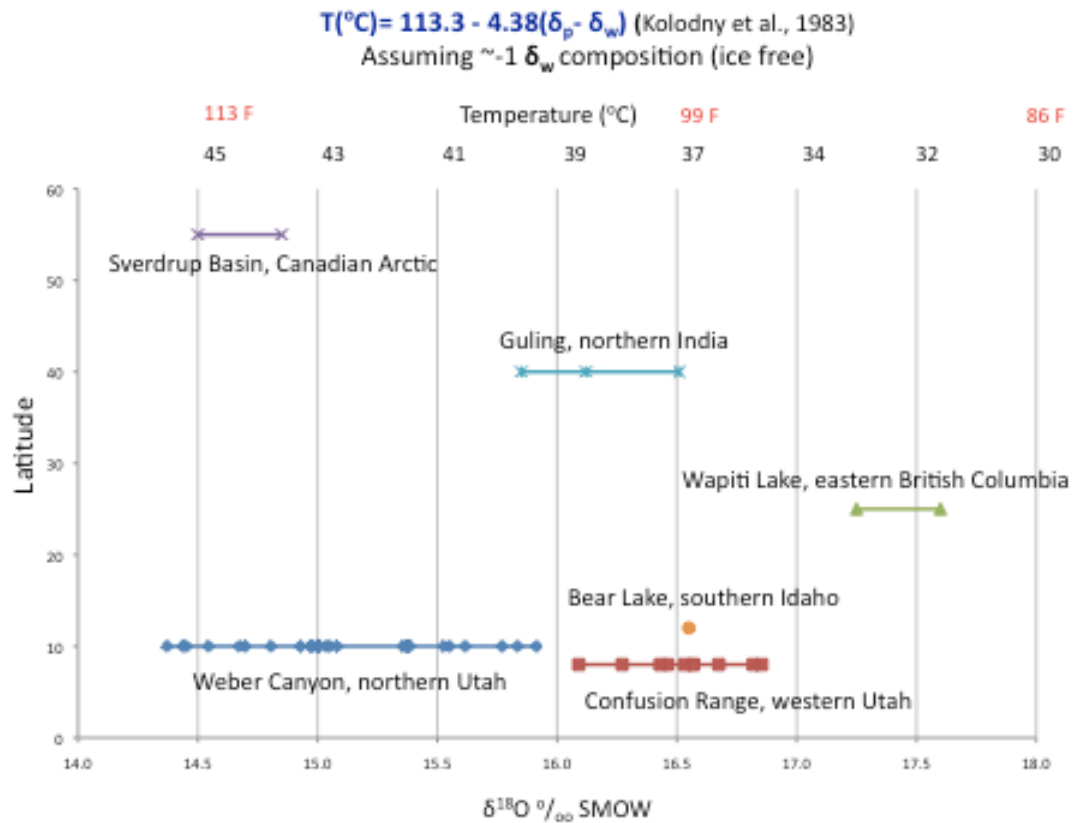


Figure 2.3: Averaged oxygen isotope measurements for the six sample locations arranged by paleolatitude. Approximate temperature calculations based on the Kolodny et al. (1983) equation are recorded on the top of the graph.

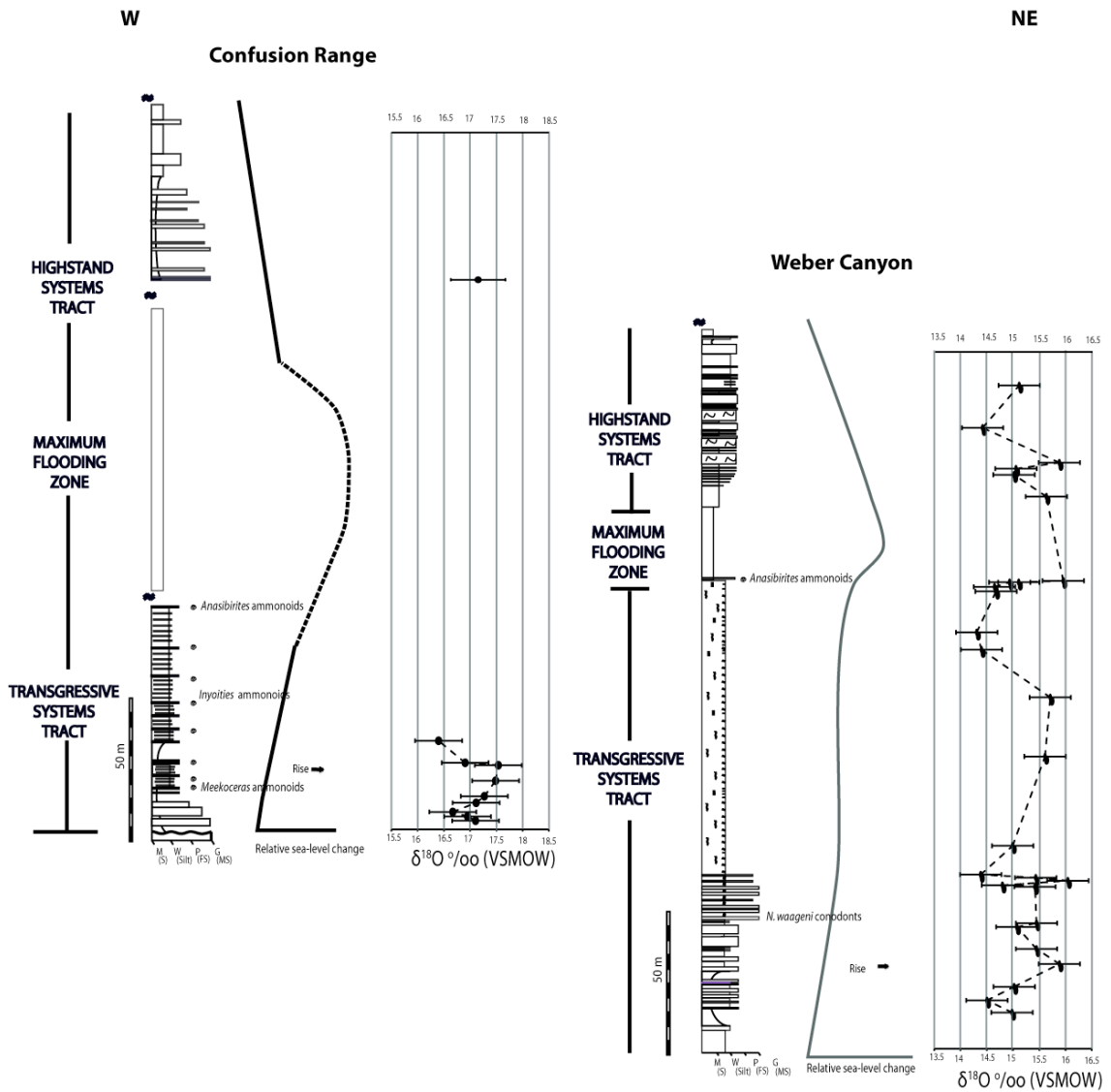


Figure 2.4: Oxygen isotopic values from the Confusion Range and Weber Canyon compared to measured and described stratigraphy. There are no apparent trends between the oxygen isotopes and the stratigraphy. In addition, there is an up to 1.5 per mil difference between the two locations. An interpreted sea-level curve determined in Chapter 1 is also plotted next to the stratigraphic columns to the left of the stratigraphic columns.

are separated by ~300 km, were significantly different or that the conodont $\delta^{18}\text{O}$ values at one or both of the Utah localities were diagenetically altered.

If the measured Utah $\delta^{18}\text{O}$ values are primary, then the lower isotopic values at Weber Canyon may represent a significant influx of fluvial (meteoric) waters and a lowering of $\delta^{18}\text{O}$ values of local coastal waters. The discharge of the modern Amazon River is one of the largest in the world; however, $\delta^{18}\text{O}$ values in coastal waters near its mouth are depleted by only ~0.5‰ with respect to open-ocean Atlantic waters (Legrande and Schmidt, 2006). Given this comparison, it is not likely that the ~1.5 ‰ lower isotopic values recorded at Weber Canyon versus Confusion Range were caused by increased fluvial discharge because the amount of fresh water influx required to offset the Weber Canyon samples would require Early Triassic river systems several times larger than the modern Amazon. This amount of fluvial influx would preclude the occurrence of typical normal marine fossils found in the lower Thaynes Formation (i.e., conodonts, echinoderms, and ammonoids). The lower $\delta^{18}\text{O}$ values at Weber Canyon might also represent higher seawater temperatures than at the Confusion Range. If this were the case, the ~1.5 ‰ difference between sites suggests greater than 4-6°C seawater temperatures at Weber Canyon than in the Confusion Range. Although possible, it is not likely such a drastic temperature changes would occur over the ~300 km distance between the two sites, which lay at a similar paleolatitude. In addition, these higher temperatures would likely prevent the occurrence of normal (though impoverished) marine fauna observed at Weber Canyon.

Alternatively, the higher $\delta^{18}\text{O}$ values recorded in the Confusion Range might represent local seawater enrichment due to enhanced evaporation rates. Typical marine $\delta^{18}\text{O}$ values in the enclosed and arid-climate Red Sea and eastern Mediterranean regions are enriched by up to 2 ‰ from adjacent open-marine waters in the upper 5 meters of the water column (Legrande and Schmidt, 2006). Such waters are typically too saline to support normal marine faunal types observed in the lower Thaynes Formation and suggests that the higher $\delta^{18}\text{O}$ conodont values in the Confusion Range are not the result of evaporative seawater conditions.

The previous arguments suggest that the $\delta^{18}\text{O}$ differences between the Smithian Utah successions are not result of differences in seawater chemistry or temperature. Instead, we suggest that $\delta^{18}\text{O}$ differences are the result of diagenetic alteration, and in particular, the Weber Canyon conodonts record the effects of alteration related to elevated diagenetic temperatures. This interpretation is supported by the higher CAI values and SEM evidence of conodont recrystallization and/or pitting at Weber Canyon, while the Confusion Range conodonts have lower CAIs and more pristine textures under SEM (Figure 2.2). These interpretations are further supported by the CAI versus $\delta^{18}\text{O}$ trends in Smithian conodonts from British Columbia and the Sverdrup Basin (Figure 2.5), where the conodonts with the lowest CAI values (least thermal alteration) record the highest $\delta^{18}\text{O}$ values and most pristine SEM textures. In contrast to these trends, the northern Indian conodonts record the highest CAI values of 5, but their $\delta^{18}\text{O}$ values lie within the same range as conodonts from the Confusion Range, British Columbia, and Idaho (CAI < 3). This suggests that CAI values *alone* cannot identify the potential effects of conodont alteration. Inorganic exchange between apatite phosphate and meteoric

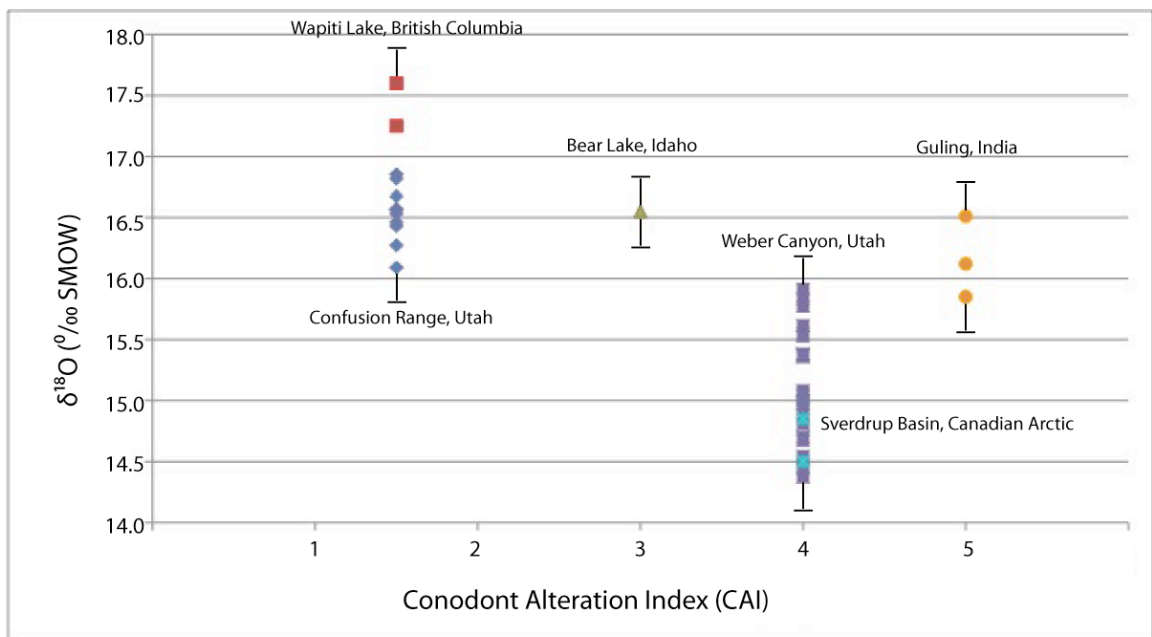


Figure 2.5: Oxygen isotopic values versus conodont alteration index for the six sample locations. Conodonts with a CAI of less than or equal to 3 have higher oxygen isotopic values than those with a CAI of 4 or higher, with the exception of the Guling section.

waters would be very difficult at low temperatures (Tudge, 1960); however Blake et al. (1997) and Lecuyer et al. (1999) have found that early diagenetic microbial degradation of organic matter can stimulate secondary apatite precipitation into available voids resulting in a shift to lower oxygen isotope values. This may explain some of the observed Smithian trends.

Figure 2.6 shows the comparison between interpreted primary or near primary Smithian $\delta^{18}\text{O}$ values (ranging from 15.85 to 17.6 ‰) from the Confusion Range, Idaho, British Columbia, and India to previously reported $\delta^{18}\text{O}$ values from Ordovician through Triassic conodonts. The Smithian values are similar to those determined from the Early Ordovician greenhouse (Trotter et al., 2008) and overlap with lower isotopic values of greenhouse time intervals including the Middle Ordovician and Early and Late Devonian. Of particular interest is that the measured Smithian values are lower than limited data from the Earliest Triassic (Griesbachian-Dienerian; Korte et al., 2004) and the Middle and Late Triassic (Rigo et al., 2010). This suggests that Smithian seawater temperatures were warmer than the Earliest Triassic and warmer than the Middle and Late Triassic.

2.7.2 Paleoclimate interpretations

At present there is no routine independent proxy for temperature (like temperature-dependent species assemblages, TEX_{86} , or alkenone paleothermometry) in deep geologic time as there is for the Cenozoic and latest Mesozoic, so estimates are made to decouple how much of the isotopic values are due to temperature versus seawater

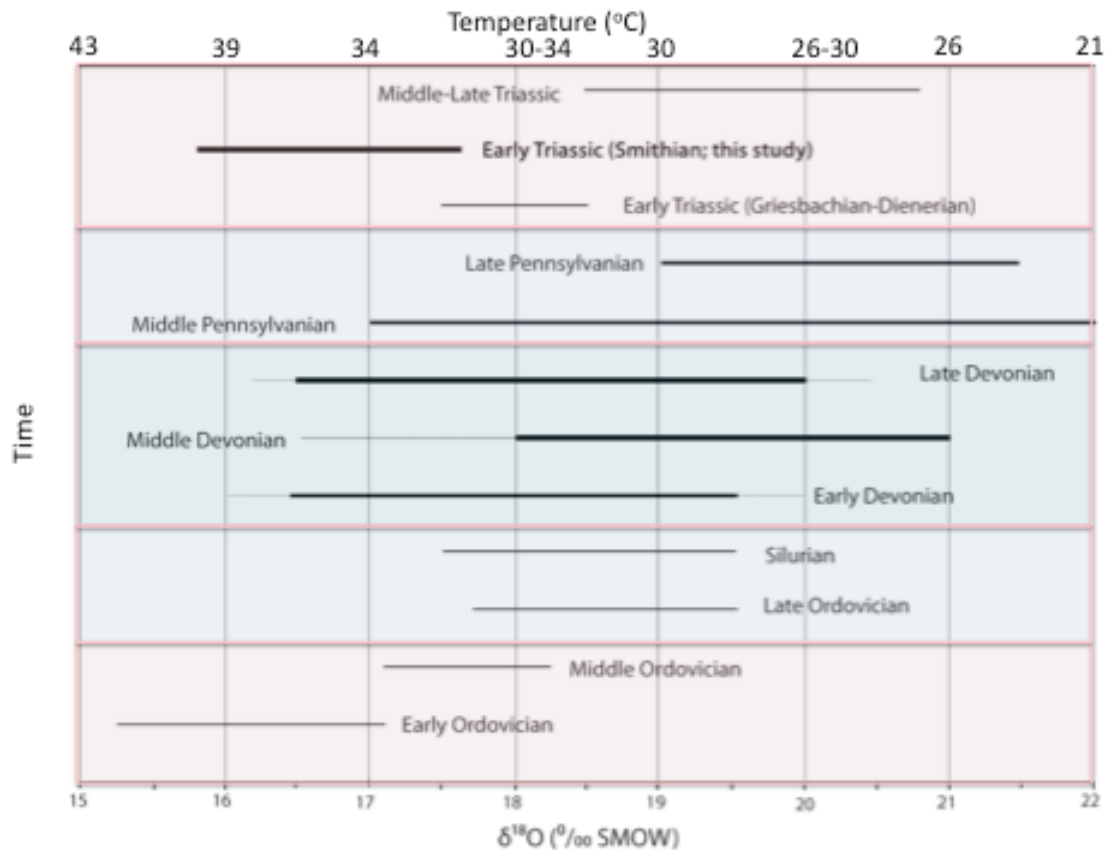


Figure 2.6: All of the published oxygen isotopic values currently published from the Early Ordovician (Basset, 2007; Trotter et al., 2008), Middle and Late Ordovician (Trotter et al., 2008), Silurian (Wenzel et al., 2000), Early Devonian (Elrick et al., 2009; Joachimski et al., 2009), Middle Devonian (Joachimski et al., 2004; 2009; Elrick et al., 2009), Late Devonian (Joachimski and Buggisch, 2002; Joachimski et al., 2004; 2009), Middle Pennsylvanian (Elrick and Scott, 2010), Late Pennsylvanian (Joachimski et al., 2006), Early Triassic (Griesbachian/Dienerian) (Korte et al., 2004), and Middle to Late Triassic (Rigo et al., 2010) are plotted. The thickness of the line indicates approximately how many data points were published for each section. The thin tails on the ends of the Devonian values indicate <2 samples. The thinnest line indicates <10 samples, the medium thickness line indicates between 10 and 25 samples, and the thickest line (including this study) indicates that >25 samples were run. The pink shaded regions indicate warm periods in Earth history, the blue are cool, and the green is in between. Temperatures are estimated based on the Kolodny et al. (1983) equation assuming $-1 \delta_{sw}$ for warm periods, 0 for in between and $+1$ for cool periods. The range of temperatures are based on combining δ_{sw} to account for a the range of possible values between warm and cool times.

The average $\delta^{18}\text{O}$ for globally mixed seawater ranges from -1 ‰ (ice free) to +1 ‰ (Pleistocene-size ice caps) with the present seawater value at ~ 0 ‰. If we assume the Confusion Range, British Columbia, Idaho, and northern India conodont isotope values record primary to near primary Smithian seawater values, then we can use the Kolodny et al. (1983) apatite temperature equation ($T(^{\circ}\text{C}) = 113.3 - 4.38 (\delta^{18}\text{O}_{\text{phosphate}} - \delta^{18}\text{O}_{\text{sea water}})$) to estimate seawater temperatures across the range of paleolatitudes.

Assuming ice-free conditions and a seawater isotope value of -1‰, seawater temperatures for the Confusion Range range from ~ 35 to 38°C , British Columbia range from ~ 32 to 34°C , the single Idaho value is $\sim 36^{\circ}\text{C}$ and India from ~ 37 to 40°C . The fact the lowest paleolatitude sites (Confusion Range and Idaho $\sim 10^{\circ}\text{N}$) record warmer temperatures than the higher paleolatitude site (British Columbian $\sim 25^{\circ}\text{N}$) further support our interpretations that these samples represent primary to near primary isotopic values. These range of temperatures come from locations spanning at least 15° of tropical to subtropical paleolatitudes and indicate a gentle low-latitude to high-latitude temperature gradient during the Smithian. Although India had a higher paleolatitude at $\sim 40^{\circ}\text{S}$, the temperatures reported for this region are similar to those recorded in the subtropics and tropics in western North America. Transport of warm paleo-Tethys surface waters south to this region may explain these warm sea-surface temperatures (Figure 2.1). The dominance of platform carbonates (~ 40 m thick) spanning the Triassic in northern India supports these warmer temperature estimates.

For comparison, modern surface-water temperatures in the western tropical Atlantic range from $\sim 27^{\circ}$ to 29°C (Antonov et al., 1998), so our data suggest that the Smithian surface ocean was $\sim 4^{\circ}$ to 10°C warmer than the present. Estimates of surface

seawater temperatures during the mid to Late Cretaceous greenhouse range from ~31 to 36°C using TEX₈₆ (Forster et al., 2007; Bornemann et al., 2008) and ~30 to 37 °C using oxygen isotopes from well preserved planktonic foraminifera (e.g., Wilson et al., 2002; Bice et al., 2006; Forster et al., 2007; Bornemann et al., 2008). These Cretaceous tropical to subtropical sea surface temperatures are similar to the ranges estimated from the primary/near primary Smithian conodonts suggesting that Early Triassic climates were comparable to the well-studied Cretaceous greenhouse.

An alternative hypothesis to explain these unusually warm temperatures is that our assumption of -1‰ (ice-free) Smithian seawaters is incorrect and instead, Early Triassic seawaters had more depleted $\delta^{18}\text{O}$ values, perhaps as low as -3‰. Calculated seawater temperatures using such depleted $\delta^{18}\text{O}$ values would decrease and lie between ~25 to 30 °C, which are similar to modern tropical seawaters. The possibility of varying seawater $\delta^{18}\text{O}$ values over geologic time has been extensively discussed and argued (e.g., Veizer et al., 1997; 1999; Jaffres et al., 2007; and Shields et al., 2007); however, resolving this issue is beyond the scope of this research.

In summary, results from the studied stratigraphic sections recording primary to near primary oxygen marine isotope values suggests a gentle tropic-to-subtropical seawater temperature gradient and overall very warm seawater conditions during the Smithian which supports previous interpretations of greenhouse or hot-house climatic conditions in the Early Triassic (e.g. Dickins, 1993; Holser and Magaritz, 1987; Frakes and Francis, 1988; Frakes et al., 1992; Jefferson and Taylor, 1983; Wignall et al., 1998; Retallack, 1999; Berner, 1999; 2002; Michaelsen and Henderson, 2000; Looy et al., 2001; Spalletti et al., 2003; Kidder and Worsley, 2004; Payne et al., 2004; Royer et al.,

2004; Kiehl and Shields, 2005; Brayard et al., 2006; Preto et al., 2010). Estimated subtropical seawater temperatures from $\delta^{18}\text{O}$ of conodont apatite (assuming -1‰ seawaters) immediately prior to the Permo-Triassic boundary range from 23 to 28 °C (Korte et al., 2004). Only two $\delta^{18}\text{O}$ apatite data points are available for the Earliest Triassic (Griesbachian-Dienerian; Korte et al., 2004) and estimated temperatures from these two values suggest increasing seawater temperatures. Combining this sparse data with the primary to near primary Smithian $\delta^{18}\text{O}$ apatite values from this study suggests continued warming conditions after the Permo-Triassic extinction and throughout the Early Triassic recovery interval. These unusually warm seawater temperatures may have aided in delaying the recovery after the Permo-Triassic extinction event.

2.7.3 What is driving My-scale sea-level change?

The original aim of this research was to collect samples of conodonts for $\delta^{18}\text{O}$ values in a stratigraphic framework to understand what drove My-scale sea-level change. This is an especially important question for the Early Triassic because it appears to be uniformly warm and ice free. In chapter 1, we established that the My-scale sea-level change that occurred in the Smithian was likely eustatic. There is no apparent relationship between the $\delta^{18}\text{O}$ values measured for the Weber Canyon and Confusion Range sections and paleoenvironmental change interpreted from facies changes (Figure 2.4). Because the Weber Canyon conodonts do not record primary $\delta^{18}\text{O}$ values, they cannot be used to evaluate the relationships between My-scale sea-level change and climate. What is left unanswered is the origin of the Early Triassic My-scale sea-level

changes. Given the warm sea surface temperatures calculated for the tropical and subtropical climates, it is unlikely that sufficient glacial ice existed at high latitudes to drive glacial eustasy. This leaves the possibility that the Smithian sea-level changes were driven by thermal eustasy; however, more samples with a low CAI would be needed to test this hypothesis.

2.8 Conclusions

1. Smithian conodont samples with a CAI > 3 do not appear to record the primary $\delta^{18}\text{O}$ values.
2. If we assume ice-free Smithian conditions, then tropical to subtropical sea-surface temperatures range from ~35-38 °C for the Confusion Range, western Utah (tropical) and ~31-34 °C for Wapiti Lake, northeastern British Columbia (subtropical). These temperatures are consistent with the Cretaceous greenhouse sea-surface temperature estimates for the similar latitudes and ~10 °C warmer than today's tropical icehouse.
3. Regardless of the specific cause of the Permo-Triassic extinction, the seawater temperatures interpreted from this study suggest that very warm seawater temperatures influenced the protracted Early Triassic biotic recovery interval.

Appendices










Appendix A- Stratigraphic Columns.....	80
Legend.....	81
Weber Canyon.....	82
Confusion Range.....	95
Guling.....	98
Appendix B- Oxygen Isotopes.....	100

APPENDIX A – STRATIGRAPHIC COLUMNS



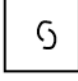

The following pages contain stratigraphic columns for Weber Canyon, northern Utah, the Confusion Range, western Utah, and Guling, Himachal Pradesh, northern India. The Weber Canyon section was measured and described on two sides of the Weber River east of Ogden, Utah on I-84. The Confusion Range section was measured and described in three locations <40 km apart. The Guling section was measured and described in one location and observed in four other places in the same valley. All three locations represent Smithian marine transgressive-regressive cycles. The first page explains the symbols used and is followed by the data.





Appendix A: Legend

Sedimentologic/biologic structures:

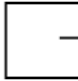
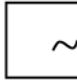
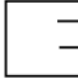
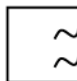
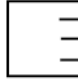
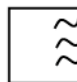

	Symmetric Ripples
	Asymmetric Ripples
	Cross Bedding
	Laminations
	Bioturbation
	Argillaceous
	Calcareous
	Soft Sediment Deformation
	Vugs

Fossils:

	Crinoids
	Ammonoids
	Abraded bivalves
	Whole bivalves
	Gastropods
	Skeletal Fragments
	Peloids
	Silicified Sponges
	Quartz sand

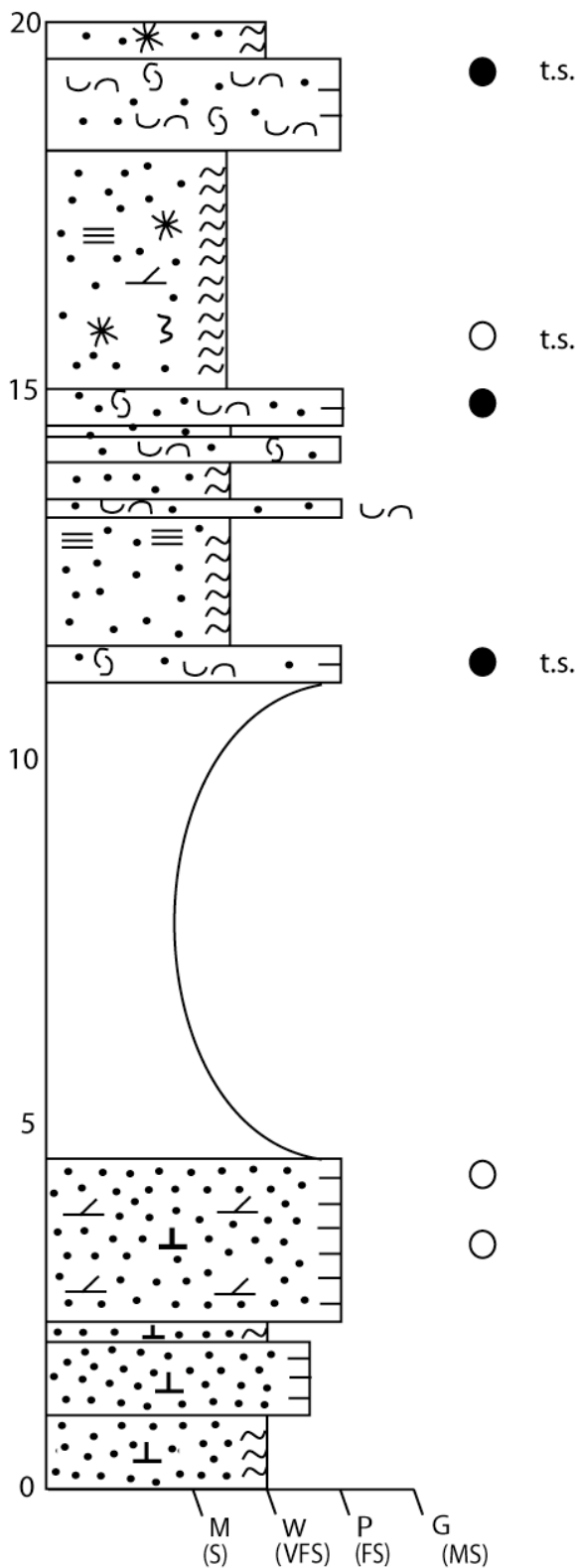
	Conodont Sample (producing)
	Conodont Sample (producing, but not enough for analyses)
	Conodont Sample (non-producing)
	t.s. Thin section

Bedding styles:

	Thick Bedding		Thick Nodular Bedding
	Medium Bedding		Medium Nodular Bedding
	Thin Bedding		Thin Nodular Bedding
	Shale		

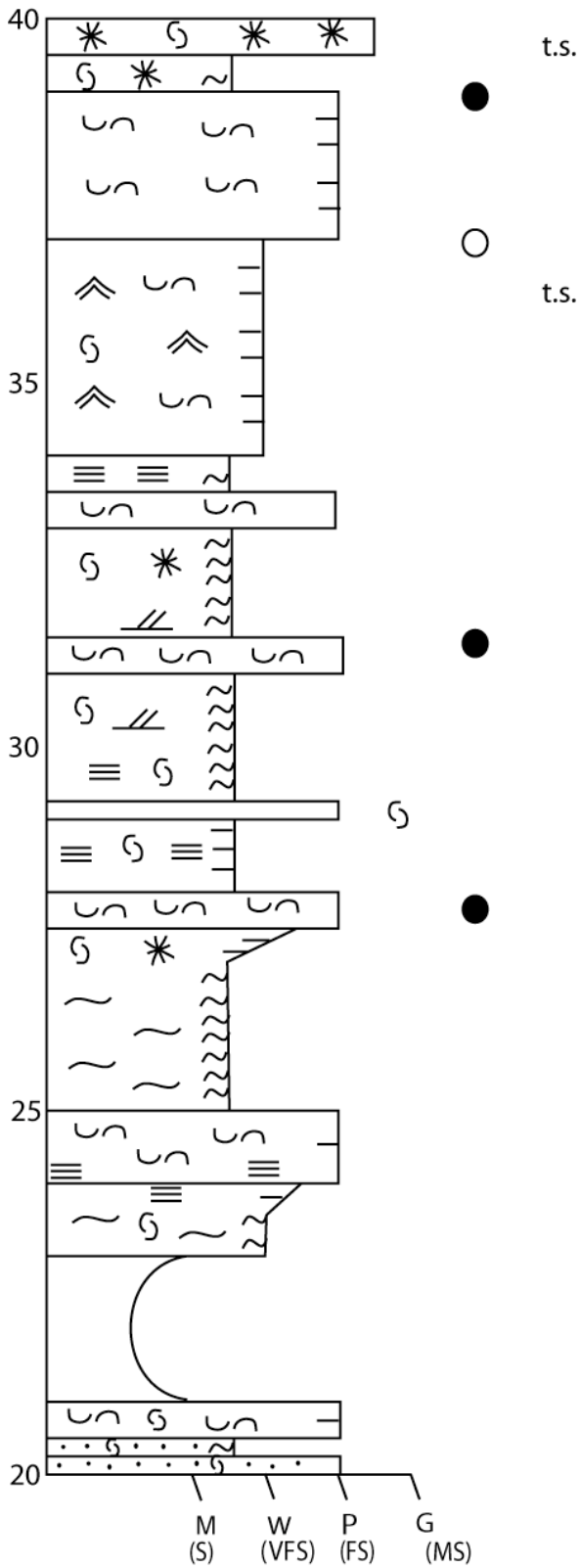
Weber Canyon, northern Utah

Notes:



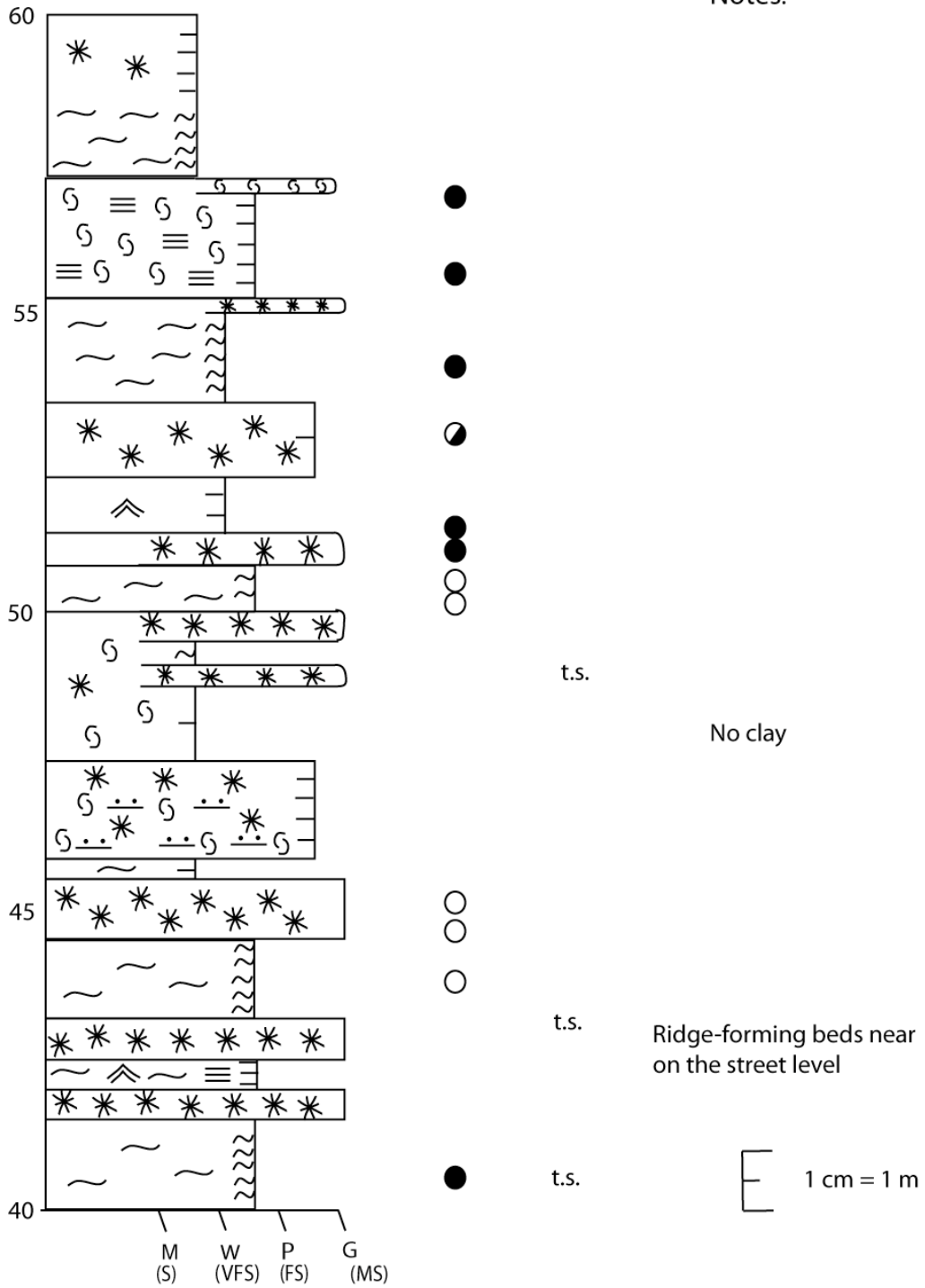
Weber Canyon, northern Utah

Notes:

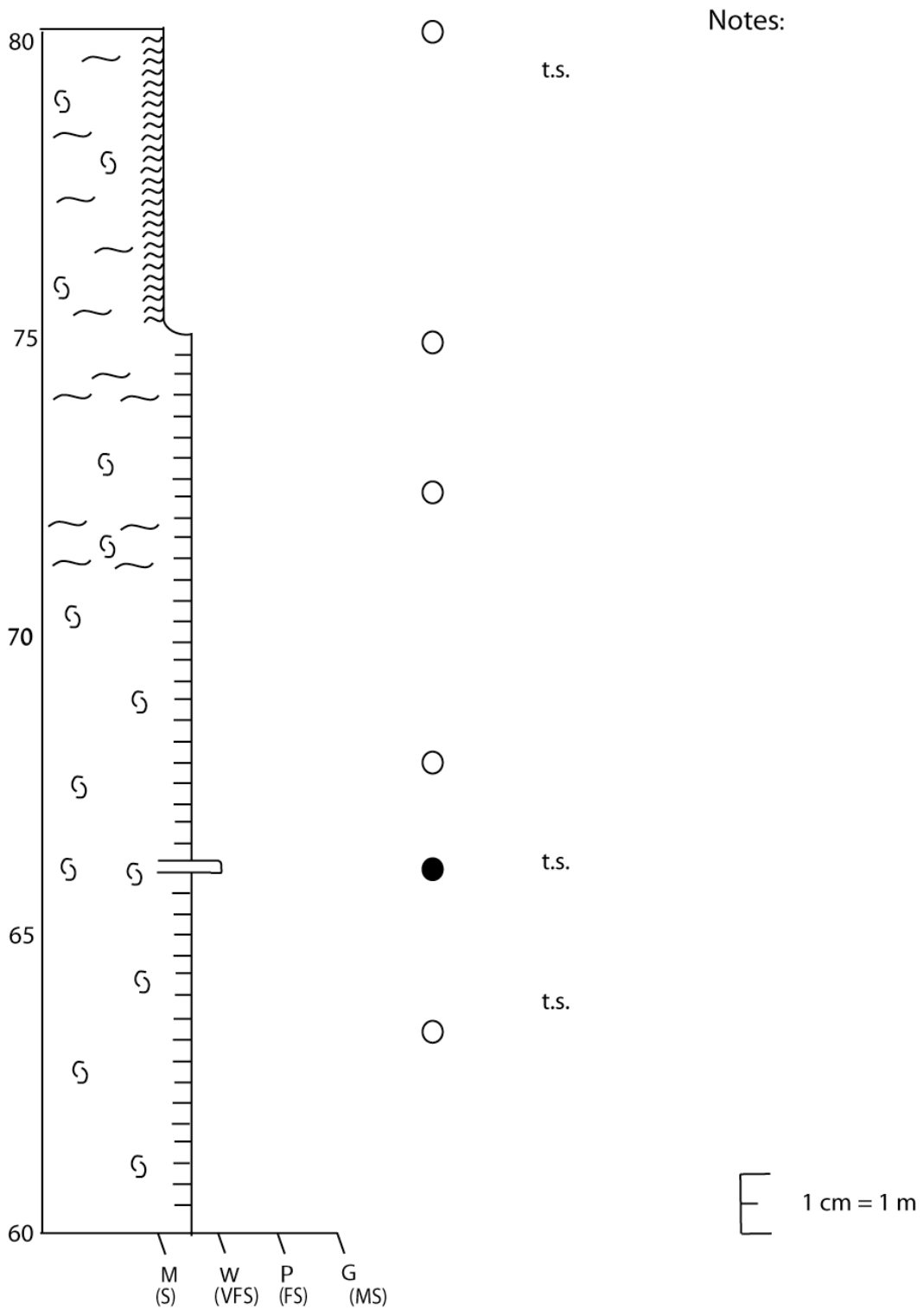


Weber Canyon, northern Utah

Notes:

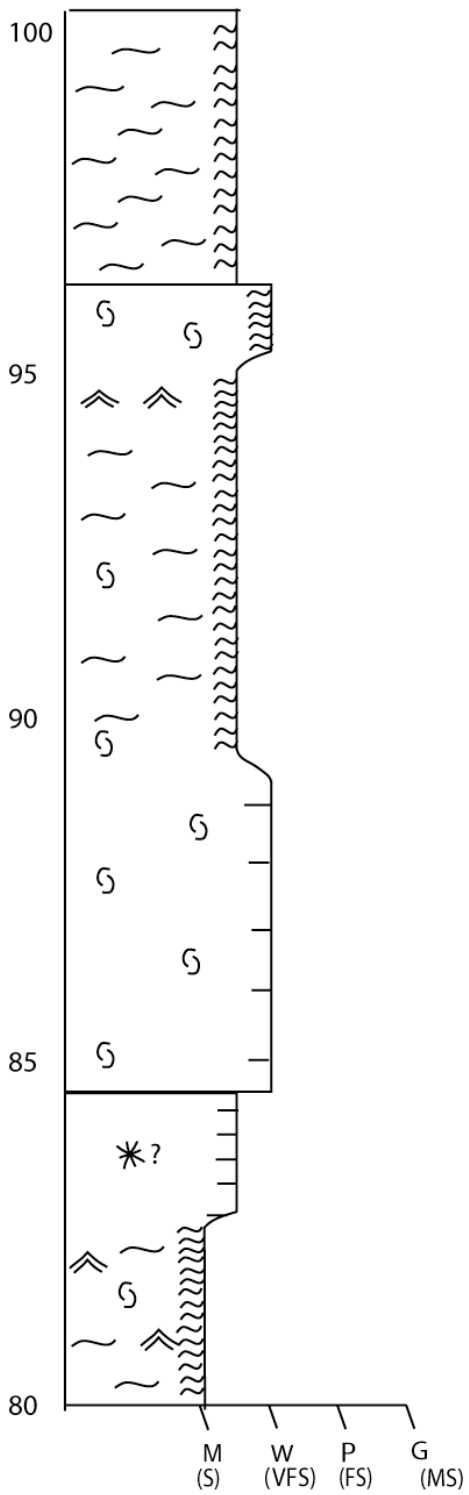


Weber Canyon, northern Utah



Weber Canyon, northern Utah

Notes:



○

●

Cleaner

○

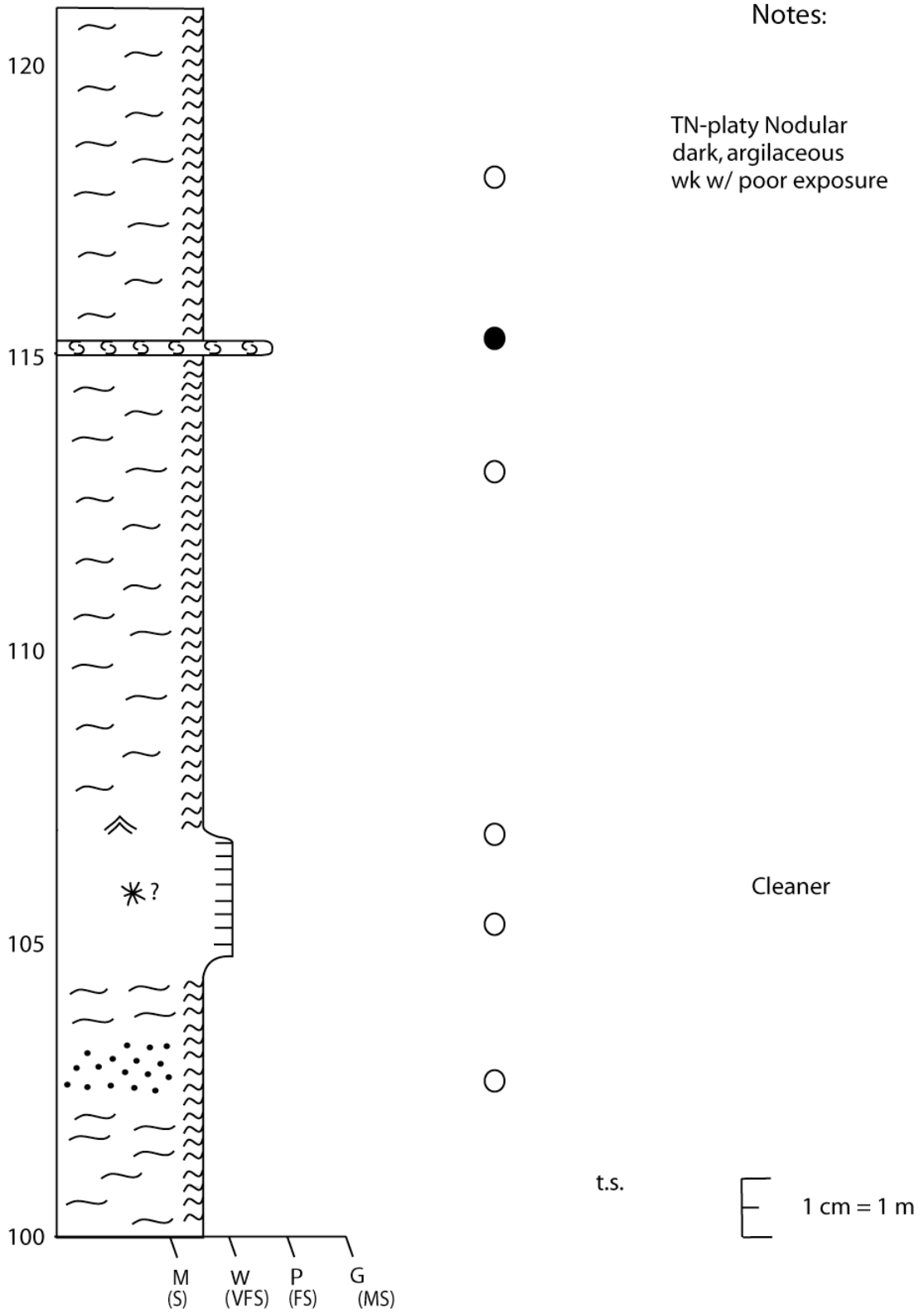
Clay

●

Cleaner

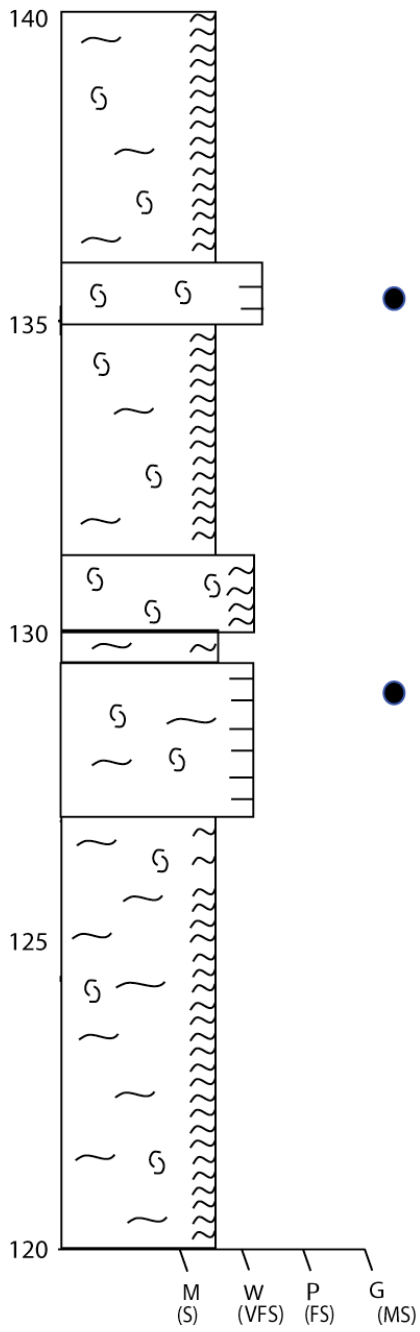
○

Weber Canyon, northern Utah



Weber Canyon, northern Utah

Notes:

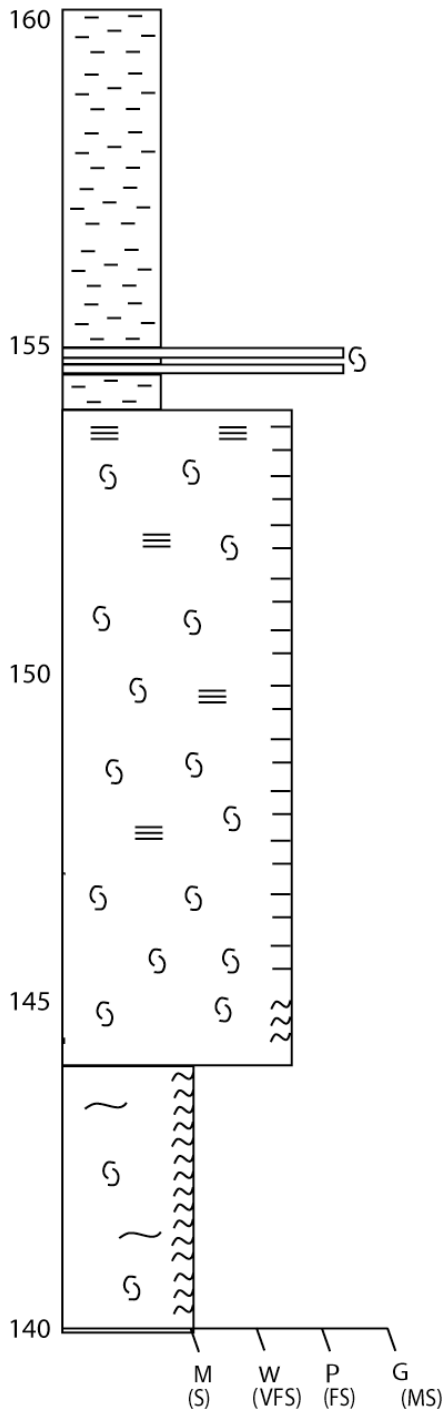


1 cm = 1 m

Started measuring from the other side of the Weber River

Weber Canyon, northern Utah

Notes:



MFZ dark shale

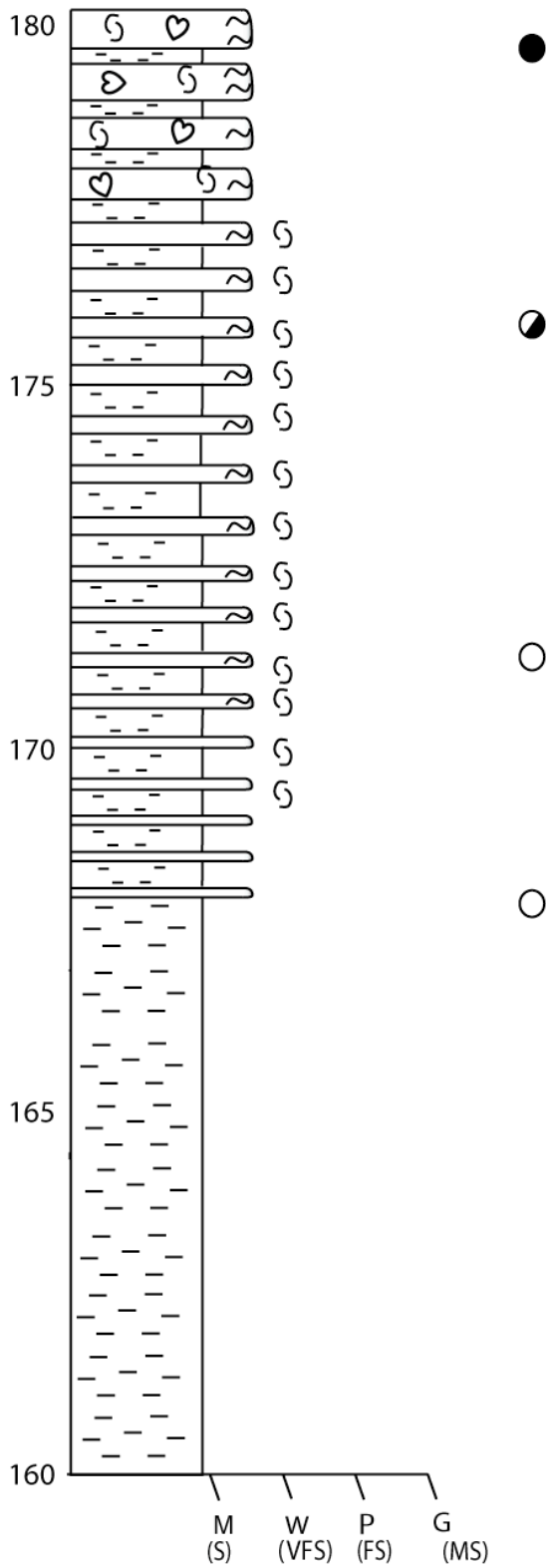
t.s.

1 cm = 1 m

Started measuring from the other side of the Weber River

Weber Canyon, northern Utah

Notes:

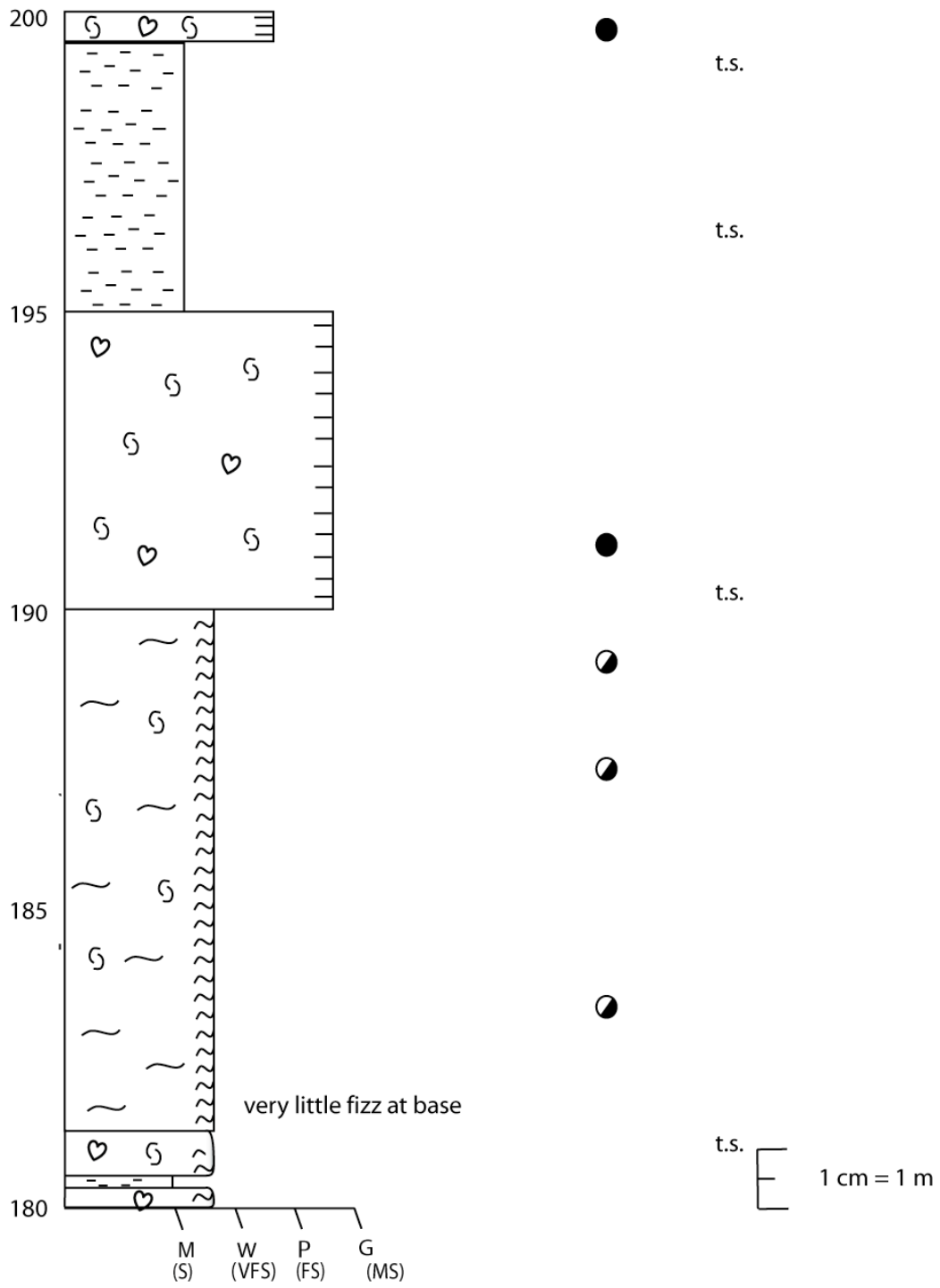


Rhythmites

1 cm = 1 m

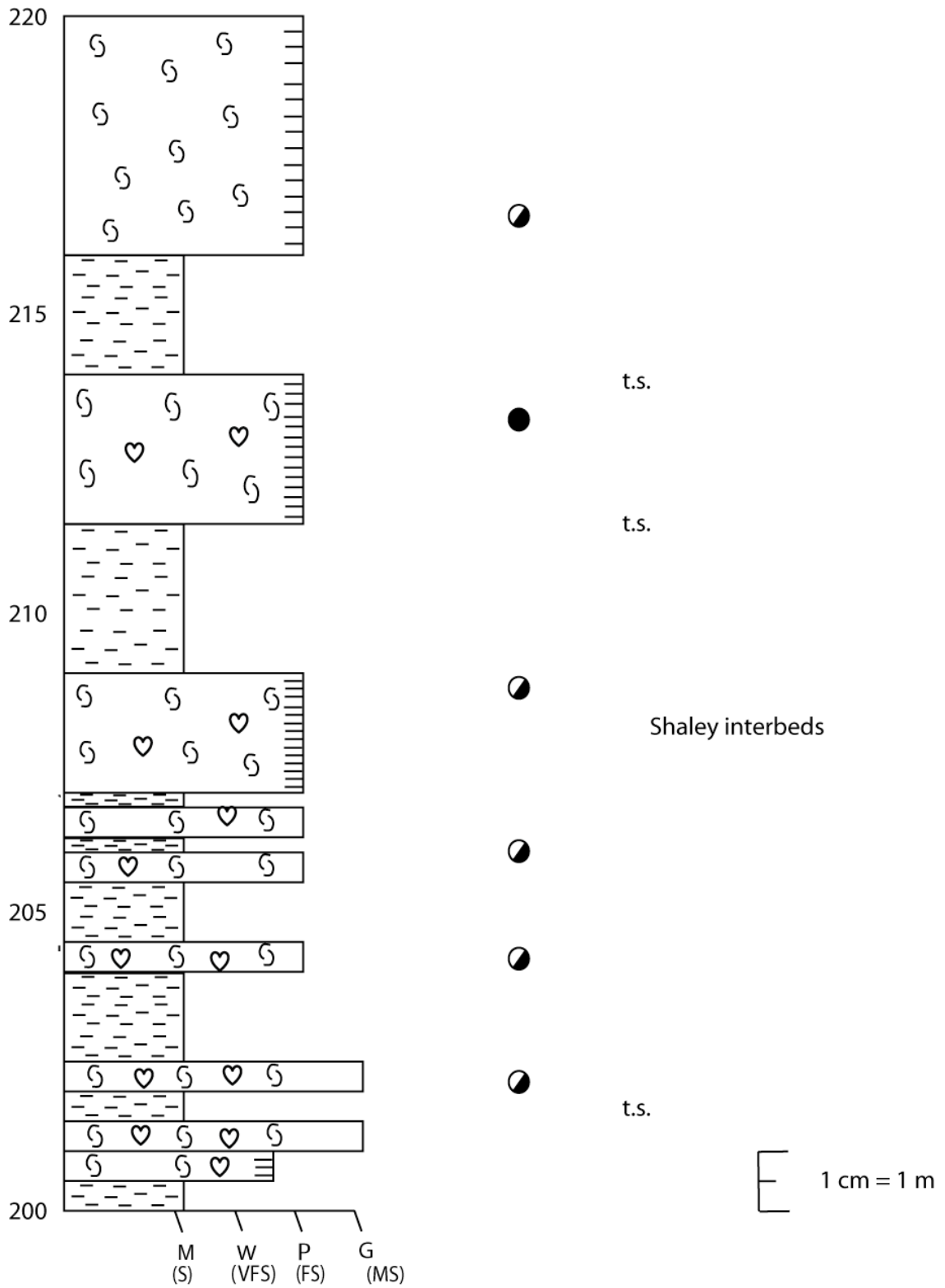
Weber Canyon, northern Utah

Notes:



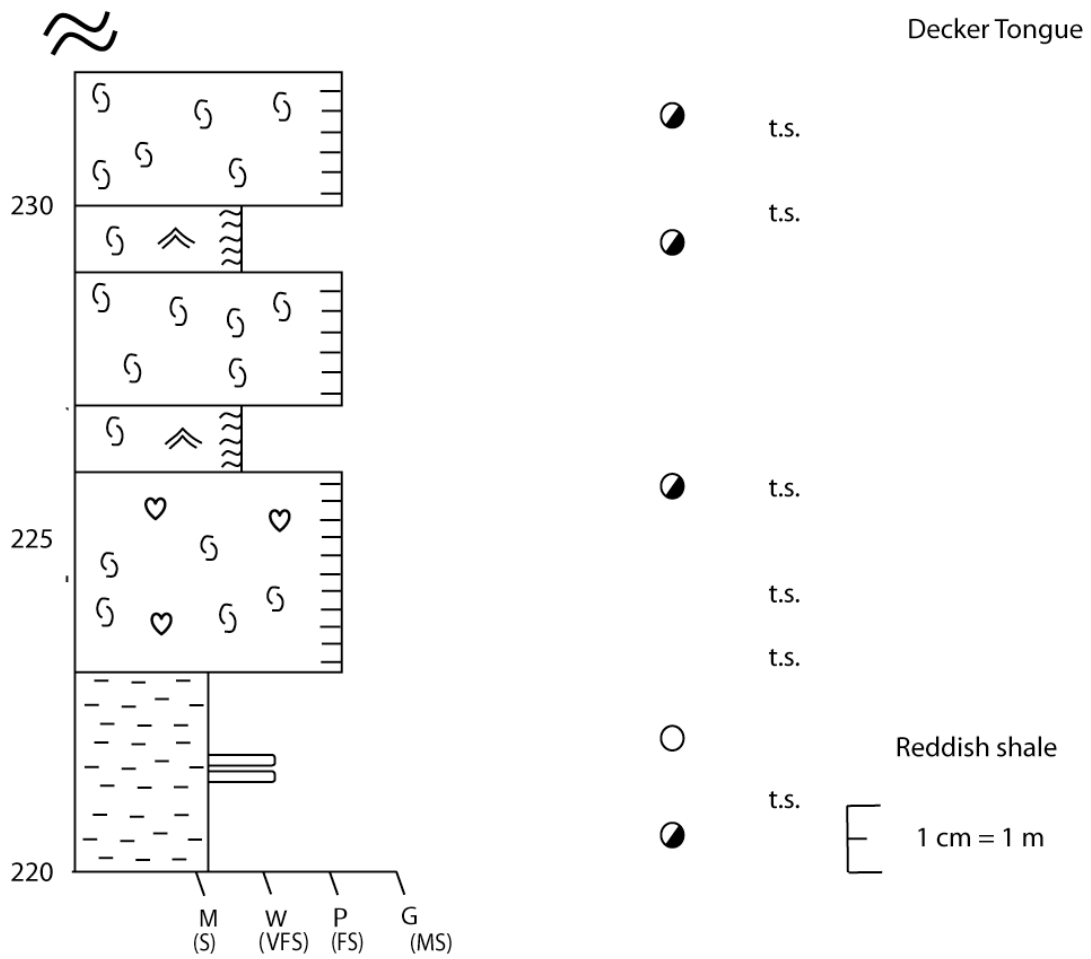
Weber Canyon, northern Utah

Notes:

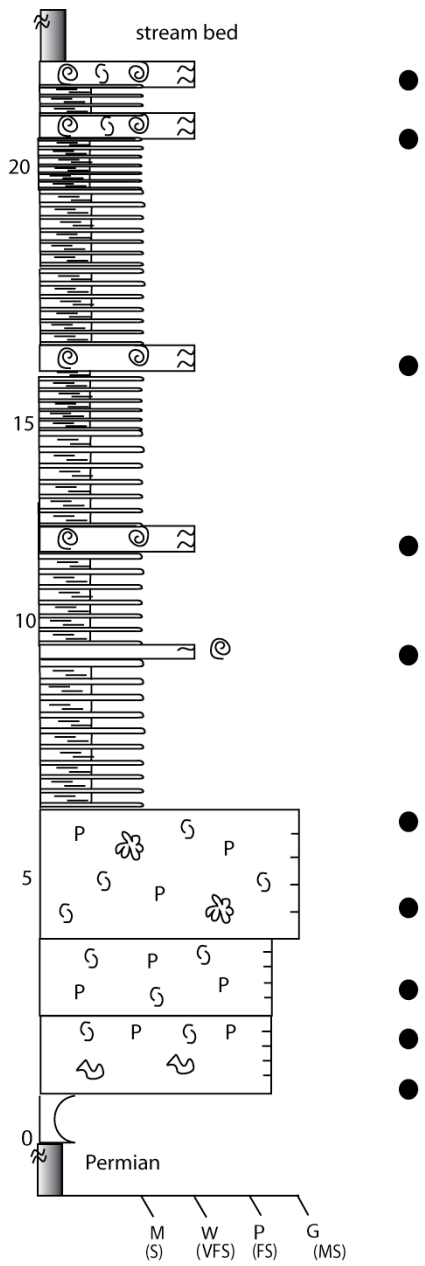


Weber Canyon, northern Utah

Notes:



Confusion Range, western Utah



Notes:

When in the field, I only measured section until here. One more same was collected right before the light calcaerous shale subfacies at ~70 m. There is ~100 m of light shale between this section and the between top of the Lower Thaynes Formation, which is on the next page.

White

Beige (rose)

Gray

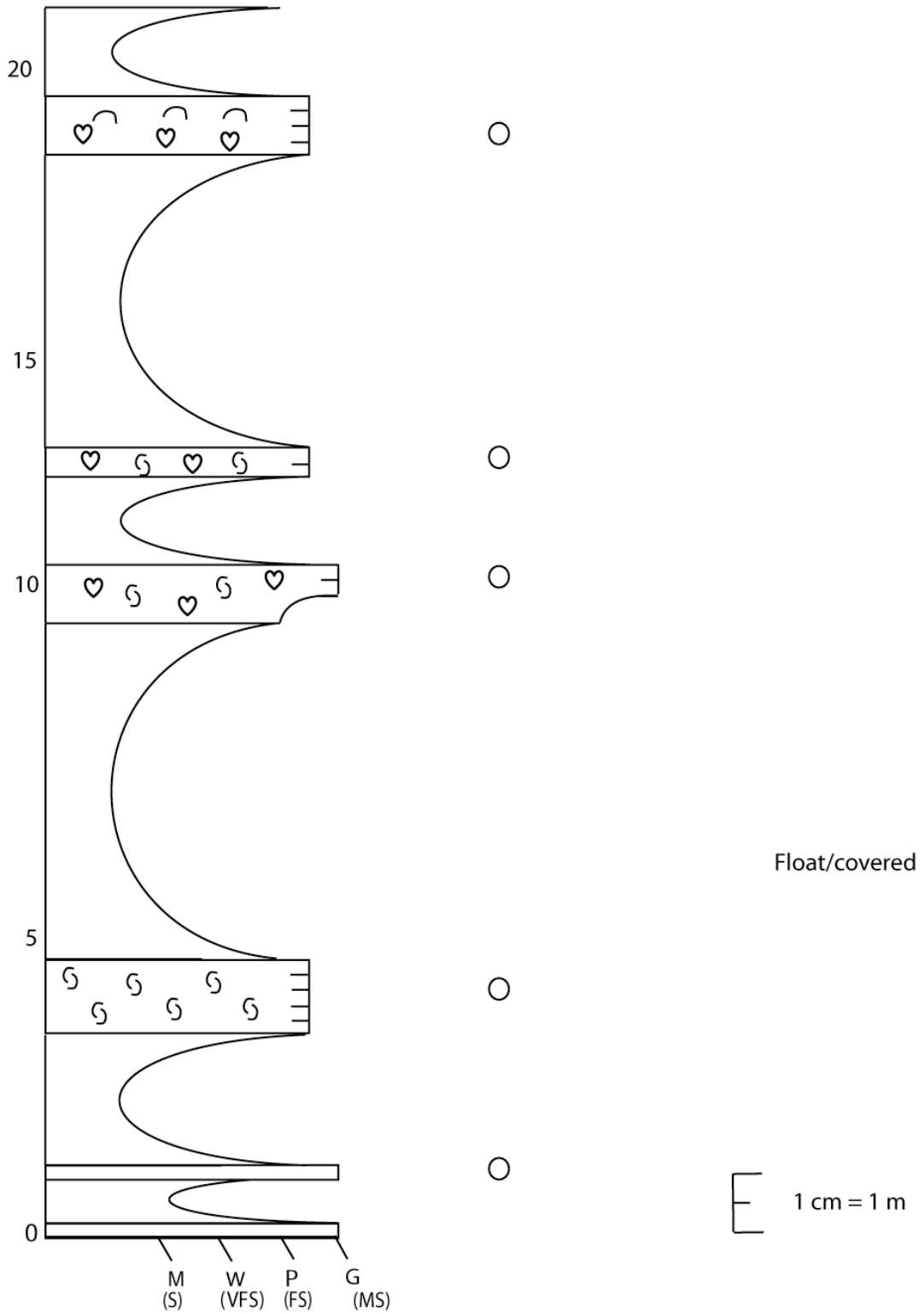
Gray

Reddish-brown

1 cm = 1 m

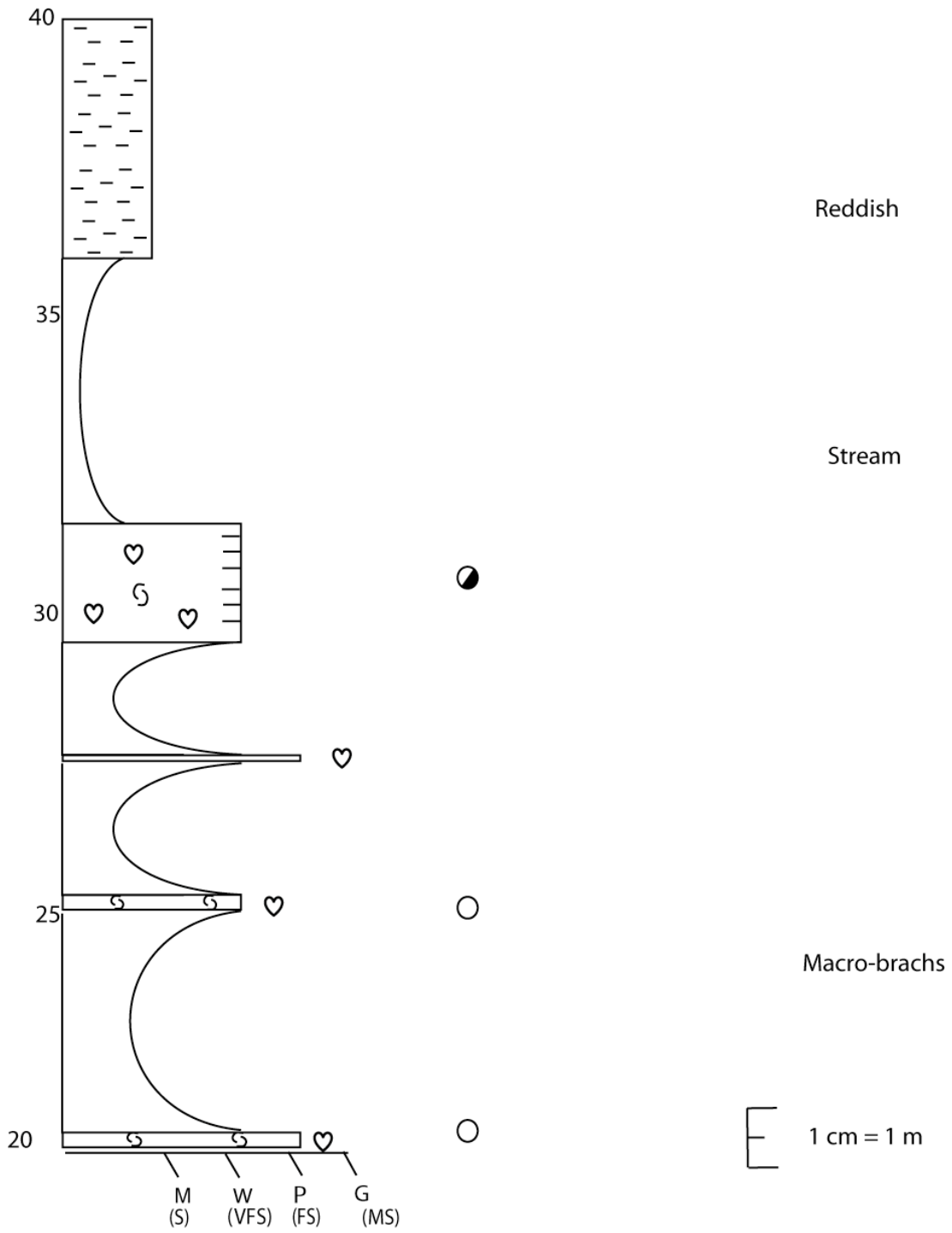
Confusion Range, western Utah

Notes:

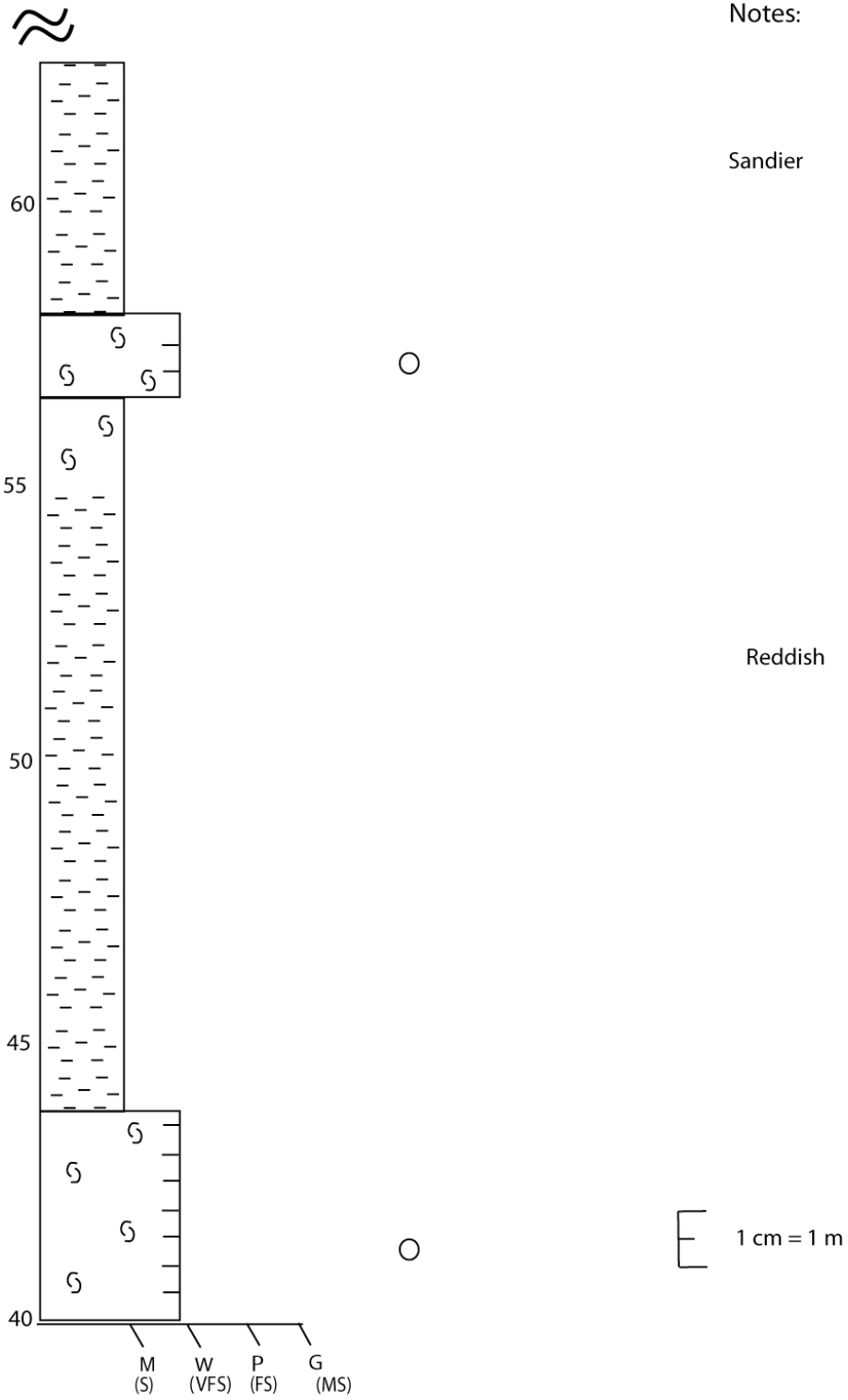


Confusion Range, western Utah

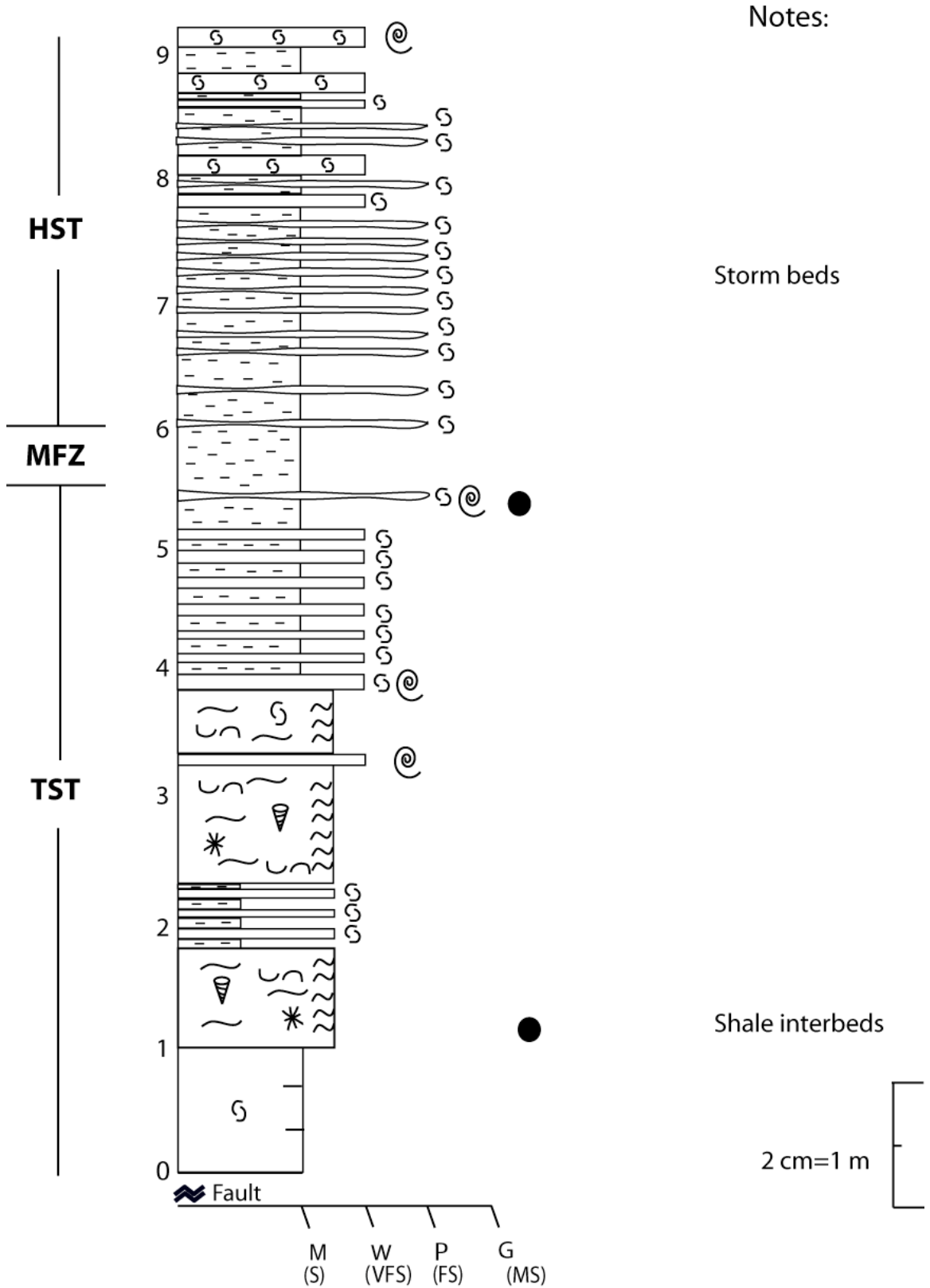
Notes:



Confusion Range, western Utah



Guling, northern India



Notes:

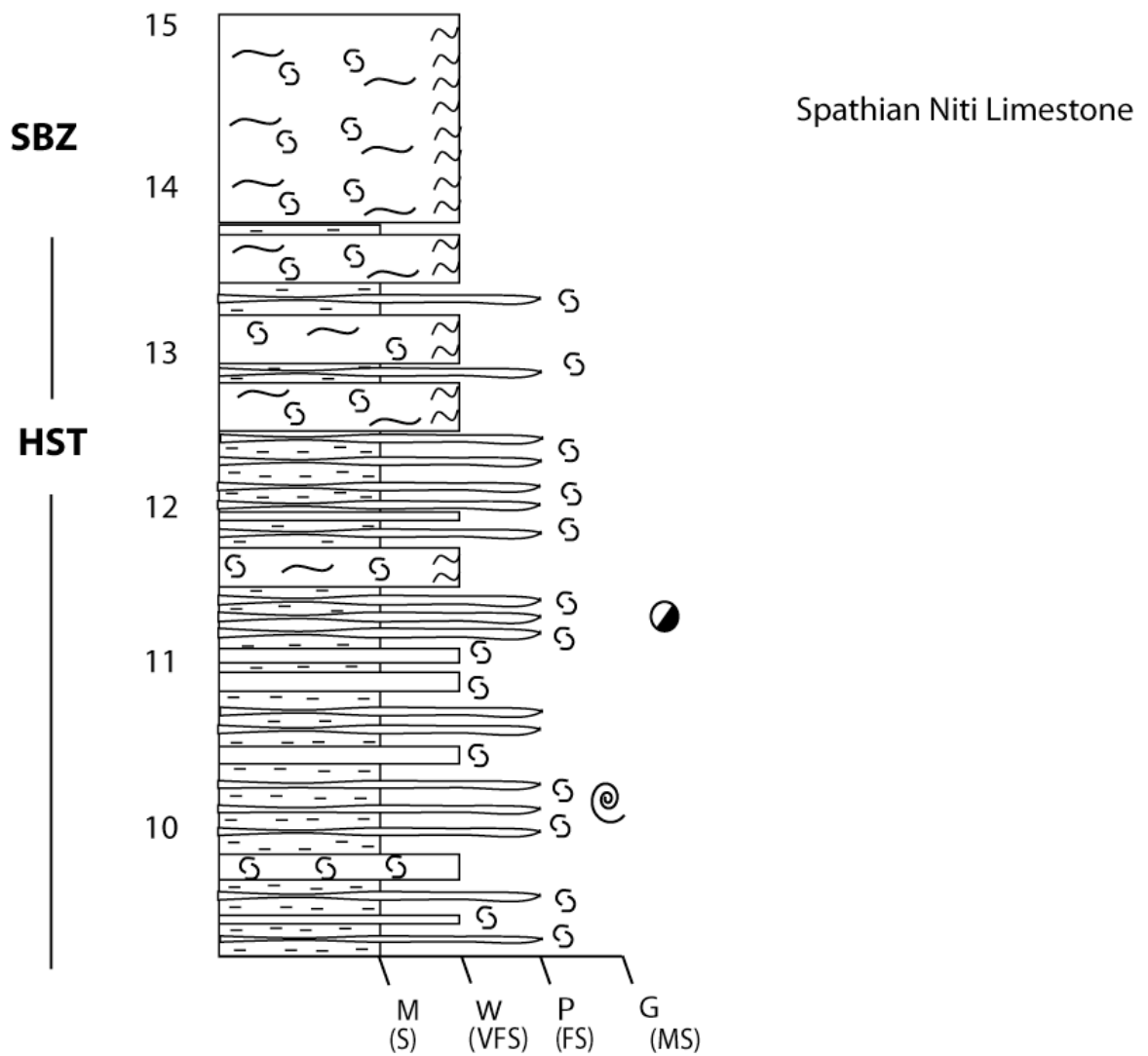
Storm beds

Shale interbeds

2 cm = 1 m

Guling, northern India

Notes:



APPENDIX B– OXYGEN ISOTOPES

The following pages contain oxygen isotope data for the six sections including the naming convention used and the measured stratigraphic location, if sampled in a stratigraphic framework. The bolded gray values represent already averaged values of up to 4 sample runs each, whereas the non-bold come from the final sample run and represent the raw data. CAI estimates are also shown in the right column.

Location/sample name	Meters	$\delta^{18}\text{O}$ values	Average	CAI
Weber Canyon, northern Utah				
WC-11	11	14.78, 14.97	14.88	4
WC-15	15	14.54	14.54	4
WC-19.5	19.5	15.00	15.00	4
WC-27	27	15.77	15.77	4
WC-32	32	15.38	15.38	4
WC-39.25	39.25	15.05	15.05	4
WC-40.5	40.5	15, 15.29, 15.38	15.22	4
WC-52.5	52.5	15.36	15.36	4
WC-53	53	14.81	14.81	4
WC-54.5	54.5	15.91	15.91	4
WC-55.5	55.5	15.37	15.37	4
WC-56.5	56.5	14.44	14.44	4
WC-66	66	14.98	14.98	4
WC-95.5	95.5	15.53	15.53	4
WC-115	115	15.34, 15.61	15.48	4
WCR-9.25	130.75	14.45	14.45	4
WCR-15	135.5	14.37	14.37	4
WCR-28.5	150	14.70	14.70	4
WCR-30	151.5	14.67	14.67	4
WCR-31.5	153	14.93	14.93	4
WC-153	153	15.08	15.08	4
WCR-32	153.5	15.83	15.83	4
WCR-59.8	181.3	15.55	15.55	4
WCR-67	188.5	15.00	15.00	4
WCR-69	190.5	15.04	15.04	4
WCR-71	192.5	15.77	15.77	4
WCR 82.5	204	14.47	14.47	4
WCR 96.5	218	15.09	15.09	4
Confusion Range, western Utah				
DH2	4	16.56	16.56	1.5
DH3	5.3	16.46	16.46	1.5
DH4	6.7	16.33, 16.27	16.30	1.5
CR 9.5	9.5	16.99, 16.48, 16.57	16.68	1.5
CR 11.5	11.5	16.68	16.68	1.5
CIR 16.25	16.25	16.82	16.82	1.5
CR21	21	16.81, 16.55	16.68	1.5
CR 21.75	21.75	16.43	16.43	1.5
CR 28.5	28.5	16.44, 16.09	16.27	1.5
DH5	75	16.53	16.53	1.5
Guling, Himachal Pradesh, northern India				
G-1	1	16.51, 16.12	16.32	5
G-5.5	5.5	15.85	15.85	5

Bear Lake, southern Idaho				
BL	-	16.55, 17.14	16.85	3
Sverdrup Basin, Canadian Arctic				
M1	-	15.02, 14.71	14.87	4
M2	-	14.38, 14.70	14.54	4
Wapiti Lake, eastern British Columbia				
M3	-	17.86, 17.12	17.49	1.5
M4	-	17.56, 17.09	17.33	1.5

References

- Aigner, T., Bachmann, G.H., 1992. Sequence-stratigraphic framework of the German Triassic. *Sedimentary Geology* 80, 115-135.
- Antonov J.I., Levitus S., Boyer T.P., Conkright M.E., O'Brien T.D., Stephens C. 1998. *World Ocean Atlas 1998 Volume 1: Temperature of the Atlantic Ocean*. NOAA Atlas NESDIS 27. US Government Printing Office: Washington, DC.
- Arthur, M.A., Sageman, B.B., 1994. Marine Black Shales - Depositional Mechanisms and Environments of Ancient-Deposits. *Annual Review of Earth and Planetary Sciences* 22, 499-551.
- Atudorei, V., Guex, J., Orchard, M.J., Lucas, G.S., Zonnewell, J.-P., 2007. The Early Triassic carbon, nitrogen and sulfur isotope record. In: Lucas, G.S, Speilman, J.A. (Eds.), *The Global Triassic*. New Mexico Museum of Natural History and Science Bulletin 41, 13-14.
- Bacon, C.S., 1948. Geology of the Confusion Range, West-Central Utah. *Bulletin of the Geological Society of America* 59, (10), 434-458.
- Bassett, D., Macleod, K.G., Miller, J.F., 2007. Oxygen isotopic composition of biogenic phosphate and the temperature of Early Ordovician seawater. *Palaios* 22 (1), 98-103.
- Baud, A., Atudorei, V., Sharp, Z., 1996. Late Permian and Early Triassic evolution of the Northern Indian margin: carbon isotope and sequence stratigraphy. *Geodynamica Acta* 9 (2), 57-77.
- Baud, A., Gaetani, M., Garzanti, E., Fois, E., Nicora, A., Tintori, A., 1984. Geological observations in southeastern Zanskar and adjacent Lahul area (northwestern Himalaya). *Eclogae Geologicae Helvetiae* 77 (1), 171-197.
- Berner, R.A., 1999. A new look at the long-term carbon cycle, *GSA Today* 9, 1-6.
- Berner, R.A., 2002. Examination of hypotheses for the Permo-Triassic boundary extinction by carbon cycle modeling. *Proceedings of the National Academy of Sciences of the United States of America* 99 (7), 4172-4177.

- Bhargava, O.N., 2008. An updated introduction to the Spiti geology. *Journal of Paleontological Society of India*, 53 (2), 113-129.
- Bhargava, O.N., Krystyn, L., Balini, M., Lein, R., Nicora, A., 2004. Revised litho- and sequence stratigraphy of the Spiti Triassic. *Albertiana* 30, 21-39.
- Bice, K.L., Birgel, D., Meyers, P.A., Dahl, K.A., Hinrichs, K.-U., Norris, R.D., 2006. A multiple proxy and model study of Cretaceous upper ocean temperatures and atmospheric CO₂ concentrations. *Paleoceanography* 21(17).
- Bissel, H.J., 1962a. Pennsylvanian and Permian rocks of Cordilleran area. In: Branson, C.C. (Ed.), *Pennsylvanian System in the United States, a symposium*, Tulsa, OK, American Association of Petroleum Geologists, 188-263.
- Bissel, H.J., 1962b. Permian rocks of parts of Nevada, Utah, and Idaho. *Geological Society of America Bulletin* 73, 1083-1110.
- Blake, R.E., O'Neil, J.R., Garcia, G.A., 1997. Oxygen isotope systematics of biologically mediated reactions of phosphate I. Microbial degradation of organophosphorous compounds. *Geochemica and Cosmochemica Acta* 61, 4411-4422.
- Blakey, R.C., 1974. Stratigraphic and depositional analysis of the Moenkopi Formation, southeastern Utah. *Utah Geological and Mineral Survey Bulletin* 10, 81.
- Blakey, R., 2010. Paleogeographic maps, <http://jan.ucc.nau.edu/~rcb7/nam.html> (last accessed November 4, 2010).
- Bornemann, A., Norris, R.D., Friedrich, O., Beckmann, B., Schouten, S., Damaste, J.S., Vogel, J., Hoffman, P., Wagner, T., 2008. Isotopic Evidence for Glaciation During the Cretaceous Supergreenhouse, *Science* 319, 189-192.
- Boutwell, J.M., 1907. Stratigraphy and structure of the Park City Mining District, Utah. *Journal of Geology* 15, 434-458.
- Boutwell, J.M., 1912. Geology and ore deposits of the Park City district, Utah: U.S. Geological Survey Professional Paper 77, 1-231.
- Boyer, D.L., Bottjer, D.J., Droser, M.J., 2004. Ecological signature of Lower Triassic shell beds of the western United States. *Palaios* 19 (4), 372-380.

- Brayard, A., Bruhwiler, T., Bucher, H., and Jenks, J., 2009. Guodunites, a Low-Palaeolatitude and Trans-Panthalassic Smithian (Early Triassic) Ammonoid Genus. *Palaeontology* 52, 471-481.
- Brayard, A., Bucher, H., Escarguel, G., Fluteau, F., Bourquin, S., Galfetti, T., 2006. The Early Triassic ammonoid recovery: Paleoclimatic significance of diversity gradients. *Palaeogeography, Palaeoclimatology, Palaeoecology* 239 (3-4), 374-395.
- Brayard, A., Escarguel, G., Fluteau, F., Bourquin, S., Galfetti, T. 2009. Smithian and Spathian (Early Triassic) ammonoid assemblages from terranes: Paleooceanographic and paleogeographic implications. *Journal of Asian Earth Sciences* 36 (6), 420-433.
- Brown, L.F., Fisher, W.L., 1977. Seismic stratigraphic interpretation of depositional systems: examples from Brazil rift and pull-apart basins. *American Association of Petroleum Geologists Memoir* 26, 213-248.
- Burchette, T.P. Wright, V.P., 1992. Carbonate ramp depositional systems. In: B.W. Sellwood (Ed.), *Ramps and Reefs. Sedimentary Geology* 79, 3-57.
- Carr, T.R. 1983. Conodont Paleocology of Lower Triassic Thaynes Formation. *American Association of Petroleum Geologists Bulletin* 67 (3), 437.
- Carr, T.R., Paull, R.K., 1983. Early Triassic stratigraphy and paleogeography of the Cordilleran miogeocline. In: Reynolds, M.W., Dolly, E.D. (Eds.), *Mesozoic Paleogeography of the West-Central United States: Rocky Mountain Section. Society of Economic Paleontologists and Mineralogists, Rocky Mountain Symposium* 2, 39-54.
- Clark, D.L. 1959. Conodonts from the Triassic of Nevada and Utah. *Journal of Paleontology* 33 (2), 305.
- Clark, D. L., Stokes, W.L., 1956. Triassic in the Eastern Great Basin. *Journal of Paleontology* 30 (4), 1009-1010.
- Collinson, J.W., 1968. Permian and Triassic biostratigraphy of the Medicine Range northeaster, Nevada. *Wyoming Geologic Association Earth Science Bulletin* 1 (4), 25-44.

- Collinson, J.W., Kendall, C.G., Marcantel, J.B., 1976. Permian-Triassic in eastern Nevada and west-central Utah. *Geological Society of America Bulletin* 87, 821-824.
- Craig, H., 1965. The measurement of oxygen isotope paleotemperatures, In: Tongiorgi, E. (Ed.), *Stables Isotopes in Oceanographic Studies and Paleotemperatures*. CNR, Lab Geol. Nucl., Pisa, 161-182.
- Davidson, E.S., 1967. Geology of the Circle Cliffs area, Garfield and Kane Counties, Utah. *U.S. Geological Survey Bulletin* 1229, 140.
- De Zanche, V., Gianolla, P., Mietto, P., Siorpaes, C., Vail, P.R., 1993. Triassic sequence stratigraphy in the Dolomites (Italy). *Memorie di Scienze Geologiche* 45, 1-27.
- Dickins, J. M., 1993. Climate of the Late Devonian to Triassic. *Palaeogeography Palaeoclimatology Palaeoecology* 100 (1-2), 89-94.
- Dubiel, R.F., 1994. Triassic Deposystems, Paleogeography, and Paleoclimate of the Western Interior. In: Caputo, M.V., Peterson, J.A., Franczyk, K.J. (Eds.), *Mesozoic Systems of the Rocky Mountain Region, USA*, 133-168.
- Elrick, M., Read, J.F., Coruh, C., 1991. Short-Term Paleoclimatic Fluctuations Expressed in Lower Mississippian Ramp-Slope Deposits, Southwestern Montana. *Geology* 19 (8), 799-802.
- Elrick, M., Hinnov, L.A., 1996. Millennial-scale climate origins for stratification in Cambrian and Devonian deep-water rhythmites, western USA. *Palaeogeography Palaeoclimatology Palaeoecology* 123 (1-4), 353-372.
- Elrick, M., Hinnov, L.A., 2007. Millennial-scale paleoclimate cycles recorded in widespread Palaeozoic deeper water rhythmites of North America. *Palaeogeography Palaeoclimatology Palaeoecology* 243 (3-4), 348-372.
- Elrick, M., Berkyova, S., Klapper, G., Sharp, Z., Joachimski, M., Fryda, J., 2009. Stratigraphic and oxygen isotope evidence for My-scale glaciation driving eustasy in the Early-Middle Devonian greenhouse world. *Palaeogeography Palaeoclimatology Palaeoecology* 276 (1-4), 170-181.
- Embry, A.F., 1988. Triassic Sea-Level Changes: Evidence from the Canadian Arctic Archipelago. In: Wilgus, C.K., Hastings, B.S., Posamentier, H., Van Wagoner, J., Ross, C.A., Kendall, C.G.S.C., (Eds.), *Sea-Level Changes: An Integrated*

Approach. Society of Economic Paleontologists and Mineralogists Special Publication 42, 249-255.

Embry, A.F. 1997. Global sequence boundaries of the Triassic and their identification in the Western Canada Sedimentary Basin. *Bulletin of Canadian Petroleum Geology* 45, 415-433.

Emiliani, C., 1955. Pleistocene Temperatures. *Journal of Geology* 63, 538-578.

Epstein, A.G., Epstein, J.B. Harris, L.D., 1977. Conodont Color Alteration - an Index to Organic Metamorphism. *Geological Survey Professional Paper* 995, 26.

Erwin, D. H., 1996. The Mother of Mass Extinctions. *Scientific American* 275 (1), 56-62.

Erwin, D.H., 1996. Understanding Biotic Recoveries: Extinction, Survival, and Preservation during the End-Permian Mass Extinction. In: Jablonski, D., Erwin, D.H., Lipps, J.J. (Eds.), *Evolutionary Paleobiology*. The University of Chicago Press, 398-418.

Erwin, D.H., 2006. *Extinction: how life on earth nearly ended 250 million years ago*. Princeton, NJ, Princeton University Press.

Erwin, D.H., 2008. Extinction as the loss of evolutionary history. *Proceedings of the National Academy of Sciences of the United States of America* 105, 11520-11527.

Erwin, D.H., Hua-Zhang, P., 1996. Recoveries and radiations: gastropods after the Permian-Triassic mass extinction. *Biotic Recovery from Mass Extinction Events*. M.B. Hart 102, 223-229.

Fisher, W.L., McGowen, J.H., 1967. Depositional systems in the Wilcox Group of Texas and their relationship to the occurrence of oil and gas. *Gulf Coast Association of Geological Societies Transactions* 17, 105-125.

Forney, G.G., 1975. Permo-Triassic Sea-Level Change. *Journal of Geology* 83 (6), 773-779.

- Forster, A., Schouten, S., Baas, Marianne, Sinninghe Damste, J.S., 2007. Mid-Cretaceous (Albian-Santonian) sea surface temperature record of the tropical Atlantic Ocean. *Geology* 35 (10), 919-922.
- Fraiser, M.L., Bottjer, D.J., 2004. The non-actualistic early triassic gastropod fauna: A case study of the lower triassic sinbad limestone member. *Palaios* 19 (3): 259-275.
- Frakes, L.A., Francis, J.E., Syktus, I., 1992. *Climate Modes of the Phanerozoic*, Cambridge University Press.
- Frakes, L.A., Francis, J.E., 1988. A guide to Phanerozoic cold polar climates from high-latitude ice-rafting in the Cretaceous. *Nature* 333, 547-549.
- Galfetti, T., H. Ovtcharova, M., Schaltegger, U., Brayard, A., Bruhwiler, T., Goudemand, N., Weissert, H., Houchuli, P., Cordey, F., Guodun, K., 2007. Timing of the Early Triassic carbon cycle perturbations inferred from new U-Pb ages and ammonoid biochronozones. *Earth and Planetary Science Letters* 258 (3-4), 593-604.
- Galfetti, T., Hochuli, P.A., Brayard, A., Bucher, H., Weissert, H, Vigran, J.O., 2007. Smithian-Spathian Boundary event: evidence for global climatic change in the wake of the end-Permian biotic crisis, *Geology* 35 (4), 291-294.
- Garzanti, E., Nicora, A., Tintori, A., 1994. Triassic stratigraphy and sedimentary evolution of the Annapurna Tethys Himalaya in Manang (central Nepal). *Rivista Italiana di Paleontologia e Stratigrafia*. 100:195-226.
- Gregory, R.T., 1991. Oxygen isotope history of seawater revisited: Timescales for boundary event changes in the oxygen isotope composition of seawater. In: Taylor, H.P., O'Neil, J.R., Kaplan, I.R. (Eds.), *Stable Isotope Geochemistry: A tribute to Samuel Epstein*. San Antonio, The Geochemical Society 3, 65-76.
- Guex, J., Hungerbühler, A., O'Dogherty, L., Atudorei, V., Taylor, D.G., Bucher, H., Bartolini, A., 2010. Spathian (Lower Triassic) ammonoids from Western USA (Idaho, California, Utah and Nevada).
- Hallam, A. 1981. The End-Triassic Bivalve Extinction Event. *Palaeogeography Palaeoclimatology Palaeoecology* 35 (1), 1-44.

- Hallam, A., Wignall, P.B., 1997. *Mass Extinctions and Their Aftermath*, Oxford University Press.
- Haq, B.U., Hardenbol, J., Vail, P.R., 1987. Chronology of Fluctuating Sea Levels since the Triassic. *Science* 235 (4793), 1156-1167.
- Haq, B.U., Hardenbol, J., Vail, P.R., 1988. Mesozoic and Cenozoic eustatic cycles. In: Wilgus, C.K., Hastings, B.S., Kendall, C.G.S.G., Posamentier, H.W., Ross, C.A., Van Wagoner, J.C., *Sea-Level changes: an integrated approach*. S.E.P.M. 42, 71-107.
- Harris, A.G., Sweet, W.C., 1989. Mechanical and Chemical Techniques for Separating Microfossils from Sediment and Residue Matrix. In: Feldmann, R.M., Chapman, R.E., and Hannibal, J.T., (Eds.), *Paleotechniques: Paleontological Society Special Publication 4*, 70-86.
- Hayden, H.H., 1904, *The geology of Spiti with parts of Bashahr and Rupsu*, *Memoirs from the Geological Survey of India* 36 (1), 121.
- Holser, W.T., Magaritz, M., 1987. Events near the Permian-Triassic boundary. *Modern Geology* 11, 155-180.
- Hose, R.K., Repenning, C.A., 1959. Stratigraphy of Pennsylvanian, Permian, and Lower Triassic rocks of Confusion Range, west-central Utah. *AAPG Bulletin* 43 (9), 2167-2196.
- Irwin, D.C., 1971. Stratigraphic Analysis of Upper Permian and Lower Triassic Strata in Southern Utah. *The American Association of Petroleum Geologists Bulletin* 5 (11), 1976-2007.
- Jaffres, J.B.D., Shields, G.A., Wallmann, K., 2007. The isotope evolution of seawater: A critical review of a long-standing controversy and an improved geological water cycle model for the past 3.4 billion years. *Earth-Science Reviews* 83, 83-122.
- Jefferson, T.H., Taylor, T.N., 1983. Permian and Triassic woods from the Transantarctic Mountains: paleoenvironmental indicators. *Antarctic Journal of the United States* 18 (5), 14-16.
- Jervey, M.T. 1988. Quantitative geological modelling of siliciclastic rock sequences and their seismic expressions. In: Wilgus, C.K., Hastings, B.S., Kendall, C.G.S.G.,

- Posamentier, H.W., Ross, C.A., Van Wagoner, J.C., Sea-Level changes: an integrated approach. *S.E.P.M.* 42, 47-69.
- Joachimski, M.M., Buggisch, W., 2002. Conodont apatite $\delta^{18}\text{O}$ signatures indicate climatic cooling as a trigger of the Late Devonian mass extinction. *Geology* 30, 711-714.
- Joachimski, M.M., van Geldern, R., Breisig, S., Day, J., Buggisch, W., 2004. Oxygen isotope evolution of biogenic calcite and apatite during the Middle and Late Devonian. *International Journal of Earth Sciences* 93 (4): 542-553.
- Joachimski, M.M., von Bitter, P.H., Buggisch, W., 2006. Constraints on Pennsylvanian glacioeustatic sea-level changes using oxygen isotopes of conodont apatite. *Geology* 34(4), 277-280.
- Joachimski, M.M., Breisig, S., Buggisch, W., Talent, J.A., Mawson, R., Gereke, M., Morrow, J.M., Day, J., Weddige, K., 2009. Devonian climate and reef evolution: Insights from oxygen isotopes in apatite. *Earth and Planetary Science Letters* 284 (3-4), 599-609.
- Kidder, D.L., Worsley, T.R., 2004. Causes and consequences of extreme Permo-Triassic warming to globally equable climate and relation to the Permo-Triassic extinction and recovery. *Palaeogeography Palaeoclimatology Palaeoecology* 203 (3-4), 207-237.
- Kiehl, J.T., Shields, C.A., 2005. Climate simulation of the latest Permian: Implications for mass extinction. *Geology* 33 (9), 757-760.
- Kolodny, Y., Kaplan, I.R., 1970. Carbon and oxygen isotopes in apatite CO_2 and co-existing calcite from sedimentary phosphorite. *Journal of Sedimentary Petrology* 40 (3), 954-959.
- Kolodny, Y., Luz, B., 1991. Oxygen isotopes in phosphates of fossil fish - Devonian to Recent. *Stable Isotope Geochemistry: A tribute to Samuel Epstein*. H. P. Taylor, J. R. O'Neil and I. R. Kaplan. San Antonio, The Geochemical Society 3, 105-119.
- Kolodny, Y., Luz, B., Navon, O., 1983. Oxygen isotope variations in phosphate of biogenic apatites, I. Fish bone apatite - rechecking the rules of the game. *Earth and Planetary Science Letters* 64, 398-404.

- Korte, C., Kozur, H.W., Bruckschen, P., Veizer, J., Schwark, L., 2004. Carbon, sulfur, oxygen and strontium isotope records, organic geochemistry and biostratigraphy across the Permian/Triassic boundary in Abadeh, Iran, *International Journal of Earth Science* 93, 565-581.
- Krystyn, L., Balini, M., Nicora, A., 2004. Lower and Middle Triassic stage and substage boundaries in Spiti. *Albertiana* 30, 40-53.
- Krystyn, L., Balini, M., Nicora, A., 2005. Lower and Middle Triassic Stage and Substage Boundaries in Spiti. *Special Publication of Association of Petroleum Geologists* 1, 66-75.
- Krystyn, L., Bhargava, O.N., Richoz, S., 2007. A candidate GSSP for the base of the Olenekian Stage: mud at Pin Valley, Himachel Pradesh (W. Himalaya), India, *Albertiana* 35, p. 5-29.
- Kummel, B., 1943. The Thaynes Formation, Bear Lake Valley, Idaho, *American Journal of Science* 241 (5), 316-332.
- Kummel, B., 1954. Triassic Stratigraphy of Southeastern Idaho and Adjacent Areas, U.S.G.S. Professional Papers, 254-H.
- Kummel, B., Steele, G. 1962. Ammonites from the *Meekoceras gracilitatus* zone at Crittenden Spring, Elko County Nevada. *Journal of Paleontology* 36 (4), 638-703.
- Lawton, T.F., 1994. Tectonic Setting of Mesozoic Sedimentary Basins, Rocky Mountain Region, United States, in the Rocky Mountains, Eastern Great Basin, and Colorado Plateau, USA. In: Caputo, M.V., Peterson, J.A., Franczyk, K.J. (Eds.), *Mesozoic Systems of the Rocky Mountain Region, USA*. 65-71.
- Lecuyer, C., Grandjean, P., Sheppard, S.M.F., 1999. Oxygen isotope exchange between dissolved phosphate and water at temperatures ≤ 135 °C: inorganic versus biological fractionations. *Geochemica and Cosmochemica Acta* 63, (6), 855-863.
- LeGrande, A.N., Schmidt, G.A., 2006. Global gridded data set of the oxygen isotopic composition in seawater. *Geophysical Research Letters* 33 (12), L12604.
- Lehrmann, D.J., Wan, Y., Wei, J., Yu, Y., Xiao, J., 2001. Lower Triassic peritidal cyclic limestone: an example of anachronistic carbonate facies from the Great Bank of Guizhou, Nanpanjiang Basin, Guizhou province, South China. *Palaeogeography Palaeoclimatology Palaeoecology* 173 (3-4), 103-123.

- Longinelli, A., 1966. Ratios of oxygen-18:oxygen 16 in phosphate and carbonate from living and fossil marine organisms. *Nature* 211, 923-927.
- Looy, C.V., Twitchett, R.J., Dilcher, D.L., Van Konijnenburg-Van Cittert, J.H.A., Visscher H., 2001. Life in the end-Permian dead zone. *Proceedings of the National Academy of Sciences of the United States of America* 98 (14), 7879-7883.
- Lucas, S.G., Goodspeed, T.H., and Estep, J.W. (2007). Ammonoid biostratigraphy of the Lower Triassic Sinbad Formation, east-central Utah. In: Lucas, G.S, Spielman, J.A. (Eds.), *The Global Triassic*. New Mexico Museum of Natural History and Science Bulletin 41, 103-108.
- Luz, B., Kolodny, J., Kovach, J., 1984. Oxygen isotope variations in phosphate of biogenic apatites, III. Conodonts. *Earth and Planetary Science Letters* 69, 255-262.
- Marzolf, J.E., 1994. Reconstruction of the Early Mesozoic Cordilleran Craton Margin Adjacent to the Colorado Plateau in the Rocky Mountains, Eastern Great Basin, and Colorado Plateau, USA. In Caputo, M.V., Peterson, J.A., Franczyk, K.J. (Eds.), *Mesozoic Systems of the Rocky Mountain Region, USA*, 181-216.
- McCormic, C.D., Picard, M.D., 1969. Petrology of Gartra Formation (Triassic), Uinta-Mountain Area, Utah and Colorado. *Journal of Sedimentary Petrology* 39 (4), 1484.
- Mckee, E.D., 1949. Ripple Marks of the Triassic Moenkopi Formation. *Geological Society of America Bulletin* 60 (12), 1941-1941.
- Michaelsen, P., 2002. Mass extinction of peat-forming plants and the effect on fluvial styles across the Permian-Triassic boundary, northern Bowen Basin, Australia. *Palaeogeography Palaeoclimatology Palaeoecology* 179 (3-4), 173-188.
- Michaelsen, P., Henderson, R.A., 2000. Facies architecture and depositional dynamics of the Upper Permian Rangal Coal Measures, Bowen Basin, Australia. *Journal of Sedimentary Research* 70 (4), 879-895.
- Mitchum, R.M., Jr, Vail, P.R. (1977). Seismic stratigraphy and global changes of sea-level, part 7: stratigraphic interpretation of seismic reflection patterns in depositional sequences. In: Payton, C.E. (Ed.), *Seismic Stratigraphy -*

Applications to Hydrocarbon Exploration. Memoir of the American Association of Petroleum Geologists, Tulsa 26, 135-144.

- Mørk, A., 1994. Triassic transgressive-regressive cycles of Svalbard and other Arctic areas: a mirror of stage subdivision. In: Guex, G. & Baud, A. (Eds.), Recent developments on Triassic Stratigraphy, *Mémoires de Géologie (Lausanne)* 22, 69-82.
- Newell, N.D., 1948, Key Permian section, Confusion Range, western Uta, *Geological Society of America Bulletin* 59, 1053-1058.
- Newell, N.D., 1959, Key Permian section, Confusion Range, Western Utah. *Bulletin of the Geological Society of America*, 59, 1053-1058.
- Newell, N.D., 1973. The very last moments of the Paleozoic Era. In: Logan, A., Hills, L.V. (Eds.), *The Permian-Triassic Systems and their mutual boundary*. Canadian Society of Petroleum Geologists Memoirs 2, 1-10.
- Ogg, J., von Rad, U., 1994. The Triassic of the Thakkhola (Nepal). II: Paleolatitudes and comparison with other Eastern Tethyan Margins of Gondwana. *Geologische Rundschau* 83 (1), 107-129.
- O'Neil, J.R., Roe, J.L., Reinhardt, E., Blake, R.E., 1994. A Rapid and Precise Method of Oxygen Isotope Analysis of Biogenic Phosphate: *Israel Journal of Earth Sciences* 43, 203-212.
- Ovtcharova, M., Bucher, H., Schaltegger, U., Galfetti, T., Brayard, A., Guex, J., 2006. New Early to Middle Triassic U-Pb ages from South China: Calibration with ammonoid biochronozones and implications for the timing of the Triassic biotic recovery. *Earth and Planetary Science Letters* 243 (3-4), 463-475.
- Paull, R.K., Paull, R.A., 1994. Lower Triassic Transgressive-Regressive Sequence in the Rocky Mountains, Eastern Great Basin, and Colorado Plateau, USA. In Caputo, M.V., Peterson, J.A., Franczyk, K.J. (Eds.), *Mesozoic Systems of the Rocky Mountain Region, USA*, 169-180.
- Payne, J. L., Lehrmann, D.J., Wei, J., Orchard, M.J., Schrag, D.P., Knoll, A., 2004. Large Perturbations of the Carbon Cycle During Recovery from the End-Permian Extinction. *Science* 305 (5683), 506-509.

- Payne, J. L., Lehrmann, D.J., Wei, J., Knoll, A., 2006. The pattern and timing of biotic recovery from the end-Permian extinction on the Great Bank of Guizhou, Guizhou province, China. *Palaios* 21 (1), 63-85.
- Payne, J. L., Lehrmann, D.J., Wei, J., Orchard, M.J., Schrag, D.P., Knoll A., 2004. Large perturbations of the carbon cycle during recovery from the end-Permian extinction. *Science* 305 (5683), 506-509.
- Picard, M.D. Beckmann, D.D., 1967. Non-Opaque and Opaque Grain Fabrics of Siltstones in Red Peak Member (Triassic) Central Wyoming - Reply to Discussion by Rees. *Journal of Sedimentary Petrology* 37 (2), 712.
- Pietzner, H., Vahl, J., Werner, H., Ziegler, W., 1968. Zur chemischen Zusammensetzung und Micromorphologie der Conodonten. *Paleontographica* 128: 115-152.
- Preto, N., Kustatscher, E., Wignall, P.B., 2010. Triassic climates -- State of the art and perspectives. *Palaeogeography, Palaeoclimatology, Palaeoecology* Triassic climates - Selected papers from the Workshop on Triassic palaeoclimatology at the Museum of Nature South Tyrol, Bolzano/Bozen, Italy, 3-8 June 2008 290 (1-4), 1-10.
- Raup, D. M., 1979). Size of the Permian-Triassic Bottleneck and Its Evolutionary Implications. *Science* 206, 217-218.
- Retallack, G. J., 1999. Postapocalyptic greenhouse paleoclimate revealed by earliest Triassic paleosols in the Sydney Basin, Australia. *Geological Society of America Bulletin* 111 (1), 52-70.
- Retallack, G. J., Veevers, J.J., Morante, R., 1996. Global coal gap between Permian-Triassic extinction and Middle Triassic recovery of peat-forming plants. *GSA Bulletin* 108 (2), 195-207.
- Rigo M., Joachimski, M., 2010. Paleoecology of Late Triassic conodonts: constraints from oxygen isotopes in biogenic apatite. *Acta Paleontologica Polonica* 55 (3), 471-478.
- Roddlund, D.L., Bottjer, D.J., 2001. Biotic recovery from the end-Permian mass extinction, behavior of the inarticulate brachiopod *Lingula* as a disaster tason. *Palaios* 16, (1), 95-101.

- Ross, C.A., Ross, J.R.P., 1987. Cushman Foundation for Foraminiferal Research Special Publication 24, 137-149.
- Ross, C.A., Ross, J.R.P., 1988. Sea-level Change: an Integrated Approach. In: Wilgus, C.K., Hastings, B.J., Posamentier, H., van Wagoner, J.C., Ross, C.A., Kendall, C.G. St. C., (Eds.), SEPM Special Publication 42, 71-108.
- Royer, D.L., Berner, R.A., Montanez, I. P., Tabor, N.J., Beerling, D.J., 2004. CO₂ as the primary driver of Phanerozoic climate. *GSA Today* 14, 4-10.
- Rüffer, T., Zühlke, R., 1995. Sequence Stratigraphy and Sea-Level Changes in the Early to Middle triassic, of the Alps: A Global Comparison. *Sequence Stratigraphy and Depositional Response to Eustatic, Tectonic and Climatic Forcing*. B. U. Haq, Kluwer Academic publishers 1, 161-207.
- Schubert, J. K., Bottjer, D.J., 1995. Aftermath of the Permian-Triassic mass extinction event: Paleoecology of Lower Triassic carbonates in the western USA. *Palaeogeography, Palaeoclimatology, Palaeoecology* 116, 1-39.
- Scotese, C., 2010, Paleogeographic maps, <http://www.scotese.com/newpage8.htm> (last accessed November 4, 2010).
- Sepkoski, J. J., Jr, 1989. Periodicity in extinction and the problem of catastrophism in the history of life. *Journal of the Geological Society of London Bulletin* 146, 7-19.
- Sharp, Z.D., Atudorei, V., Furrer, H., 2000. The effect of diagenesis on oxygen isotope ratios of biogenic phosphates. *American Journal of Science* 300 (3), 222-237.
- Shemesh, A., Kolodny, Y., Luz, B., 1988. Isotope geochemistry of oxygen and carbon in phosphate and carbonate of phosphorite francolite. *Geochimica et Cosmochimica Acta* 52, 2565-2572.
- Shields, G.A., Kasting, J.F., 2007. Paleoclimatology: Evidence for hot early oceans? *Nature* 447, E1-E2.
- Silberling, N.J., 1975. Age relationships of the Golconda thrust fault, Sonoma Range, North-Central Nevada: Boulder, Colorado, *Geological Society of America Special Paper* 163, 28.

- Smith, H. P. (1969). The Thaynes Formation of the Moenkopi Group North-Central Utah: Unpublished Ph.D. Dissertation, University of Utah, Salt Lake City, UT.
- Smith, D.L., 1977. Transition from deep to shallow-water carbonates, Paine Member, Lodgepole Formation, central Montana. In: Enos, P., Cook, H.E. (Eds.), SEPM Special Publication 25, 87-201.
- Spalletti, L.A., Arabe, A.E., Morel, E.M., 2003. Geological factors and evolution of southwestern Gondwana Triassic plants. *Gondwana Research* 6 (1), 119-134.
- Stanley, S.M., 1990. The general correlation between rate of speciation and rate of extinction: Fortuitous causal linkages, In: Ross R.M., Allmon W.D. (Eds.), *Causes of Evolution*. University of Chicago Press, Chicago, 103–172.
- Stephen, D.A., Bylund, K.G., Bybee, P.J., Ream, W.J., 2010. Ammonoid beds in the Lower Triassic Thaynes Formation of western Utah, USA. In: Tanabe, K., Shigeta, Y., Hirano, H. (Eds.), *Cephalopods Present and Past*. Tokai University Press, Tokyo, 243-252.
- Tudge, A.P., 1960. A Method of Analysis of Oxygen Isotopes in Orthophosphate - Its Use in the Measurement of Paleotemperatures. *Geochimica Et Cosmochimica Acta* 18 (1-2), 81-93.
- Trotter, J.A., Williams, I.S., Barnes, C.R., Lecuyer, C., Nicoll, R.S., 2008. Did cooling oceans trigger Ordovician biodiversification? Evidence from conodont thermometry. *Science* 321, 550-554.
- Urey, H. C., Lowenstam, H.A., Epstein, S., McKinney, C.R., 1951. Measurement of paleotemperatures and temperatures of the Upper Cretaceous of England, Denmark and the Southern United States. *Bulletin of the Geological Society of America* 62, 399-416.
- Vail, P.R., Mitchum, R.M.J., Thompson, S., 1977. Seismic stratigraphy and global changes of sea level, part 4: Global cycles of relative changes of sea level. In: Payton, C.E. (Ed.), *Seismic Stratigraphy--Applications to Hydrocarbon Exploration*, Memoir of the American Association of Petroleum Geologists 26, 83-97.
- Van Wagoner, J.C., Posamentier, H.W., Mitchum, R.M., Vail, P.R., Sarg, J.F., Loutit, T.S., Hardenbol, J., 1988. An overview of the fundamentals of sequence stratigraphy and key definitions. In: Wigus, C.K., Hastings, B.S., Kendall, C.G.S.K., Posamentier, H.W., Ross, C.A., van Wagoner, C.J. (Eds.), *Sea-Level*

Changes: An Integrated Approach. Special Publication, Society of Economic Paleontologists and Mineralogists, Tulsa 42, 39-45.

Van Veen, P.M., Skjold, L.J., Kristensen, S.E., Rasmussen, A., Gjelberg, J., Stoølan, T., 1992, Triassic sequence stratigraphy in the Barents Sea. In: Vorren, T.O., Bergsager, E., Dahl-Stammes, Ø.A., Holter, E., Johansen, B., Lie, E., Lund, T.B., (Eds.), Arctic Geology and Petroleum Potential. Amsterdam, Norwegian Petroleum Society, NPF Special Publication 2, Elsevier, 457-479.

Van Wagoner, J.C., Mitchum, R.M., Jr., Campion, K.M. Rahmanian, V.D., 1990. Siliciclastic Sequence Stratigraphy in Well Logs, Cores and Outcrops: Concepts for High Resolution Correlation of Time and Facies. American Association of Petroleum Geologists Methods in Exploration Series, Tulsa 7.

Veizer, J., Bruckschen, P., Pawellek, F., Diener, A., Podlaha, O.G., Carden, G.A.F., Jasper, T., Korte, C., Strauss, H., Azmy, K., Ala, D., 1997. Oxygen isotope evolution of Phanerozoic seawater. *Palaeogeography, Palaeoclimatology, Palaeoecology* 132, 159-172.

Veizer, J.P., Ala, D., Azmy, K., Bruckschen, P., Buhl, D., Bruhn, F., Carden, G., Diener, A., Ebner, S., Godderis, Y., Jasper, T., Korte, C., Pawellek, F., Podlaha, O.G., Strauss, H., 1999. $^{87}\text{Sr}/^{86}\text{Sr}$, $\delta^{13}\text{C}$, and $\delta^{18}\text{O}$ evolution of Phanerozoic seawater. *Chemical Geology* 161, 59-88.

Wenzel, B., Lecuyer, C., Joachimski, M.M., 2000. Comparing oxygen isotope records of Silurian calcite and phosphate - $\delta^{18}\text{O}$ compositions of brachiopods and conodonts. *Geochimica Et Cosmochimica Acta* 64 (11), 1859-1872.

Wheeler, H.E., Scott, W.F., Thompson, T.L., 1949. Permian-Mesozoic stratigraphy in northeastern Nevada, *Geological Society of America Bulletin* 60, 1928.

Wignall, P.B., Morante, R., Newton, R., 1998. The Permo-Triassic transition in Spitsbergen: $\delta^{13}\text{C}_{(\text{org})}$ chemostratigraphy, Fe and S geochemistry, facies, fauna and trace fossils. *Geological Magazine* 135, 47-62.

Wignall, P. B., Twitchett, R.J., 1996. Oceanic Anoxia and the End Permian Mass Extinction. *Science* 272, 1155-1158.

Wilson, P.A., Norris, R.D., Cooper, M.J., 2002. Testing the Cretaceous greenhouse hypothesis using glassy foraminiferal calcite from the core of the Turonian tropics on Demerara Rise. *Geology* 30 (7), 607-610.

Ziegler, A.M., Scotese, C.R., Barrett, S.F., 1983. Mesozoic and Cenozoic paleogeographic maps, In: Brosche, P., Sundermann, J., (Eds.), Tidal friction and the earth's rotation, II, Berlin, Springer-Verlag, 240-252.